PEOPLE'S DEMOCRATIC REPUBLIC OF ALGERIA

Ministry of Higher Education and Scientific Research

Amar Telidji University - Laghouat

Faculty of technology

Department of Electronics

A thesis presented in fulfillment of the requirement for the degree of

Doctor of Sciences

In Electrical Engineering

Presented by:

TOUATI Zohra

Thesis Title

Hybrid (L_1, H_2, H_∞) For Optimal Order Reduction Of PEM Fuel Cell Controller Using Meta-Heuristic Optimization Approaches

Committee members:

Mr. AMEUR Aissa	Chair	Professor	U.A.T Laghouat
Mr. SAADI Slami	Supervisor	Professor	U.Z.A Djelfa
Mr. KIOUS Mecheri	Co-supervisor	Professor	U.A.T Laghouat
Mr. MAZOUZ Lakhdar	Examiner	M.C	U.Z.A Djelfa
Mr. HADJ AISSA Boubakeur	Examiner	M.C	U.A.T Laghouat
Mr. GHEZAL Hadj Ahmed	Examiner	Professor	U.Z.A Djelfa

July 2022

الملخص

الغرض من هذه الدراسة هو العثور على نموذج طلب مخفض مثالي للنظام الديناميكي المعقد اللاخطي للخلية الوقود لتوليد الطاقة .باستخدام خوارزميات وصفية جديدة . من وجهة نظر نظام الخلية . يمكن اعتبار كلا من غازي الهيدروجين والاكسجين مدخلين في حين يكون كلا من الجهد والتيار مخرجي النظام .با ستخدام تقنية تحديد الهوية .تم انشاء النموذج الخطي لفضاء الحالة لمكدس الخلية الوقودية وذلك بتنفيذ إجراء نمذجة الخارجية ذاتية الانحدار الغير الخطية بواسطة الشبكة العصبية. تم تخفض النموذج الخطي المحصول عليه بواسطة التقنيات الوصفية مثل تحسين النظام البيئي الاصطناعي و إعتلاف اسماك شيطان البحر(مانتا) .ان خورزمية تحسين النظام البيئي يحاكي تدفق الطاقة بين الكائنات الحية في النظام البيئي .في حين تحاكي خورزمية مانتا استراتجيات اسماك شيطان البحر في البحث عن الغذاء في مياه المحيط حيث تعيش .كلا الخوارزميتين تعمل على تقليل معايير التآزر (ال1.اتش2.اتش انفيني) و التآزر(اتش2.اتش انفيني) للخطأ بين النموذج الخطي الكامل للخلية الوقودية ونماذج الطلبات المخفضة. تمت مقارنة النتائج بين تلك التي تم الحصول عليها بوسطة الخورزميتين مع طريقة الاقتطاع المتوازن. أكدث النتائج التجربية أن النموذج التقريبي الذي تم الحصول عليه بواسطة الخورزمية المقترحة مانتا له تقارب أسرع وأداء تقريبي أفضل في كلا التآزرين مقارنة بخورزمية النظام البيئي . بالإضافة إلى ذلك ، أثبت أن كل من الخوارزميتين أنها دقيقة وموثوق بها للتحقيق في نموذج الطلب المنخفض العالمي مع الحفاظ على السلوك الرئيسي للخلية الوقودية 500وات .

الكلمات المفتاحية :الخلية الوقودية 500 وات– خوارزميات النظام البيئي الاصطناعي و إعتلاف اسماك شيطان - الشبكة العصبية- نمذجة الخارجية ذاتية الانحدار الغير الخطية- معايير التآزر - تقنية نموذج طلب مخفض

Abstract

The purpose of this study is to find an optimal reduced order model for large-scale order multi-input multi-output dynamical nonlinear PEMFC SR-12 500W system using novel meta-heuristic algorithms. From the point view of the PEMFC system, the hydrogen and oxygen can be considered as two inputs, the cell voltage and current as two outputs. By implementation of identification technique, the linear state space model of PEMFC stack is generated using neural network nonlinear autoregressive exogenous (NN-NLARX) modeling procedure, the obtained linear model is reduced its order by meta-heuristic techniques such as Artificial Ecosystem Optimization (AEO) and Manta Rays Foraging Optimization (MRFO) algorithms. The AEO mimics the energy flow behaviour between living organisms in a natural ecosystem, while the MRFO is inspired by foraging strategies of manta rays which are living in ocean waters. These algorithms used to minimize the hybrid (L_1, H_2, H_∞) and hybrid (H_2, H_∞) norms of error between full linear PEMFC model and its reduced order models. The obtained results are compared with the other standard method such as balanced truncation (BT) , and they confirm that, the approximate model obtained by proposed MRFO has faster convergence and better approximation performance in hybrid (L_1, H_2, H_∞) and hybrid (H_2, H_∞) norm than obtained by AEO.in addition, both algorithms and BT method are proven to be accurate and reliable to investigate the PEMFC optimum global reduced order model which preserving the main behavior of original PEMFC SR-12 500W model.

Keywords: (L_1, H_2, H_∞) norms; hybrid; nlarx; PEMFC500W; model order reduction; AEO and MRFO algorithms; neural network.

Résumé

Le but de cette étude est de trouver un modèle d'ordre réduit optimal pour le système piles à combustible à membrane échangeuse de protons (PEMFC SR-12 500W) complexe non linéaire

multi-entrées multi-sorties en utilisant de nouveaux algorithmes méta-heuristiques. Point de vue du cette pile, les pressions l'hydrogène et l'oxygène peuvent être considérés comme deux entrées, tandis que la tension et le courant comme deux sorties. Par l'implémentation de la technique d'identification, le modèle linéaire d'espace d'état de la pile PEMFC est généré à l'aide de la procédure de modélisation exogène autorégressive non linéaire avec réseau neuronal (NN-NLARX), L'ordre de modèle linéaire résultant est réduit à l'aide de techniques méta-heuristiques telles que les algorithmes d'optimisation de l'écosystème artificiel (AEO) et d'optimisation de la recherche de nourriture des espèces (MRFO). L'AEO imite le comportement des flux d'énergie entre les organismes vivants dans un écosystème naturel, tandis que le MRFO s'inspire des stratégies de recherche de nourriture des espèces qui vivent dans les océans.
Ces algorithmes sont utilisés pour minimiser les normes d'erreur hybrides (L_1, H_2, H_∞) and (H_2, H_∞) entre le modèle PEMFC linéaire complet et ses modèles d'ordre réduit. Les résultats obtenus sont comparés avec la méthode standard telle que la troncature équilibrée (BT), et ils sont confirmés que les modèles approximantes obtenu par le MRFO proposé a une convergence plus rapide et une meilleure performance d'approximation en hybrides (L_1, H_2, H_∞) and (H_2, H_∞) que celle obtenue par AEO. De plus, les algorithmes et la méthode BT se sont avérés précis et fiables pour étudier le modèle d'ordre réduit global optimal de PEMFC qui a préservé le comportement principal d'origine PEMFC SR-12 500W Modèle.

Mots-clés: piles à combustible 500W ; Réduction optimale ; normes (L_1, H_2, H_∞); hybrides; nlarx; techniques méta-heuristiques; réseau neuronal.

DEDICATION

….dedicate

To the Soul of my father YOUCEF which I cannot forget him

*To my mother **FATNA** and*

To my beloved sisters Aida, Khadjija, Embarka, Addala ,

Zineb, Houria, Aicha , Fatima

To my wonderful brother Khaled Omar Mokhtar

And my nephew Houssam Allaa eddine

To my best friend Rabhia Bensalem

for their continuous support and encouragement

ACKNOWLEDGEMENT

Firstly, Praise be to **ALLAH** , Lord of all creation who give me power and confidence to complete this dissertation , By **ALLAH**'s grace and mercy, I could to achieve this work.

I would like to express my gratitude and thanks to my supervisor, Pr. SAADI Slami, who guided me with patience and dedication during last six years. He helped me to grow up and explore my potential. also, I appreciated the great freedom that he granted me in managing this thesis.

A special thanks to Pr. KIOUS Mecheri from University of Amar Telidji Laghouat, who generous help, encouragement, flexibility and for their support in hard times. Also, I am greatly thankful for all administrative steps, his assistance to defending this thesis.

Special thanks to Pr. AMEUR Aissa for accepting the presidency of the jury, sincere gratitude also to Dr. MAZOUZ Lakhdar, Dr. HADJ AISSA Boubakeur and Pr. GHEZAL Hadj Ahmed who honored me by examining my thesis and their valuable and constructive comments to review and improve this work.

Finally, special thanks addressed to my mother, who encouraging me when everything seemed weak. Without her love and caring, I will be a drifting empty bottle.

List of Publications

1. Z. Touati, S. Saadi, M. Kious, and K. O. M. Touati, "Synergy of (H 2 , H ∞) norms for nonlinear optimal PEMFC dynamic MIMO model reduction using a novel EAO approach," *Int. J. Syst. Assur. Eng. Manag.*, vol. 13, no. 3, pp. 1396–1409, 2022, doi: 10.1007/s13198-021-01485-1.

2. Z. Touati, "H2 –norm optimal of linear complexes discrete MIMO models reduction using data interpolation". Conference: The 2nd International Workshop on Signal Processing Applied to Rotating Machinery Diagnostics SIGPROMD'2018, Djelfa, Algeria. April 2018

Table of Contents

Abstract ..... **i**
DEDICATION ..... **iii**
ACKNOWLEDGEMENT ..... **iv**
Table of Contents ..... **vi**
List of figures ..... **x**
List of Tables ..... **xii**
List of Abbreviations ..... **xiii**
List of symbols ..... **xiv**
General Introduction **1**
Chapter 1 Fuel cells Literature review **3**
1.1 Introduction 3
1.2 Fuel Cells History 4
1.3 Operating Principle of Fuel Cell 6
1.4 Fuel Cell Systems Types 7
1.5 The Proton-Exchange Membrane Fuel Cells (PEMFC) 9
1.5.1 Structure of Proton Exchange Membrane Fuel Cell 9
1.5.1.1 Bipolar Plates 10
1.5.1.2 The Electrodes 11
1.5.1.3 The Catalyst 12
1.5.1.4 The Electrolyte 12
1.6 Auxiliary Devices 13
1.6.1 Hydrogen and Air Supplies 14
1.6.2 The Humidifier 15
1.6.3 The Cooling Circuit 15
1.6.4 DC/DC Converter 16
1.7 Efficiency of PEM fuel cell System 16
1.8 Fuel cells applications 17
1.8.1 Transport Applications 17
1.8.2 Portable Applications 18
1.8.3 Stationary Applications 18
1.9 Advantages and Disadvantages of Fuel Cells 20

1.10 Conclusion 22
Chapter 2 Nonlinear modeling of Proton exchange membrane fuel cell PEMFC 500W….. ……..... 23
2.1 Introduction..... 23
2.2 Proton Exchange Membrane Fuel Cell Stack Nonlinear Modeling 23
2.2.1 Static modeling..... 24
2.2.1.1 Activation Voltage Loss..... 25
2.2.1.2 Ohmic Voltage Loss 26
2.2.1.3 Concentration Voltage Loss 26
2.2.2 Dynamic Modeling..... 27
2.2.2.1 Net Mole Flow Rate Equations of Gases 28
2.2.2.2 Equations of Pressure Gases..... 29
2.2.2.3 Equations of the Net Temperature..... 31
2.2.2.4 Equivalent Electrical Circuit Equations for PEM Fuel Cell..... 34
2.3 Evaluation of Mathematical Modeling 37
2.3.1 Evaluation of Mathematical Modeling for Partial Pressures Gases..... 38
2.3.2 V-I Characteristics of the Proton Exchange Membrane Fuel Cell 41
2.3.3 Evaluation of Voltage Losses..... 43
2.3.4 P-I Characteristics Curve of the Proton Exchange Membrane Fuel Cell..... 47
2.4 Conclusion 49
Chapter 3 Neural Network Nonlinear Autoregressive Exogenous Modeling of PEMFC 500 W ……..……..……..50
3.1 Introduction..... 50
3.2 Nonlinear Model Identification..... 50
3.3 Nonlinear Autoregressive Exogenous (NLARX) Model..... 52
3.4 Artificial Neural Network..... 53
3.5 The Proposed Cascade Forward Neural Network 56
3.6 Neural Network Nonlinear Autoregressive Exogenous Model Identification 60
3.7 Model Validation 61
3.7.1 Mean Square Error 61
3.7.2 Best Fit Criterion..... 61

3.7.3 Final Prediction Error 62
3.8 Result and Analysis 62
3.8.1 Preparing and Preprocessing of the Data 63
3.8.2 Neural Network Estimation of PEMFC 500W Stack 63
3.8.3 NN-NLRAX Model Linearization 66
3.9 Conclusion 75
Chapter 4 Model Order Reduction Literature 76
4.1 Introduction 76
4.2 Model Order Reduction 77
4.3 Classical methods 80
4.3.1 Model order reduction for linear systems 80
4.3.2 Model Order Reduction For Nonlinear Systems 81
4.4 Optimal Model Reduction 82
4.4.1 Signal Norms 82
4.4.2 System Norms 83
4.4.2.1 H2 Norm 83
4.4.2.2 H∞ Norm 85
4.4.2.3 L1 Norm 86
4.4.3 H2 Norm Model Reduction 86
4.4.4 H∞ Norm Model Reduction 87
4.4.5 L1 Norm Model Reduction 88
4.5 Meta-Heuristic Techniques for Model Reduction 89
4.6 Conclusion 90
Chapter 5 Meta-Heuristic Algorithms 91
5.1 Introduction 91
5.2 Artificial Ecosystem-Based Optimization (AEO) 91
5.2.1 Application of AEO Algorithm 99
5.3 Manta Ray Foraging Optimization (MRFO) Algorithm 100
5.3.1 Application of MRFO Algorithm 108
5.4 Conclusion 109

Chapter 6 Hybrid (L1 ,H2 , H∞) Norms For Optimal Order Reduction of PEMFC 500W Model……..…110

6.1 Introduction 110

6.2 Statement of Problem 110

6.3 Numerical Results 111

6.3.1 Hybrid (L1, H2, H∞) Norm 112

6.3.1.1 Comparative Study of the Meta-Heuristic Algorithms 113

6.3.1.2 Norms and Steady State Errors 114

6.3.1.3 Impulse Responses 115

6.3.1.4 Step Responses 116

6.3.1.5 Frequency Responses and Steady State Error 118

6.3.1.6 Comparative study of The Hybrid (L1, H2, H∞) Reduced Models and Nonlinear PEMFC Model 121

6.3.2 Hybrid (H2, H∞) Norms 123

6.3.2.1 Comparative Study of the Two Algorithms 124

6.3.2.2 Norms and Steady State Errors 125

6.3.2.3 Impulse Responses 126

6.3.2.4 Step Responses 127

6.3.2.6 Frequency Responses and Steady State Error 129

6.3.2.7 Comparative Study of The hybrid (H2, H∞) Reduced Models And Nonlinear PEMFC Model…. 132

6.4 PEMFC Meta-Heuristic Model Reduction Approaches vs. Previous Studies 134

6.4.1 Model identification 134

6.4.2 Balanced Model Order Reduction 135

6.5 Conclusion 137

General Conclusion 138

Bibliography 140

Annex A 149

List of figures

Figure 1. 1 External view of the fuel cell stack ……....**3**
Figure 1. 2 Grove's gas battery……..……**4**
Figure 1. 3 PEM Fuel cell uses **6**
Figure 1. 4 Fuel Cell basic working **7**
Figure 1. 5 Structure of PEM fuel cell stack……...**10**
Figure 1. 6 single- fuel cell **10**
Figure 1. 7 Bipolar plates structure **11**
Figure 1. 8 Membranes fuel cell ……..….....**13**
Figure 1. 9 Nafion molecular structure..... **13**
Figure 1. 10 Different components of a fuel cell system..... **14**
Figure 1. 11 Fuel cell electric automobile **18**
Figure 1. 12 200 kW PAFC on-site plant **19**

Figure 3. 1 Flowchart of identification technique……....**51**
Figure 3. 2 Nonlinear ARX Model Structure **52**
Figure 3. 3 Structure of static neural network..... **54**
Figure 3. 4 Structure of dynamic feedforward neural network..... **55**
Figure 3. 5 Structure of dynamic feedback neural network..... **56**
Figure 3. 6 Structure of cascade-forward neural network (CFNN)..... **57**
Figure 3. 7 NN-NLARX model structure..... **60**
Figure 3. 8 (a) Data estimation , (b) Data validation of predicted outputs model for ([2 0, 2 0], [2 2, 0 0], [1 1, 1 1] at [2 4 2] **69**
Figure 3. 9 (a) Data estimation , (b) Data validation of predicted outputs model for ([2 0, 2 0], [2 2, 0 0], [1 1, 1 1] at [2 5 2]. **70**
Figure 3. 10 (a) Data estimation, (b) Data validation of predicted outputs model for ([2 0, 2 0], [2 2, 0 0], [1 1, 1 1] at [2 6 2]. **71**
Figure 3. 11 Step responses of linear and nonlinear models **72**
Figure 3. 12 Step responses of linear and nonlinear models with hidden layers [2 5 2] **73**
Figure 3. 13 Step responses of linear and nonlinear models with hidden layers [2 6 2] **73**
Figure 4. 1 Overall picture of model order reduction ……..**77**
Figure 5. 1 Flow energy in an ecosystem; (a) food chain, (b) food web.....**93**
Figure 5. 2 An ecosystem in AEO technique [91] **94**
Figure 5. 3 Flowchart of AEO algorithm **98**
Figure 5. 4 (a) A foraging manta ray, (b) manta ray structure.....**100**
Figure 5. 5 Chain foraging strategy.....**102**
Figure 5. 6 Cyclone foraging strategy in a 2-D space **103**
Figure 5. 7 Somersault foraging strategy.....**105**
Figure 5. 8 Flowchart of MRFO algorithm **107**

Figure 6. 1 Convergence rate of AEO and MRFO for hybrid (L1 H2, H∞) norms **113**

Figure 6. 2 Impulse responses of original PEMFC model and hybrid (L1, H2, H∞) reduced models via AEO, MRFO and BT **115**
Figure 6. 3 Initial values of the impulse responses of original PEMFC model and hybrid (L1, H2, H∞) reduced models **116**
Figure 6. 4 Step responses of original PEMFC model and hybrid (L1, H2, H∞) reduced models via AEO,MRFO and BT **117**
Figure 6. 5 Initial values of the steps responses of original PEMFC model and hybrid (L1, H2, H∞) reduced models **118**
Figure 6. 6 Frequency responses of original PEMFC model and hybrid (L1, H2, H∞) reduced models via AEO,MRFO and BT **119**
Figure 6. 7 Step error comparison between the original PEMFC model and AEO, MRFO, BT reduced order models **120**
Figure 6. 8 Comparison the outputs of hybrid (L1, H2, H∞) reduced models, the linearized 8th order model, nonlinear model with PEMFC measured data **121**
Figure 6. 9 Step responses of nonlinear ,linear PEMFC models and hybrid (L1, H2, H∞) reduced models via AEO, MRFO and BT.....**122**
Figure 6. 10 Convergence rate of AEO and MRFO for hybrid (H2, H∞) norms **124**
Figure 6. 11 Impulse responses of original PEMFC model and hybrid (H2, H∞) reduced models via AEO, MRFO and BT **126**
Figure 6. 12 Initial values of the impulse responses of original PEMFC model and hybrid (H2, H∞) reduced models **127**
Figure 6. 13 Step responses of original PEMFC model and hybrid (H2, H∞) reduced models via AEO, MRFO and BT **128**
Figure 6. 14 Initial values of the step responses of original PEMFC model and hybrid (H2, H∞) reduced models **129**
Figure 6. 15 Frequency responses of original PEMFC model and hybrid (H2, H∞) reduced models via AEO, MRFO and BT **130**
Figure 6. 16 Step error comparison between original PEMFC model and hybrid (H2, H∞) reduced models **131**
Figure 6. 17 Comparison the outputs of hybrid (H2, H∞) reduced models, the linearized 8th order model, nonlinear model with PEMFC measured data **132**
Figure 6. 18 Step responses of nonlinear ,linear PEMFC models and hybrid (H2, H∞) reduced models **133**

List of Tables

Table 1. 1 Different types of fuel cells……...**8**

Table 2. 1 The PEM Fuel Cell 500 W Model characteristics **38**

Table 3. 1 Effect of the number of units in the hidden layers and the regressors on ze and zv of NN-NLRAX models……..**64**

Table 3. 2 Loss function for NLRAX structures with neural network estimator……**65**

Table 3. 3 MSE performance for model structures with neural network estimator..... **66**

Table 3. 4 Effect of the number of units in the hidden layers and the regressors on ze and zv for identified linear ARX models **67**

Table 3. 5 LN and FPE results for estimated using ARX from data set **68**

Table 6. 1 Comparison between the relative L1, H2, H∞, hybrid (L1, H2, H∞) norms of errors and SSE……**114**

Table 6. 2 Comparison between the relative L1, H2, H∞, hybrid (H2, H∞) norms of error and SSE.... **125**

Table 6. 3 Comparisons results of the hybrid (L1, H2, H∞) norms and Shady's reduced models..... **136**

List of Abbreviations

AEO	Artificial Ecosystem-Based Optimization
AFC	Alkaline Fuel Cell
ARX	Auto Regressive eXogenous
BT	Balanced Truncation
CFNN	Cascade-Forward Neural Network
DMFC	Direct Methanol Fuel Cell
FPE	Final Prediction Error
GA	Genetic Algorithm
MCFC	Molten Carbonate Fuel Cell
MEA	Membrane Electrode Assembly
MIMO	Multi Input Multi Output
MOR	Model order reduction
MRFO	Manta Ray Foraging Optimization
MSE	Mean Square Error
NLARX	Non-Linear Auto-Regressive eXogenous
NN	Neural Network
NN-NLARX	Neural Network Non-Linear Auto-Regressive eXogenous
PAFC	Phosphoric Acid Fuel Cell
PEM	Prediction Error Method
PEMFC	Proton Exchange Membrane Fuel Cell
PSO	Particle Swarm Optimization
SI	System Identification
SISO	Single Input Single Output
SOFC	Solid Oxide Fuel Cell
SSE	Steady State Error
TDL	Time Delay
TPWL	Trajectory Piece-Wise Linear method

List of symbols

A_s	Area of a single cell
a_0	Constant in Tafel equation
a, b	Constants in Tafel equation
C	Capacitance due to charge double layer (F)
C_0	Concentration of surface at the reaction sites
C_i	Biggest concentration in gas channels
C_{fc}	Specific heat capacity of PEM fuel cell stack ($J/(molK)$)
E_0^{Cell}	Reference potential at standard operating conditions (V)
E_{Nernst}	cell potential Nernst (V)
h_S	Convective heat transfer coefficient $W/(m^2.K)$
e	Number of participating electrons
ΔG	Gibbs free energy (J/mol)
ΔG^0	Change in a Gibb's free energy at standard operating conditions(J/mol)
F	Faraday's constant (C/mol)
Is	Stack current (A)
I_L	Current limit of PEM fuel cell (A)
Id	Exchange current density(A/m^2)
i_{fc}	Output current
K_I	Constant in computation of $R_O(\Omega/A)$
K_T	Constant in computation of $R_O(\Omega/K)$
M_{fc}	Fuel cell mass
$(M_{H_2})_{in}$	Input hydrogen mole flow rate at anode (mole/s)
$(M_{H_2})_{out}$	Output hydrogen mole flow rate at anode (mole/s)
$(M_{H_2})_{net}$	Net mole flow rate of hydrogen(mole/s)
$(M_{H_2O})_{net}$	Net mole flow rate of water (mole/s)
$(M_{H_2O})_{in}^{a}$	Anode water mole flow rate (mole/s)
$(M_{H2O})_{in}^{c}$	Cathode water mole flow rate (mole/s)
$(M_{O_2})_{in}$	Input oxygen mole flow rate at cathode (mole/s)
$(M_{O_2})_{out}$	Output oxygen mole flow rate at cathode (mole/s)

$\left(\mathrm{M}_{\mathrm{O}_2}\right)_{\mathrm{net}}$	Net mole flow rate of oxygen (mole/s)
n_{s}	Number of stack cells
$\mathrm{P}_{\mathrm{H}_2}$	Hydrogen partial pressure (*atm*)
$\mathrm{P}_{\mathrm{O}_2}$	Oxygen partial pressure (*atm*)
$\mathrm{P}_{\mathrm{H}_2\mathrm{O}}$	Water partial pressure (*atm*)
$(\mathrm{P}_{\mathrm{H}_2\mathrm{O}})_{\mathrm{in}}^{\mathrm{a}}$	Water partial pressure at anode (*atm*)
$(\mathrm{P}_{\mathrm{H}_2\mathrm{O}})_{\mathrm{in}}^{\mathrm{c}}$	Water partial pressure at cathode (*atm*)
P_{stack}	Output power
Q_{C}	Electrochemical reaction heat (J)
Q_{E}	Electrical output heat of PEM fuel cell (J)
Q_{L}	Heat loss due to the air convection (J)
R	Universal gas constant $[J/(mole.K)]$
R_{O}	Ohmic resistance of the PEM fuel cell (Ω)
$\mathrm{R}_{\mathrm{O}}^{\mathrm{c}}$	Constant in computation of $R_O(\Omega)$
T	Stack temperature (K)
T_{t}	Room temperature (K)
$\mathrm{u}_{\mathrm{P_A}}$	Channel pressure of hydrogen (*atm*)
$\mathrm{u}_{\mathrm{P_C}}$	Channel pressure of oxygen (*atm*)
V_{a}	Volume of anode (m^3)
V_{c}	Volume of cathode (m^3)
V_{act}	Activation voltage loss (V)
$\mathrm{V}_{\mathrm{conc}}$	Concentration voltage loss (V)
V_O	Ohmic voltage loss (V)
V_{out}	Output voltage
y_p	Predicted output
λ_{A}	Flow delay at anode (sec)
λ_{C}	Flow delay at cathode(sec)
$[n_a, n_b, n_k]$	Standard regressors
$\mathbb{R}$	Set of real numbers
x	State vector of the system
u	Input vector of system

y	Output vector of system
$(A_N, B_N, C_N, D, K_N, x_N)$	Full system
$(A_n, B_n, C_n, D, K_n, x_n)$	Reduced order system
t, k	Continuous time, discrete time
z, s	Frequency variables in continuous time, in the discrete time
$G_N(z)$, $G_n(z)$	Transfer function of original model and reduced order model
$\|y\|_p$	Vectors norms (p = 1, 2, ∞)
$\|\mathrm{G}\|_\mathrm{p}$	Matrix norms (p = 1, 2, ∞)
$\mathcal{P}/\mathcal{Q}$	controllability and observability grammians

General Introduction

General Introduction

Recently, renewable energy technologies are preparing to play an important role in overcoming global pollution, climate change, global warming and the fossil fuel depletion. Among these technologies, the conversion of an electrochemical energy which is considered the most suitable, sustainable and eco-friendly. Proton Exchange Membrane Fuel Cells (PEMFCs) are one of the most prominent examples of electrochemical energy conversion technologies in progress, due to their high efficiency, robustness, lightweight, high density, zero emission level, fast start-up, lower operation temperature (less than 100 ◦C) and solid-state of the electrolyte. As a result of these characteristics, the PEMFC is an appropriate device for automotive vehicles, portable power generators, and emergency backup power application.

The main goal of the PEMFC control system is providing the power at levels equal to those required by the command signal while achieving a wide range of power conditions. Modeling methodology and controller design play a substantial role in the investigation of this objective[1]. the PEMFC stack is considered a multi-input/multi-output, nonlinear, and complex high scale system, as result, it requires a high order modeling in order to represent it well. Therefore, most of the difficulties lay in simulation and designing a large-scale PEMFC model, which in turn lead to difficulty in designing the highly complex controller of PEM fuel cell model.

Model order reduction (MOR) is a significant tool was developed in the field of systems and control literature to study properties of dynamical systems in order to reduce their complexity (or simplification), while capture the essential features of the original systems and preserving their input-output behavior as much as possible[2].

The main contributions of this study can be summarized in the following points:

- System identification was implemented to model the nonlinear behavior for PEMFC model. the nonlinear autoregressive exogenous (NLARX) structure with neural network estimator was chosen to reproduce the best voltage/current outputs of the nonlinear PEMFC system, the resulting of nonlinear neural network model is linearized at a given input signal to obtain the linear state space PEMFC model.

- Meta-heuristic optimization algorithms were proposed to reduce the order of linear PEMFC model via minimizing both of the hybrids (L_1, H_2, H_∞) and (H_2, H_∞) norms of errors between full linear state space PEMFC model and reduced model. Artificial Ecosystem Optimization (AEO) and Manta Rays Foraging Optimization (MRFO) are the best techniques that provide competitive results with balanced truncation (BT).

The outline of this dissertation is as follows:

Chapter 1 introduces an overall literature review on Proton Exchange Membrane Fuel Cell such as history, operating principle, composition and structure of single PEM fuel cell, auxiliary devices, advantages and disadvantages of fuel cells.

Chapter 2 describes and implements the nonlinear state space equations of a 500-W PEM fuel cell stack using the internal physical processes inside the PEM fuel cell system. The performance of dynamic behavior for PEM fuel cell stack is evaluated by using the V-I and P-I Characteristics.

Chapter 3 demonstrates the system identification technique to model the behavior of the PEM fuel cell using neural network nonlinear autoregressive exogenous model (NN-NLARX) structure. The development of forward cascade neural network to model the nonlinear behavior of the PEM fuel cell 500W stack is shown. The obtained neural network model is linearized to get the linear space state PEMFC model.

Chapter 4 presents a brief overview on model order reduction with their methods including classical techniques for linear and nonlinear systems, optimal model reduction methods, and meta-heuristic techniques.

Chapter 5 contains a detailed discussion about two meta-heuristic algorithms: Artificial Ecosystem Optimization (AEO) and Manta Rays Foraging Optimization (MRFO), as a two bright techniques to deal with optimal model order reduction problems hybrids (L_1, H_2, H_∞) and (H_2, H_∞) norms for complex PEMFC 500 W model.

Chapter 6 presents the results discussion of AEO and MRFO model reduction methods for PEMFC 500W model and compare them with balanced truncated (BT) approach using the step, impulse responses and frequency responses as well as steady state error. Finally a general conclusion is given with some proposed future works.

Chapter 1

Fuel cells Literature review

1.1 Introduction

The objective of this chapter is to present the art state of fuel cells: its history, its operating principle, its types, its applications, its advantages and its disadvantages. In general, fuel cells are considered as generators that directly convert the internal energy of a fuel into electrical energy, using an electrochemical process (instead of a thermal reaction of combustion, the mechanical work which is converted into electricity).

This chapter focus particularly on Proton-Exchange Membrane Fuel Cells PEMFC type with details of its stack structure. Figure (1.1) gives an image of a fuel cell with few cells are connected in series configuration, the fluid supply and discharge pipes (fuel, oxidizer and coolant) as well as the assembly system (bipolar plates).

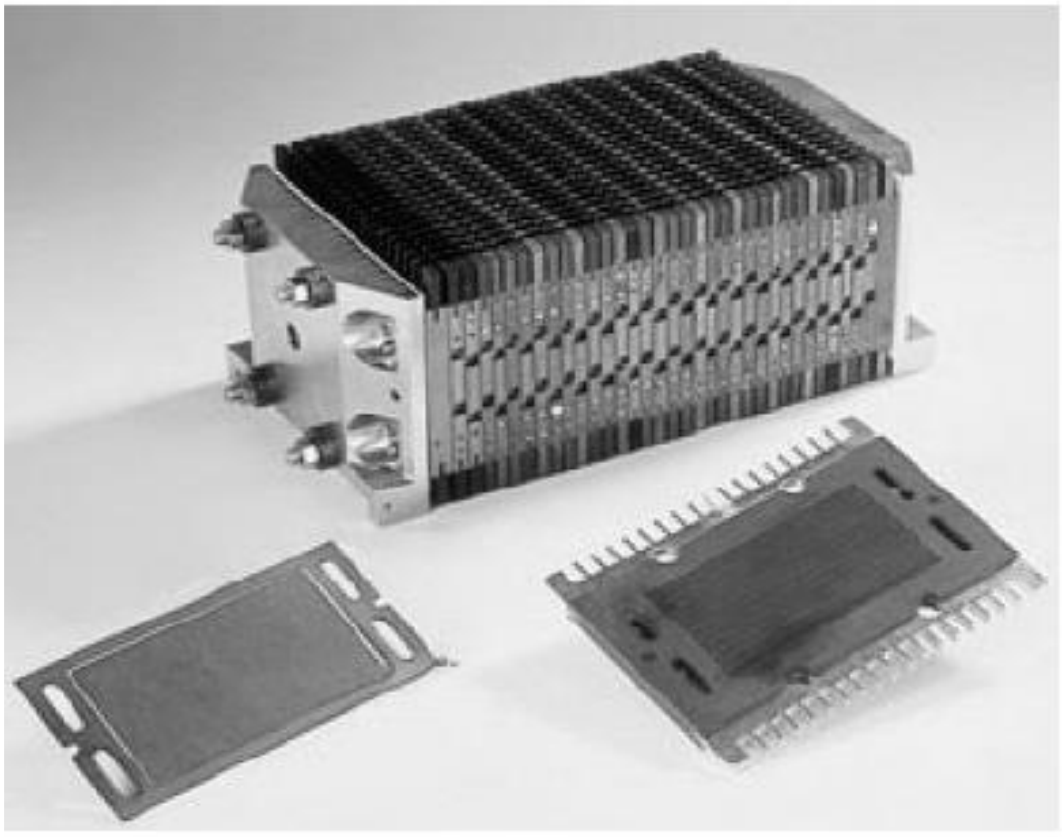

Figure 1.1 External view of the fuel cell stack [3]

1.2 Fuel Cells History

The first crude fuel cells were invented by Sir William Grove in 1839 through an experimental set-up using two platinum electrodes partially immersed in a sulphuric acid of copper and dilute .Each electrode had one end immersed in acid and the other end in a sealed container of hydrogen and oxygen, respectively. Grove observed the current flow between the electrodes was constant. In addition, the containers maintain water as well as the gases, and he noted an increasing in water level in both of them as the current flowed. Thus, Grove's gas battery was the first experimental fuel cell in that period figure (1.2). The electrochemical reactions which occurred in the cell were still unknown in that era and because it was useless to use it. This invention remained almost locked in drawers until the early twentieth century.

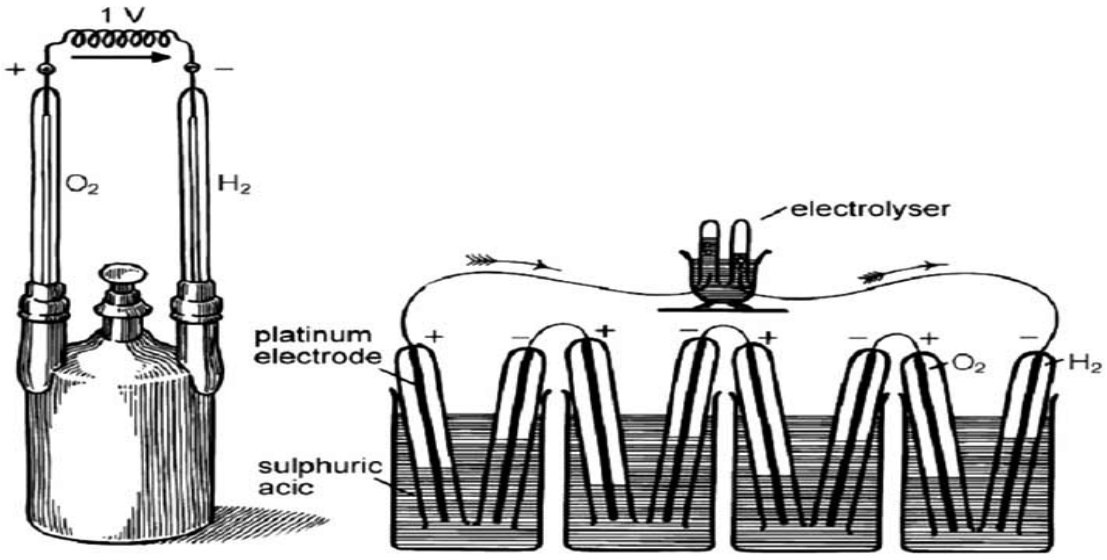

Figure 1.2 Grove's gas battery

In 1932, an engineer Francis Bacon from Cambridge University made a significant development to fuel cell system he replaced platinum electrodes with less expensive nickel gauze and substituted the sulphuric acid electrolyte for alkali potassium hydroxide, a less corrosive substance. In 1959, Bacon built a 5-kW alkaline fuel cell, capable to power a welding machine[4].

In the early sixties, the PEM fuel cell was invented by General Electric (GE) scientists Willard Thomas Grubb and Leonard Niedrach, they used the sulfonated polystyrene membranes for electrolytes. Later, it were replaced by Nafion ionomer, which proved to be superior in performance and durability to sulfonated polystyrene. This fuel cell type was used in the famous spacecraft "Gemini" for US National Aero Space Agency (NASA) to generate electricity for manned space missions because both nuclear generation and solar power were too dangerous. This considered the principal achievements of the initiative between GE and NASA. This was the first commercial use of a PEM fuel cell[5]. Next, NASA replaced the PEM fuel cell by alkaline fuel cells (AFC) in the "Apollo" program and in the Space Shuttle. Hence, the cells in those two spacecraft were large and expensive, but they performed their tasks without any errors and were able to provide an electric current as well as a source of clean drinking water in spacecraft.

Since the 1970s, very large industrial companies have made many research efforts to develop fuel cells by developing its manufactured materials, reducing its weight and increasing its life time until they became the first source for the production of energy used in NASA's space shuttle. Then its use expanded to more applications for transportation , portable and stationary systems as a promising source for power generation for these applications ,and this was shown by both M. W. Ellis et al[6] and et J. H. Hirschenhofer [7], in their research papers as they proved that the fuel cell coupled with a tank in portable applications can provide higher energy and more convenient than conventional batteries. In addition to providing better performance than thermal engines besides Generators.

For high-power stationary applications, PEM fuel cells can be used to supplement the existing electrical grid without emitting locally contaminated gases. Moreover, PEM fuel cell systems can be connected directly to buildings in order to supply the electrical and thermal energy efficiently co-generation up to 80%. The figure (1.3) shows an example to uses of PEM fuel cell stack in all applications.

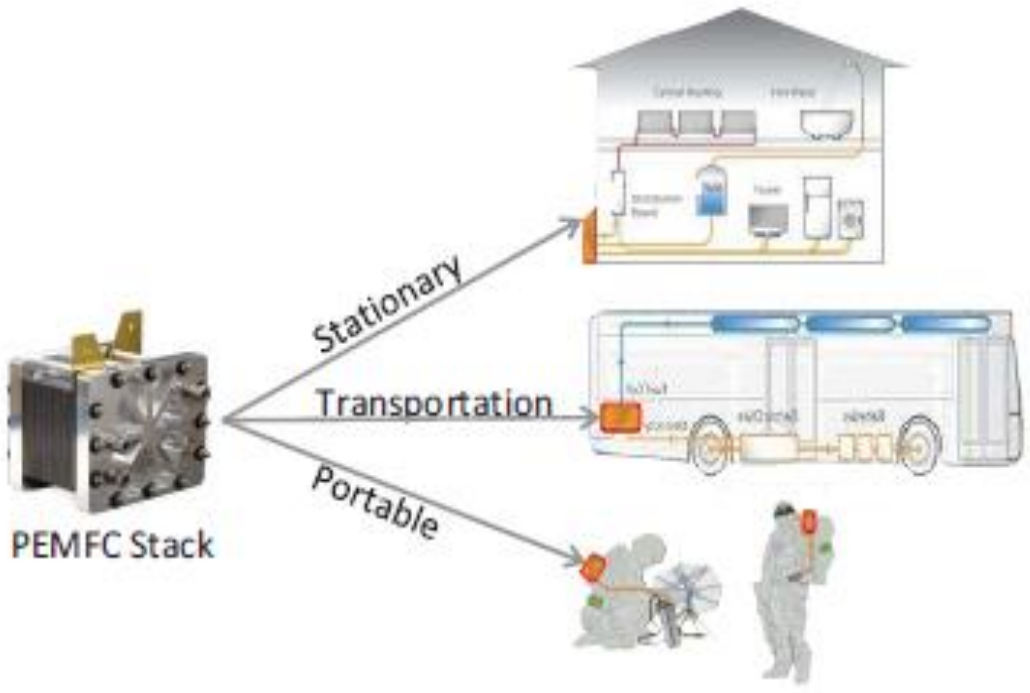

Figure 1.3 PEM Fuel cell uses [8]

1.3 Operating Principle of Fuel Cell

The basic principle work of all fuel cells is converting the chemical energy which exist in hydrogen atoms into electrical energy. There are three main components in fuel cell :a positive charged electrode(anode) is supplied by hydrogen gas, a negative charged electrode(cathode) is supplied by air and electrolyte placed between them to permit only hydrogen ions flows from the anode to the cathode side for combining with electrons and oxygen to produce the water [9]. The free electrons flow through an external circuit in form electric energy. Besides the energy released from chemical reactions, the heat are also produced.

Given that the electrochemical process does not involve a Carnot cycle, efficiency can be very high, could reach 80–85%. Fuel cells have no moving parts, make no noise and are scalable[4]. The basic chemical equations in anode/cathode of fuel cell are the following:

$$
\begin{aligned}
2H_2 &\longrightarrow 4H^+ + 4e^- \quad \text{half reaction of anode} \\
O_2 + 4H^+ + 4e^- &\longrightarrow H_2O \quad \text{half reaction of cathode} \\
H_2 + \tfrac{1}{2}\, O_2 &\longrightarrow H_2O + \text{electricity} + \text{heat} \quad \text{overall reaction}
\end{aligned}
\tag{1.1}
$$

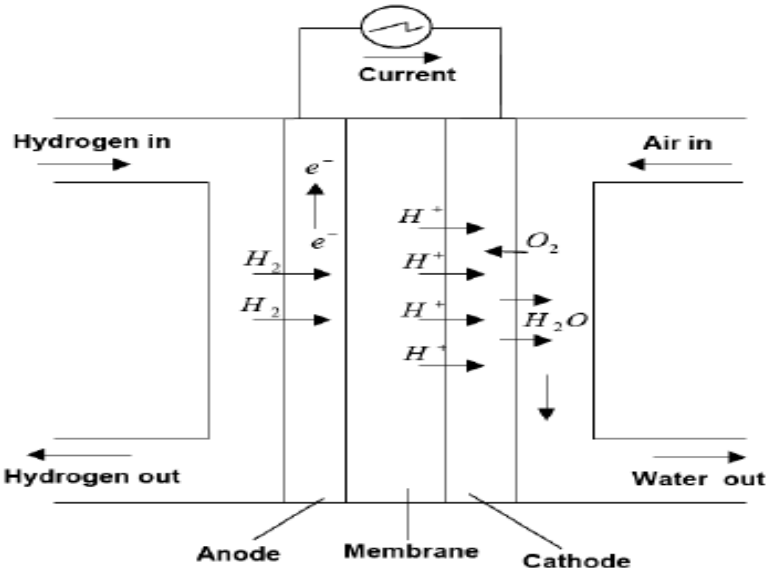

Figure 1.4 Fuel Cell basic working

Figure (1.4) shows a schematic representation of a single fuel cell with reactant gases (H_2/O_2) and the direction of ion flow through the cell. generally many fuel cells are connected electrically in series configuration to form a stack which provides a fairly large energy at higher voltage. A single fuel cell produces an open-circuit voltage about at 0.7-1.23V.

1.4 Fuel Cell Systems Types

The electrolyte must be an electronic dielectric and an ionic conductor. It can be either liquid or solid. The bipolar plates allow the access of gases to the reaction sites by the presence of channels[10].

The fuel cell is classified according to the nature of used electrolyte, electrode materials and their temperature of operation. There are six main fuel cell types, the table (1.1) summarizes the different types of fuel cells and their characteristics.

Table 1. 1 Different types of fuel cells

Fuel Cell types	Electrolyte	Temperature	fuel	oxidant
Alkaline fuel cells (AFC)	KOH solution	23^0C to 70^0C	H_2 pur	Air or O_2 pur
Solid Oxide fuel cell(SOFC)	ceramic	500 to 1000 °C	H_2,CH_4,CH_3OH, CO	Air
Direct Methanol fuel cell(DMFC)	proton exchange membrane	50–120 °C	CH_3OH	Air or O_2 pur
Phosphoric Acid fuel cell (PAFC)	phosphoric acid	150 to 200 °C	H_2,CH_4,CH_3OH	Air
Molten Carbonate fuel cell(MCFC)	a molten carbonate-salt-impregnated ceramic	600-700 °C	H_2,CH_4	Air
Proton Exchange Membrane fuel cell(PEMFC)	proton exchange membrane	50 to 100 °C	H_2 pur	Air or O_2 pur

Every fuel cell type has disadvantage that reduces its effectiveness, whether that was the efficiency is as low as DMFC cell around 10%[11], so they are aimed especially to portable applications, or in terms of its limited applications, such as a AFC cell which used only in the space sector.

For the SOFC and MCFC cells, they face a huge challenge because of its short lifetime due to increase operating temperature which causes the degradation of electrolyte materials . In addition, the need for a relatively long start time (ten minutes for SOFC cell starting cold). Nevertheless, it does not prevent its use in the production of electrical energy[12].

This study focus on the Proton Exchange Membrane Fuel Cells (PEMFC 500w) which considered the most suitable as energy source for portable applications like small robots , transportation applications (vehicles)and stationary application (residential homes), because of

their appropriate characteristics such as high power density, high efficiency , lighter weight, smaller size, low operation temperature, fast power response and environmental friendliness[13].

1.5 The Proton-Exchange Membrane Fuel Cells (PEMFC)

Proton-exchange membrane fuel cells (PEMFC), also known as polymer electrolyte membrane (PEM) fuel cells, they are the most promising energy system used for transportation applications like electric vehicles[14] as well as for stationary fuel-cell applications and portable.

Recently, this technology experienced tremendous progress in material industry with the discovery of new Nafion-type membranes b by DuPont's Walther Grot, this eventually increase the power density and make the device more efficient and reliable. The distinguishing features of these cells include the efficiency is about to 50% , the temperature operation (80 °C) and its density of power is up to 350–600 mW/cm^2 [15].

1.5.1 Structure of Proton Exchange Membrane Fuel Cell

In general, a proton exchange membrane fuel cell stack composed of cells which are connected electrically in series configuration to form a stack as shown in figure (1.5). Each elementary cell is consisted of the membrane electrode assembly (MEA), catalyst layer and membrane between the electrodes. The figure (1.6) presents the internal structure of single proton exchange membrane cell.

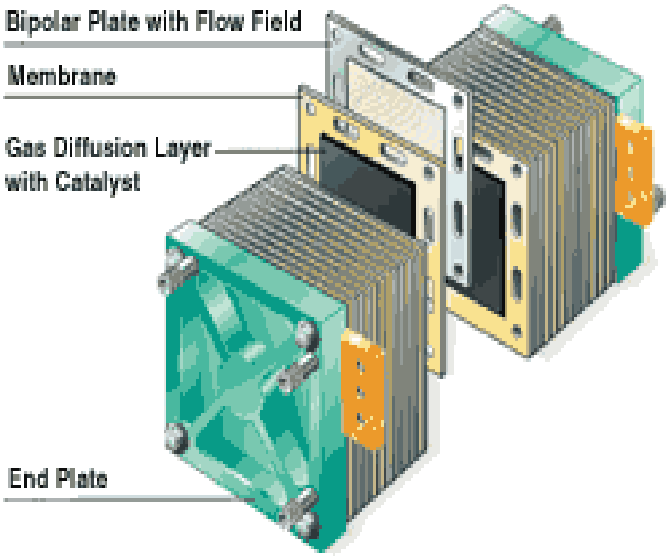

Figure 1.5 Structure of PEM fuel cell stack

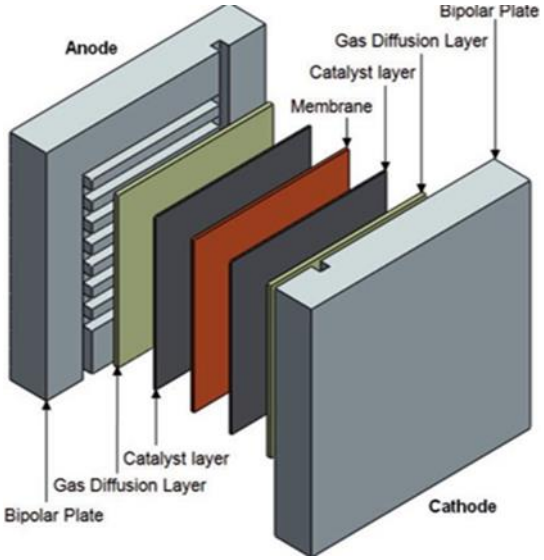

Figure 1. 6 single- fuel cell[16]

1.5.1.1 Bipolar Plates

Also named collectors, separators or supports on both sides of electrodes, and they have many functions in a fuel cell system, the most important are the following:

- Collect the electrons (the current) through electrical connection between individual cells of the stack
- Must be impermeable to hydrogen and oxygen gases among adjacent cells inside PEMFC systems
- Must be characterized by the robustness and light weight to structural support to the cell.
- Manage flows of the water and conduct the heat efficiently.
- Must be conductive as well as allow homogeneous diffusion of gases towards to electrodes.

Usually, these plates are made of non-metallic material such as graphite which is considered the most corrosion resistant material due to the pH of PEM cells is between 2 and 3 (acid environment), and the temperature in the range of 60–80 °C [4]. Figure (7.1) shows the structure of bipolar plates.

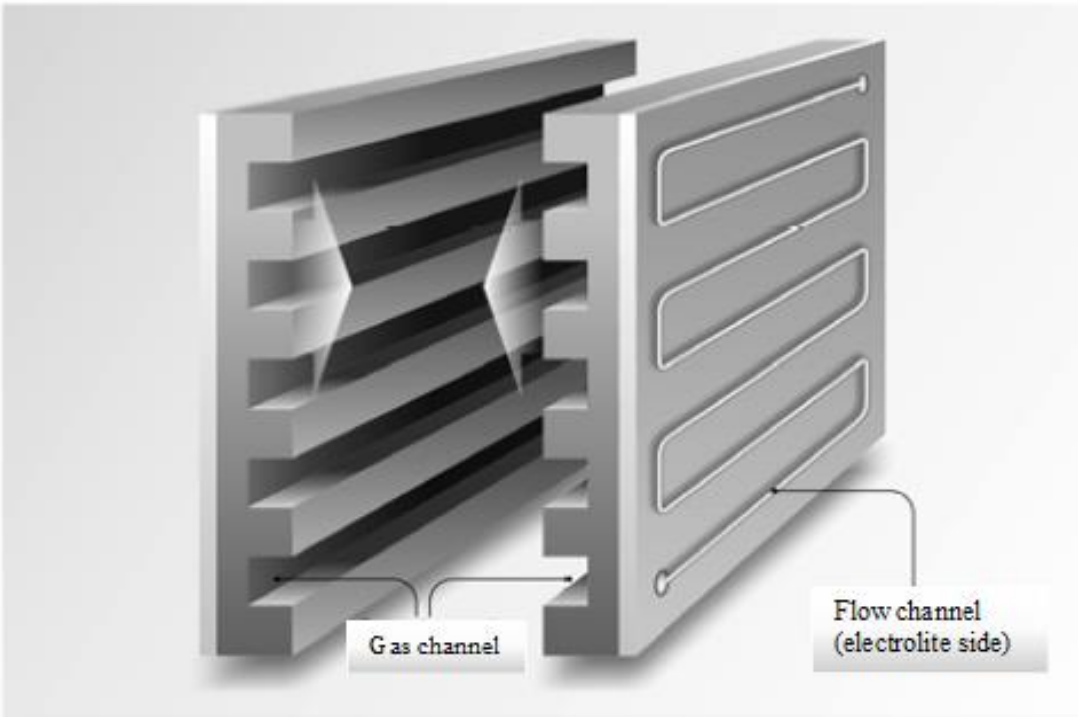

Figure 1. 7 Bipolar plates structure[17]

1.5.1.2 The Electrodes

The electrodes are the sites of redox reactions in order to synthesis the water and producing the electricity from hydrogen and oxygen gases with the presence of the platinum catalyst (solid catalyst). Where the oxidation reaction takes place in anode channel, while the reduction reaction takes place in the cathode side as mention in equation (1.1).

Typically these sites are considered triple contact for each of gases, electrolyte and catalyst. To promote the creation this contact, the electrodes must have the following characteristics:

- Be porous to transition protons from the catalytic sites of hydrogen oxidation to oxygen reduction sites with the presence of ionic polymer. It is usually made of carbon paper or carbon felt.
- Be impregnated with a paste consisted of catalyst containing platinum carbon, on contact surface with the electrolyte. In which the part of the electrode impregnated with paste constitutes the active zone. The non-impregnated part constitutes the diffusion zone[18].

1.5.1.3 The Catalyst

The catalyst is a metal material used to catalyze (accelerate) the electrochemical reactions which occur in the electrodes. Usually, the most used metal is pure platinum Pt (noble metal) or alloyed with the elements Nickel (Ni), Cobalt (Co), Iron (Fe). It is also a resistant material to corrosion in this acidic chemical environment. This catalyst works to break the molecular bond of the atomic gaseous reactants which occur when hydrogen oxidation at the anode channel and oxygen reduction at the cathode side. The functions of catalyst include electron conduction, proton transport and mass transport of the reactants. Each task is necessary for a reaction to occur on the catalyst surface. Therefore, the use of catalyst must determined by the satisfaction of three criteria: proton access, gas access and electronic path continuity[19].

1.5.1.4 The Electrolyte

The electrolyte is a polymer membrane inserted between the electrodes to allow the hydrogen ions (H^+) which were formed due to the oxidation of hydrogen at the anode to transit to the cathode side. Whereas the electrons (e^-) are converted to an external circuit to create a current. Where they recombine with the positively charged ions and an oxidant to form the water at the cathode[20].

Typically, each cell distinguished by the type of electrolyte material used in charge transport. However, the most important characteristics of the electrolyte are:

- Have high proton conductivity.
- Have low permeability of gases reactants.
- Good thermal stability and high durability.
- It should be low cost.

The electrolyte of the proton exchange membranes fuel cell PEMFC is a solid membrane with thickness of a hundred micrometers($100\mu m$) figure(1.8) it is made from Nafion material (sulfonated tetrafluoroethylene) which is developed by DuPont company in 1960s[21]. Currently, Nafion and its derivatives considered as standard materials for polymeric electrolyte fuel cells figure (1.9).

Figure 1.8 Membranes fuel cell

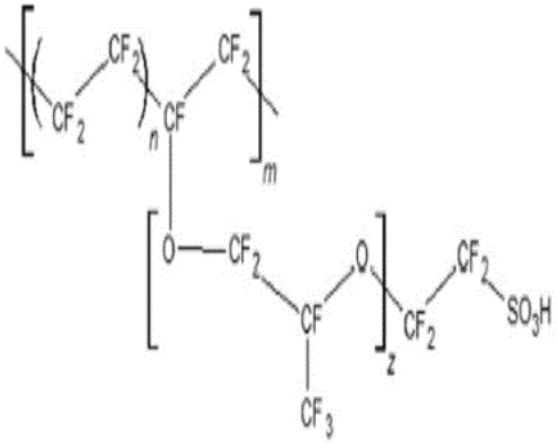

Figure 1. 9 Nafion molecular structure[22]

These basic components (bipolar plates, electrodes, the catalyst, and electrolyte) make up the core of the PEM fuel cell. For proper functioning of this device, the necessary auxiliaries be add such as air compressor , the fuel tanks ,pumps for fuel and water, heat exchangers to cool the fuel cell , DC converter.

1.6 Auxiliary Devices

The fuel cell system consists of six fundamental subsystems:

- The stack presented previously
- The hydrogen supply, consists of a hydrogen tank connected with a reducer of pressure
- The air supply which consists of compressor coupled to a turbine
- The humidifier, to keep gas and membrane hydration
- The cooling circuit, to extract the heat produced by electrochemical reaction
- DC/DC converter

The design of each subsystem of the overall fuel cell system is a fundamental task in achieving efficient fuel cell systems. The pressures and flow rates of both the fuel and the oxidizer must be adjusted. In addition, the gases must be humidified and the system temperature controlled. The figure (1.10) shows the basic components of a fuel cell system.

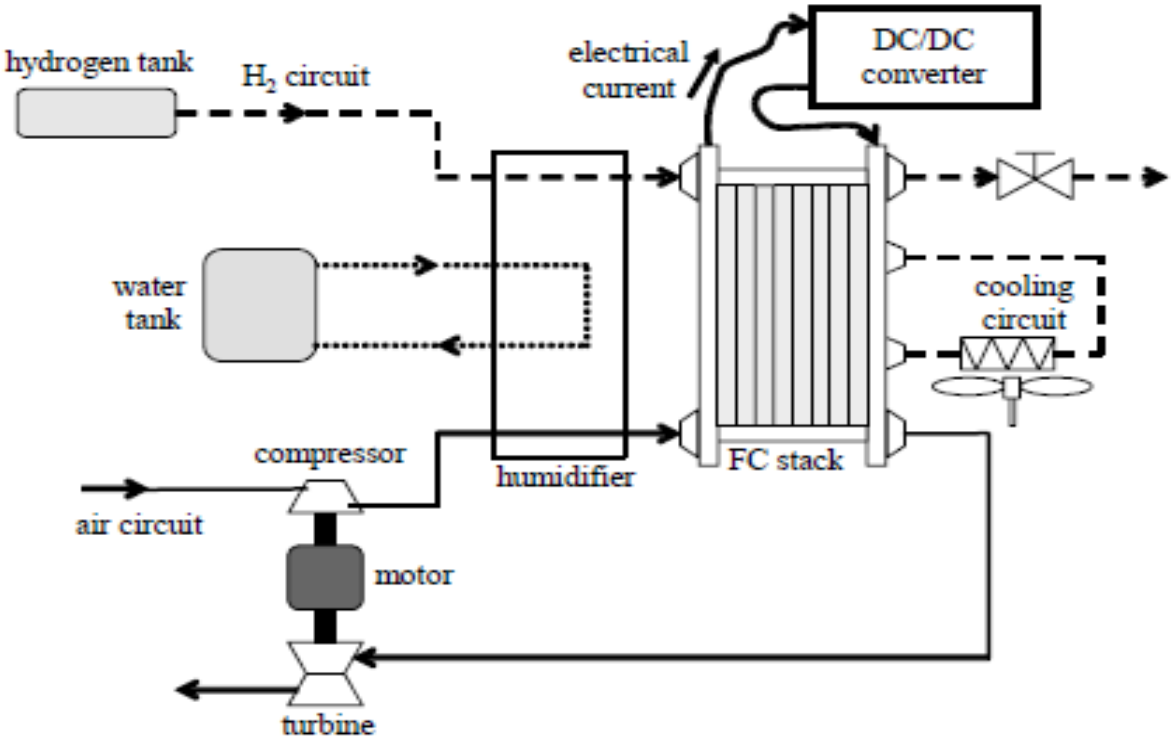

Figure 1. 10 Different components of a fuel cell system[23]

1.6.1 Hydrogen and Air Supplies

The anode side of the PEMFC is supplied by pure hydrogen, which does not exist in the original state in the nature because it is always associated with other elements. Pure hydrogen is usually produced widely in four different ways: thermochemical technology, photo-biological technology, photochemical technology and electrolysis technology[24]. Generally the hydrogen pressure is not a big problem since the gas is stored in tanks at several hundred bar (300 up to 700 bar).

On the other hand, the air supplied to the cathode comes from the atmosphere. Where its injection depends on the area of use and the power of PEM device. The low-power PEM are supplied directly by atmospheric. While, the high power PEM fuel cells use a compressor system for air injecting at high speed. This compressor consumes some delivered power by PEM fuel cell. therefore the net power that reach the customer will be the result of the total produced power

subtracting the power consumed by the compressor and the other electronic components[25]. To ensure proper performance of a PEM, it is necessary to reach a sufficient and suitable level of pressure and air flow to increase the efficiency and the power of the cell [24].

1.6.2 The Humidifier

In a fuel cell system, the humidifier is a circuit used to minimize the temperature of the incoming gases and stack cells to avoid drying out the membrane, that through injecting water into the air stream or hydrogen (humidify of gases). This is important for ensuring good ionic conductivity of the membrane by ensuring the hydration of the AME, thus reducing potential losses. the water of humidifier it can be obtained from exhaust gases produced by electrochemical reactions in fuel cell, usually the impact of the humidification of hydrogen on the performance of the cell is comparatively smaller than that of the humidification of the air[12].

The Humidification circuit often composed of an evapor-condenser (with walls or membrane), one or three separators to recover liquid water, a tank and a pump[26].

1.6.3 The Cooling Circuit

Typically a PEM fuel cell stack produces almost as much thermal energy as electrical energy. As a result of inside electrochemical reactions and power generation of this cell[27], therefore, it is important to cool down the thermal path of PEMFC by using operational cooling system in order to keep the operating temperature of fuel cell stack's at its optimal, in the temperature range from 60 to 80°C. This system provides coolant material usually consisting of water, Glycol and Corrosion inhibitor.

Generally the system of cooling includes:

- A pump with a flow control device
- A radiator
- A parallel by-pass of the cell fuel (valve controlled)
- A parallel by-pass of the radiator (valve controlled)

1.6.4 DC/DC Converter

The output voltage delivered by the PEM fuel cell is irregular due to the small voltage of each individual cell is heavily influenced by changes in electric current, partial pressure of gases , level of reactants humidity , gas speed, temperature and membrane water content. Therefore, it is necessary to use a DC/DC converter to adapt load requirements as interface or an electronic conditioning system between the PEM fuel cell and the electricity bus.in general, this converter is connected with a supervisory electronic control to ensure proper management of batteries or super-capacitors charge/discharge cycles[4].

1.7 Efficiency of PEM fuel cell System

The standard method to calculate the efficiency of any electrical generation device is the ratio between output energy and input energy. In the case of the PEM fuel cell, the input energy is the hydrogen enthalpy which can be converted to work, while the output energy is measured by the Gibbs free energy which is converted to electric energy, hence the efficiency represented by[28]:

$$\text{Efficiency} = \frac{\text{Electricity produced}}{\text{feul cell enthalpy}}$$

theoretically the maximum limit the electrical efficiency of the PEM fuel cell system with the value of heat combustion of hydrogen (energy) 285.8 KJ/mole at 25 C^0 (298K) and the value of the Gibbs free energy of output 237.2KJ/mole is represented by:

$$\eta_{\max} = \frac{-\Delta G}{-\Delta H} = \frac{237.2}{285.8} = 0.83$$

When the hydrogen enthalpy is converted to electric energy by $\Delta H/2F$ and the Gibbs free energy is converted to voltage by $\Delta G/2F$, the voltage efficiency of the fuel cell stack can be given by:

$$\eta_{max} = \frac{-\Delta G}{-\Delta H} = \frac{\Delta G/2.F}{\Delta H/2.F} = \frac{1.229}{1.481} = 0.83$$

In practice, the fuel cells cannot achieve this maximum value of electrical efficiency due to existence of the resistance losses inside them. Considering that, the maximum energy production

from the fuel cell is capable of producing only 154 KJ of electricity per mole of hydrogen consumed, the value of electrical efficiency is 0.53[28]. As for rest of energy producing is formed as generated heat inside the system.

1.8 Fuel cells applications

The field of fuel cell applications is very wide due to the diversity of the characteristics of each type of fuel cell. It can replace a traditional energy generator or the current energy storage element such as batteries, in addition, the power production of each these fuel cells can range from a few watts up to several megawatts, for these reasons we can mainly distinguish three types of applications:

- Transport applications
- Portable applications
- Stationary applications

1.8.1 Transport Applications

In the recent decades, researches have increased in fuel cells for transportation applications due to the augmentation interest of the vehicle manufacturers in order to solve the increasing problems of oil prices and degradation of climate, these applications involve buses, automobiles, utility vehicles, and bicycles. The most widely used types of fuel cell in these applications are PEMFC, DMFC and AFC, the puissance of each cell can vary from a few kilowatts to several hundred kilowatts according to characteristics and the energy production rate of each cell. Figure (1.11) presents an example of fuel cell automobile.

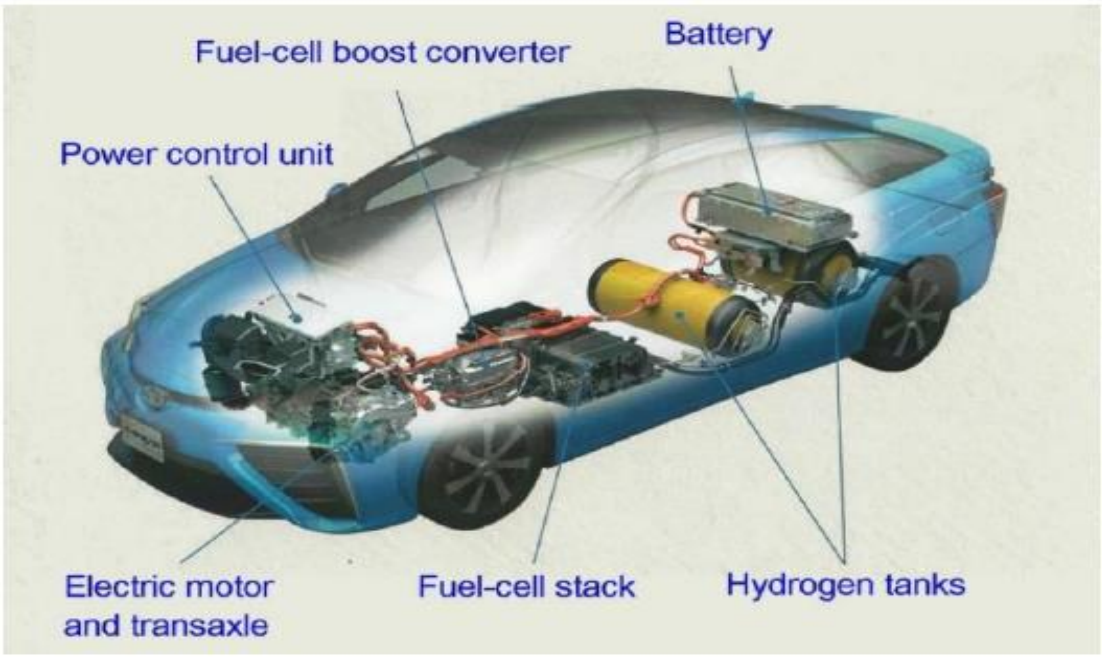

Figure 1.11 Fuel cell electric automobile[29]

1.8.2 Portable Applications

This type of applications are designed to provide energy to portable devices such as phone, laptop, camera, camping or military gear, telecommunications installations , by integrate them into these devices in order to facilitate the process of carrying and moving them. These cells are characterized by lightweight, long-lasting, in addition they prolong the time amount a device can be used without recharging. Unlike secondary batteries are require recharge from other batteries . The most commonly used types in this application are PEMFCs and DMFCs. because these two cells are characterized by their low temperature of operation (between 60 °C and 80 °C), which reduces thermal management problems. However, their size minimization remains a great challenge from an architectural point of view.

1.8.3 Stationary Applications

This type of applications is considered the most versatile and used among all applications due to several reasons, including:

- Their ability to use various types of fuel cells which leads to inclusion of wide spectrum of power from few kW to several MW.

- It is considered as cogeneration or combined heat and power (CHP) to provide electrical and heat energy to a house or small business.
- It is considered as emergency power systems to provide backup resources in a crisis or when regular systems fail. It's used in residential homes, hospitals, scientific laboratories, data centers, and telecommunication. The type of fuel cell used in these applications is PEMFC
- It is used in the electric grid (distributed generation) to provide an electricity as supplemental power device or as backup power , the most commonly used types in this application are PEMFC, PAFC,MCFC and SOFC, figure (1.12) shows PAFC type the first to enter the commercial market for stationary application[30].
- It is used to supply electrical energy to places where an electric network is not available as independent power system for isolated areas and military bases, in this application the fuel cell type used is AFC. in addition, this type of application, it meet the needs of several types of possible customers (individuals, businesses, public services, military) with different objectives, specifications and budgets[29].

Figure 1.12 200 kW PAFC on-site plant[30]

1.9 Advantages and Disadvantages of Fuel Cells

- **Advantages**

In general, fuel cells are characterized by the following advantages:

- High energy efficiency: the energy efficiency depends on the type of the cell, its size and its uses, usually ranging between 40% and 70% without taking into account the overall system with the auxiliaries (pumps, exchanger, reformer, humidifier and converter) which lower these percentages. In transportation applications, the PEM cell efficiency is between 38% and 50%. While in the stationary applications the overall energy efficiency is much higher, ranging between 85% to 90% due to the existence of thermal energy beside electrical energy, which increases the efficiency value.
- Different operating temperatures: the fuel cells have a wide range of operating temperatures depending on their types. This makes it possible to cover many fields of application. For example, low temperature cells are used for mobile or portable applications that do not need the produced heat. In contrast, in stationary applications, the high temperature fuel cells are more suitable for domestic applications where the heat generated is used for hot water and heating. They are also suitable for industrial applications where the produced heat is exploited for coupling with a turbine.
- Low emissions of gaseous: fuel cells that run on pure hydrogen produce nothing (zero emissions), while those that run on methanol or ethanol produce low amounts of CO2, CH4 and CO.
- Low noise emissions: the fuel cells are silent during operation. Only certain components such as compressors, pumps and the ventilation system produce a slight noise. This advantage is suitable to integrate it in an urban environment.
- Modular construction: the fuel cells have modular construction according to the power demand, through adapting the number of cells and the surface area of each them to obtain all the possible energies.
- The absence of rotating parts: there is no rotating parts in a fuel cells and no movement therefore no mechanical corrosion to the core of the cells. This gives it an advantage for its lifetime

from a mechanical point of view. However, the lifetime is limited by other factors related to the chemical resistance of the internal components.

- **Disadvantages**

Despite the great interest caused by the fuel cells recently, however it is still far from a real penetration in the market. Its current situation requires further researches and developments before it can be commercialized .Hence, the some problems which hinder in the development of fuel cells are:

- High cost: the use of noble metals such as platinum at the electrodes and the cost of manufacturing the membrane and the bipolar plates leads to a high cost of manufacture.
- The weight and the volume: they are considered the main constraints for the applications of transport due to existence the auxiliaries that increase the weight and the volume of fuel cell system which effects on performance of the vehicle.
- The short life: the fuel cell undergoes a decrease in voltage and efficiency because the degradation of the different parts of the system over time, starting from the electrodes to the membrane via the catalyst.
- Production and storage of the fuel: the pure hydrogen gas is not widely available in the nature, therefore its production considered the biggest issue remains unsolved for fuel cell application. However, it can be obtained from many sources such as water electrolysis, solar and wind power, reformation of methanol, gasoline and natural gas, but these sources still expensive. Furthermore, the hydrogen storage and construction of the refueling infrastructure increases the overall cost[15].

1.10 Conclusion

This chapter covered various points concerned on the fuel cells such as historical reminders of the development of fuel cells, its operating principle, its types, its applications. And focused mainly on proton-exchange membrane fuel cells (PEMFC) and their structure. Finally, the advantages and disadvantages of fuel cells and its performance have been mentioned.

The fuel cells at a phase of pre-industrialization have been subjugated to many experiments in different fields with the development of multiple tests in real operating situation .In this context many laboratories and industrial companies are interested in fuel cells. In addition to integration into systems that require the development of simple and efficient assistants, the main work is still necessary at the cell level. However, all the elements of an elementary cell can still be improved. Whether it is the catalyst (improvement of the existing one and research of new catalysts), the membrane (functioning membrane at higher temperatures) or the cell structure itself (geometric shape, material of the bipolar plates, cooling modes).

Chapter 2

Nonlinear modeling of Proton exchange membrane fuel cell PEMFC 500W

2.1 Introduction

The description and understanding of the internal physical phenomena of PEM fuel cell systems are considered to be one of the obstacles preventing the progress of this technology. In this context, mathematical modeling occupies an important place in their development, due to its ease to express the physical phenomena involved in the fuel cell through algebraic or differential equations. These equations are considered powerful tool for designing, simulation, analysis of temporal and spatial behavior of the PEM fuel cell system and synthesis the appropriate controller.

The last decade has recognized the development of a significant number of FC models. These proposed models vary in terms of their level of complexity, validation domain, the scales of time and dimensions on which the studied phenomena take place and area to be modeled of the system (part or all of a cell, the entire stack, the stack with auxiliary systems)[31].

It has become essential to define the objectives beforehand for the future use of the model. Which leads to establishing criteria for using the model such as speed, precision, flexibility, graphical interface and implementation in software. From these usage criteria, it is necessary to determine model design criteria (theoretical or semi-empirical approach, dynamic or static model, mono, two or three-dimensional model, black box…etc.)[12][32].

The main goal of this study is modeling a fuel cell energy system for transport application. This motivates us to calculate the evolution of voltage and current using static and dynamic approaches resulting from the work presented by[31] [33].

2.2 Proton Exchange Membrane Fuel Cell Stack Nonlinear Modeling

The main measurements to evaluate the PEM fuel cell performances is the (V–I) polarization curve, which is a plot of cell output voltage versus density of the current. This V–I curve is the most common way to compare and describe the efficiency of fuel cells to other released data. The polarization curve explains the nonlinear relation of the voltage/current to operational conditions such as hydrogen and oxygen pressures, mole flow rates of gases, temperature and humidity. This relation could be represented through mathematical modeling equations that

would explain the internal phenomena occurring in the fuel cell in order to facilitate the design process, analysis, simulation and control.

Generally, there are two types of fuel cell models that have been considered in the literature: static and dynamic models. The first one focuses on simulation of the fuel cell V-I polarization curve while the second pays more attention to electrical and partial pressures models. In the next sections the static and dynamic models are studied in details to obtain the voltage/current outputs. The following assumptions, commonly made in the literature, are also used to simplify the simulation and analysis[32][34]:

- The treatment of flow and diffusion of gases is done in one dimensional of PEM fuel cell.
- Constant partial pressures in the fuel cell gas flow electrodes.
- The gases distribution is uniform and ideal.
- The individual cells parameters can be gathered to shape a PEM fuel cell stack.
- PEM fuel cell works under 100°C and the product of reaction is in liquid phase.
- The fuel is humidified hydrogen and the oxidant is humidified air.
- On the anode channel, the effective water vapor pressure is 50%, while on the cathode channel the saturated vapor pressure up to 100% .
- Thermodynamic properties are evaluated at the average stack temperature, taking into account the variations of temperature across the stack.
- The overall specific heat capacity is taken into account in the stack.

2.2.1 Static modeling

The main part of this modeling is the reversible cell potential that obtained by a thermodynamic balance of open circuit. This potential is generated by the flow of electrons from anode channel to cathode side by an external circuit. The reversible cell potential can be expressed by Nernst equation E_{Nernst} as following [31][33]:

$$E_{Nernst} = \mathrm{E_{cell}} = E_0^{Cell} + \frac{RT}{2F}\ ln\left(\frac{P_{H_2}\sqrt{P_{O_2}}}{P_{H2O}}\right) \quad (2.1)$$

The individual open-circuit output voltage of one cell is approximately 1.23V at standard conditions of pressure and temperature. Accordingly that, the open-circuit output voltage of all the PEM fuel cell stack can be represented by:

$$V_{O.FC} = n_s \cdot E_0^{Cell} + \frac{n_s R.T}{2F} \; ln\left(\frac{P_{H_2}\sqrt{P_{O_2}}}{P_{H2O}}\right) \quad (2.2)$$

n_s : is number of cells

The actual voltage of the PEM fuel cell is less than the one calculated with Nernst's equation when the operation of a fuel cell, caused many voltage losses: activation voltage loss, ohmic voltage loss, and concentration voltage loss [35] . Figure (2.1) shows the V-I characteristics of the output voltage with losses which are represented by three evolution regions:

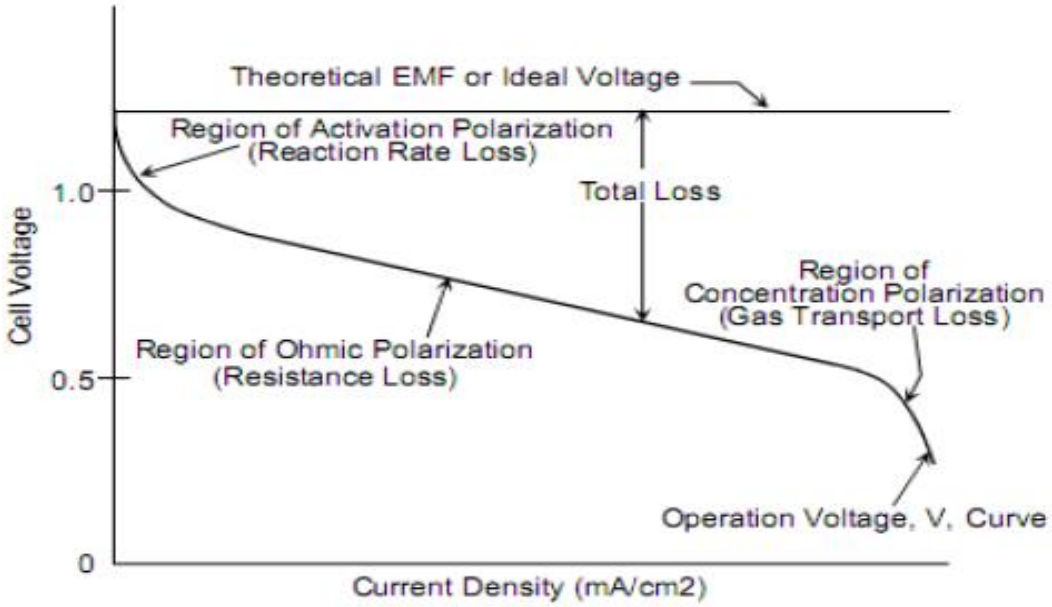

Figure 2.1 Polarization curve of PEMFC

2.2.1.1 Activation Voltage Loss

The activation loss is caused by the speed of the electrochemical reaction at the electrodes surface. This loss is considered as an extra voltage necessary to start electrochemical reactions

inside PEM fuel cell and to proceed at demanded rate similar to the necessary spark to start an internal combustion engine. The activation loss can be expressed by Tafel equation which shows a logarithmic relationship with the current density as following [33]:

$$V_{act} = \frac{RT}{2F} \ln\left(\frac{I}{I_d}\right) = a_0 + a.T + T.b.\ln(I) = V_{act1} + V_{act2} \quad (2.3)$$

Where I_d denotes exchange current density

$V_{act1} = (a_0 + a.T)$ represents the voltage loss of the temperature

$V_{act2} = [T.b.\ln(I)]$ represents the activation voltage loss.

2.2.1.2 Ohmic Voltage Loss

Ohmic loss exist due to charges transport (electrons e^-, ions H^+) from the electrode channels where they are generated to the load where they are consumed inside PEM fuel cell. The electronic charge losses are due to the degree of contact that the plates make with each other at electrodes sides[36] , while the ionic losses are due to travel the ions from anode to cathode channel through electrolyte layer in the membrane of PEM fuel cell [32]. Its expression can be given by:

$$V_O = I.R_O = V_O^A + V_O^C + V_O^M \quad (2.4)$$

The resistance of electrodes depends on the current and temperature of the stack, hence we can calculate the ohmic resistance of the PEM fuel cell by[33]:

$$R_O = R_O^c + K_I.I + K_T.T \quad (2.5)$$

2.2.1.3 Concentration Voltage Loss

The concentration voltage loss is formed due to the limitation of protons diffusion (or mass transport) through the membrane. This limitation caused by slowing the electrochemical reactions rates within the catalyst layers at cathode side than those on the anode side. This resultant slowness in turn, is caused by many factors such as the weak diffusion of the gas through the porous electrodes, concentration gradient of reactants, diffusion the reactants or

products from the reaction site to the electrolyte or vice versa. The loss of concentration is given by the following equation [31][34]:

$$V_{conc} = -\frac{RT}{eF} \ln\left(1 - \frac{C_0}{C_i}\right) \quad (2.6)$$

Where C_0 is the concentration of surface at the reaction sites, C_i is the biggest concentration in gas channels, and e is the electrons number. According to the first law of Fick and the law of Faraday [10][34], Equation (2.6) can be expressed as a function of current :

$$V_{conc} = -\frac{RT}{eF} \ln\left(1 - \frac{I}{I_L}\right) \quad (2.7)$$

I_L the current limit of PEM fuel cell (A)

Therefore, the equivalent resistance for the concentration loss can be given by following [32][33]:

$$R_{conc} = \frac{V_{conc}}{I} = -\frac{RT}{eF.I} \ln\left(1 - \frac{I}{I_L}\right) \quad (2.8)$$

Hence, the actual output voltage of the PEM fuel cell can be concluded through subtraction the voltage losses from the open-circuit output voltage of the PEMFC as:

$$V_{fc} = V_{O.FC} - n_s.(V_{act} + V_O + V_{conc}) \quad (2.9)$$

2.2.2 Dynamic Modeling

In this part, the performance of dynamic model of a PEM fuel cell is discussed through focusing on electrical approach and partial pressures dynamic equations of fuel/oxidant gases. These dynamics are represented by non-linear differential equations of the PEMFC system which are formed as state-space representation[31] . This representation displays many advantages such as control studies, identification and optimization of data. Besides it provides a robust tool for simulation and estimation of parameters.

As mentioned earlier, the structure of fuel cell stack system is built by accumulating together multiple single cell. Consequently, the fuel cell stack is an electrically connected serially by these cells, which encourages us to focus on a single cell modeling instead of entire fuel cell stack because in a serial connection, the single cell voltage is added up.

According to these hypothesis, firstly, the PEMFC modeling process is presented by identifying nonlinear equations of both partial pressures and flow rates of hydrogen, oxygen and the water, then, the equation temperature of the PEM fuel cell stack is defined. After, the electrical equation is derived by determination the relation between voltage and current. Finally, the overall nonlinear state space of PEM fuel cell is modeled.

2.2.2.1 Net Mole Flow Rate Equations of Gases

The flow of oxygen and hydrogen in the PEM fuel cell cannot pursue changes in the load instantly, there is a time lag between the change in the load current, and mol flow both of fuel (H_2) and oxidant (O_2). So, the net mole flow rate of these gases can be calculated by the difference between the mole flow gases coming inside the fuel cell electrodes and mole flow of gases going outside. For hydrogen gas the net mole flow rate is given by the following equation [32][33]:

$$\frac{d\left(M_{H_2}\right)_{net}}{dt} = \frac{I_s}{2.\lambda_A.F} - \frac{\left(M_{H_2}\right)_{net}}{\lambda_A} \tag{2.10}$$

Let: $x_1 = \left(M_{H_2}\right)_{net}$

So:

$$\dot{x}_1 = \frac{d\left(M_{H_2}\right)_{net}}{dt} = \left(\frac{I_s}{2.\lambda_A.F}\right) - \left(\frac{1}{\lambda_A}\right)x_1 \tag{2.11}$$

The same way for the net mole flow rate of oxygen, it can be calculated by the difference between the mole flow oxygen coming inside and mole flow of oxygen going outside of the fuel cell cathode such as [32][33]:

$$\frac{d(M_{O_2})_{net}}{dt} = \frac{I_s}{4.\ \lambda_C.F} - \frac{(M_{O_2})_{net}}{\lambda_C} \quad (2.12)$$

Let: $x_2 = (M_{O_2})_{net}$

So:

$$\dot{x}_2 = \frac{d(M_{O_2})_{net}}{dt} = \left(\frac{I_s}{4.\lambda_C.F}\right) - \left(\frac{1}{\lambda_C}\right)x_2 \quad (2.13)$$

The net mole flow rate of water can be provided by subtracting the rate of net flow water vapor across the cell from the rate of water production in the cell. It can be represented by the following equation [33]:

$$\frac{d(M_{H_2O})_{net}}{dt} = \frac{I_s}{2.\lambda_C.F} - \frac{(M_{H_2O})_{net}}{\lambda_C} \quad (2.14)$$

Let $x_3 = (M_{H_2O})_{net}$

So:

$$\dot{x}_3 = \frac{d(M_{H_2O})_{net}}{dt} = \left(\frac{I_s}{2.\lambda_C.F}\right) - \left(\frac{1}{\lambda_C}\right)x_3 \quad (2.15)$$

2.2.2.2 Equations of Pressure Gases

The expressions of hydrogen, oxygen and water pressures at electrodes channels and its effective values at sites of actual reaction are derived in terms of the fuel-cell-operating parameters as pressures of electrodes, gases mole flow rates and temperature of fuel cell. These partial pressures are used to calculate the output voltage of the fuel cell. The equations of the effective partial pressures of hydrogen, oxygen and water in the electrodes channels can be calculated through the ideal gas equation $P.V = n.R.T$ as[37]:

- **For hydrogen**:

$$\frac{dP_{H_2}}{dt} = \left(\frac{RT}{V_a}\right).(M_{H_2})_{in} - \left(\frac{RT}{V_a}\right).(M_{H_2})_{out} - \left(\frac{RT}{V_a}\right).\frac{I_s}{2F} \quad (2.16)$$

Where $(M_{H_2})_{in}$ and $(M_{H_2})_{out}$ are input and output hydrogen mole flow rate at anode respectively, they can be expressed by following equations[32][37]:

$$(M_{H_2})_{in} = \frac{(M_{H_2O})_{in}^{a}}{(P_{H_2O})_{in}^{a}} . u_{P_A} \quad (2.17)$$

$$(M_{H_2})_{out} = (M_{H_2})_{in} . \frac{(2.P_{H_2} - u_{P_A})}{u_{P_A}} \quad (2.18)$$

By replacing equations (2.17) and (2.18) into equation (2.16) and solving moreover to get [33]:

$$\frac{dP_{H_2}}{dt} = \left(\frac{RT}{V_a}\right) . \frac{(M_{H_2O})_{in}^{a}}{(P_{H_2O})_{in}^{a}} . u_{P_A} - \left(\frac{RT}{V_a}\right) . (M_{H_2})_{in} . \frac{(2.P_{H_2} - u_{P_A})}{u_{P_A}} - \left(\frac{RT}{V_a}\right) . \frac{I_s}{2F} \quad (2.19)$$

By taking:

$x_4 = T$,$x_5 = P_{H_2}$, $\alpha = (M_{H_2O})_{in}^{a}$ And $\beta = (P_{H_2O})_{in}^{a}$

And compensate them in the equation (2.19), to get:

$$\dot{x_5} = \frac{dP_{H_2}}{dt} = \frac{2.\alpha.R.x_4}{\beta.V_a}[u_{P_A} - x_5] - \frac{R.x_4}{2.V_a.F} . I_s \quad (2.20)$$

- **For Oxygen:**

In the same manner, the dynamic equation of the partial pressure of oxygen at cathode can be expressed by:

$$\frac{dP_{O_2}}{dt} = \left(\frac{RT}{V_c}\right) . (M_{O_2})_{in} - \left(\frac{RT}{V_c}\right) . (M_{O_2})_{out} - \left(\frac{RT}{V_c}\right) . \frac{I_s}{4.F} \quad (2.21)$$

$(M_{O_2})_{in}$ and $(M_{O_2})_{out}$ are input and output hydrogen mole flow rate of anode respectively, they can be expressed by following equations:

$$(M_{O_2})_{in} = \frac{(M_{H_2O})_{in}^{c}}{(P_{H_2O})_{in}^{c}} . u_{P_C} \quad (2.22)$$

$$M_{out} = (M_{O_2})_{in} . \frac{(2.P_{O_2} - u_{P_C})}{u_{P_C}} \quad (2.23)$$

By replacing equations (2.22) and (2.23) into equation (2.21) and solving moreover, to obtain:

$$\frac{dP_{O_2}}{dt} = \left(\frac{RT}{V_c}\right).\frac{(M_{H_2O})^c_{in}}{(P_{H_2O})^c_{in}}.u_{P_C} - \left(\frac{RT}{V_c}\right).\left(M_{O_2}\right)_{in}.\frac{(2.P_{O_2} - u_{P_C})}{u_{P_C}} - \left(\frac{RT}{V_c}\right).\frac{I_s}{4.F} \quad (2.24)$$

By taking:

$$x_6 = P_{O_2} \quad , \quad (M_{H_2O})^c_{in} = \alpha \text{ And } (P_{H_2O})^c_{in} = \beta$$

And compensate them in the equation (2.24), to get:

$$\dot{x_6} = \frac{dP_{O_2}}{dt} = \frac{2.\alpha.R.x_4}{\beta.V_c}\left[u_{P_C} - x_6\right] - \frac{R.x_4}{4.V_C.F}.I_s \quad (2.25)$$

- **For Water:**

The change rate equation of the partial pressure of water at cathode can be written as[32][33] [37]:

$$\dot{x_7} = \frac{dP_{H_2O}}{dt} = 2.\left[\frac{R.(M_{H_2O})^c_{in}.(P^{in}_{H_2O})}{V_c.(P_{H_2O})^c_{in}}\right].x_4 - 2.\left[\frac{R.(M_{H_2O})^c_{in}.P_{H_2O}}{V_c.(P_{H_2O})^c_{in}}\right].x_4 + \left[\frac{R.x_4}{2.V_c.F}\right].I_s \quad (2.26)$$

By taking:

$$x_7 = P_{H_2O} \quad ,(M_{H_2O})^c_{in} = \alpha \quad ,(P_{H_2O})^c_{in} = \beta \text{ and } P^{in}_{H_2O} = 2.\beta$$

And compensate them in the equation (2.26), to get:

$$\dot{x_7} = \frac{dP_{H_2O}}{dt} = 4.\left[\frac{R.\alpha}{V_c}\right].x_4 - 2.\left[\frac{R.\alpha.x_7}{V_c.\beta}\right].x_4 + \left[\frac{R.x_4}{2.V_c.F}\right].I_s \quad (2.27)$$

2.2.2.3 Equations of the Net Temperature

Generally, the fuel cell temperature is non-homogenous, even when there is a steady flow rate of the mass in the channels, due to dissipation of most of the consuming energy produced in the PEMFC electrochemistry reaction in form of heat energies. It is necessary to know the nature of this dissipation in order to preserve the operation of stack within reasonable temperature [38].

These heat energies can be divided mainly to electrochemical reaction heat $\mathcal{Q}_{\mathrm{C}}$, electrical output heat of PEM fuel cell $\mathcal{Q}_{\mathrm{E}}$, and the heat loss due to the air convection $\mathcal{Q}_{\mathrm{L}}$. Then the net temperature of the PEM fuel cell stuck can be given as:

$$\dot{x_4} = \frac{dT}{dt} = \frac{1}{M_{fc}.C_{fc}}[\mathcal{Q}_C - \mathcal{Q}_E - \mathcal{Q}_L] \tag{2.28}$$

a. Equation of electrochemical reaction heat

When electrochemical reaction occurs in the PEM fuel cell, the free energy change associated with a chemical reaction is converted directly to electrical energy which increases the PEM fuel cell temperature [39]. This change in energy is named Gibbs's free energy. During the reaction of an electrochemical at constant pressure and temperature, the Gibbs free energy is given by following equation:

$$\Delta \mathrm{G} = \Delta \mathrm{G}^0 - \mathrm{RT}\ln\left(\frac{\mathrm{P_{H_2}}\cdot\sqrt{\mathrm{P_{O_2}}}}{\mathrm{P_{H_2O}}}\right) \tag{2.29}$$

The heat produced during an electrochemical reaction at constant pressure and temperature, $\mathcal{Q}_{\mathrm{C}}$ is a function of the Gibbs free energy and the mole flow of hydrogen, given by the following [33]:

$$\mathrm{Q_C} = \Delta \mathrm{G}.\mathrm{M_{H_2}} \tag{2.30}$$

Where:

$$\mathrm{M_{H_2}} = \frac{\mathrm{I_s}}{2.\mathrm{F}} \tag{2.31}$$

$\mathrm{M_{H_2}}$: The net mole flow rates of hydrogen at steady state

By replacing equations (2.29) and (2.31) into equation (2.30), we get:

$$\mathrm{Q_C} = \left[\Delta \mathrm{G}^0 - \mathrm{RT}\ln\left(\frac{\mathrm{P_{H_2}}\cdot\sqrt{\mathrm{P_{O_2}}}}{\mathrm{P_{H_2O}}}\right)\right].\frac{\mathrm{I_s}}{2.\mathrm{F}} \tag{2.32}$$

Hence, the heat generation during an electrochemical reaction of the PEM fuel cell stack with compensation of all parameters: $x_4 = T$, $x_5 = P_{H_2}$, $x_6 = P_{O_2}$ and $x_7 = P_{H_2O}$ into equation (2.32) is given by :

$$Q_C = \left[\frac{n_s .\Delta G^0}{2.F} - \frac{n_s .R.x_4}{2.F} . \ln\left(\frac{x_5.\sqrt{x_6}}{x_7}\right)\right]. I_s \quad (2.33)$$

b. Equation of electrical output heat

In the PEM fuel cell, the heat produced due to an electrical output power depends on both the output voltage and stack current of the cell, which is expressed by the following $\mathcal{Q}_E$ [33]:

$$\mathcal{Q}_E = V_{fc}. I_s \quad (2.34)$$

Substituting equations (2.2) and (2.9) and by compensation of all parameters $x_4 = T$, $x_5 = P_{H_2}$, $x_6 = P_{O_2}$ and$x_7 = P_{H_2O}$ into equation (2.34), then solving it, we get:

$$\mathcal{Q}_E = \left[n_s . E_0^{Cell} + \frac{n_s R.x_4}{2F} \ln\left(\frac{x_5\sqrt{x_6}}{x_7}\right) - n_s.(V_{act} + V_O + V_{conc})\right]. I_s \quad (2.35)$$

c. Equation of the air convection heat

The heat loss $\mathcal{Q}_L$occurring in a fuel cell is due to air convection, which can be expressed as following [33]:

$$\mathcal{Q}_L = n_s. h_s A_s. \Delta T \quad (2.36)$$

and:

$$\Delta T = T - T_t \quad (2.37)$$

Where: T is stuck temperature

T_t is room temperature

By replacing equation (2.37) in (2.36), and compensation of the parameter $x_4 = T$, we get:

$$\mathcal{Q}_L = n_s. h_s. A_s[T - T_t] \quad (2.38)$$

By replacing equations (2.33), (2.35) and (2.38) into equation (2.22) and solving moreover, we get:

$$\dot{x_4} = \frac{dT}{dt} = \frac{n_s \,.\, h_s . A_s}{M_{fc} \,.\, C_{fc}} . T_t - \left[\frac{2 . n_s .. E_0^{Cell}}{M_{fc} \,.\, C_{fc}} + \frac{n_s . R . x_4}{F . M_{fc} \,.\, C_{fc}} \ln\left(\frac{x_5 \sqrt{x_6}}{x_7} \right) - (V_{act} + V_O + V_{conc}) \right] . I_s - \frac{n_s . h_s . A_s}{M_{fc} \,.\, C_{fc}} . \; x_4 \qquad (2.39)$$

2.2.2.4 Equivalent Electrical Circuit Equations for PEM Fuel Cell

The modeling of the PEM fuel cell system as an equivalent circuit is quite helpful due to the presence of electrical effects of its components which were produced by the electrochemical reaction inside the fuel cell. These effects can be represented by resistances and charge capacity of this circuit. More precisely, R_{act}, R_{ohm} and R_{conc} can be expressed as equivalent resistances of the circuit through the three types of voltage losses i.e. activation resistance, ohmic resistance and concentration resistance. While the phenomenon of the double layer between electrodes and a solid membrane can be represented by equivalent capacity C. This layer formed due to the passage of the positive hydrogen ions H^+ from the anode toward the cathode through polymer membrane, at the same time flowing of electrons (e^-) from the anode to cathode by the external load where both electrons and protons gathered with O_2 at the cathode side, this capacitance is very large and can be in the order of hundreds Farads [40].

In fact, by inserting the potential of electrochemical reaction E in the equivalent RC circuit model of the resistances and the charge capacity, the overall PEM fuel cell equivalent circuit can be obtained as shown in figure (2.2).

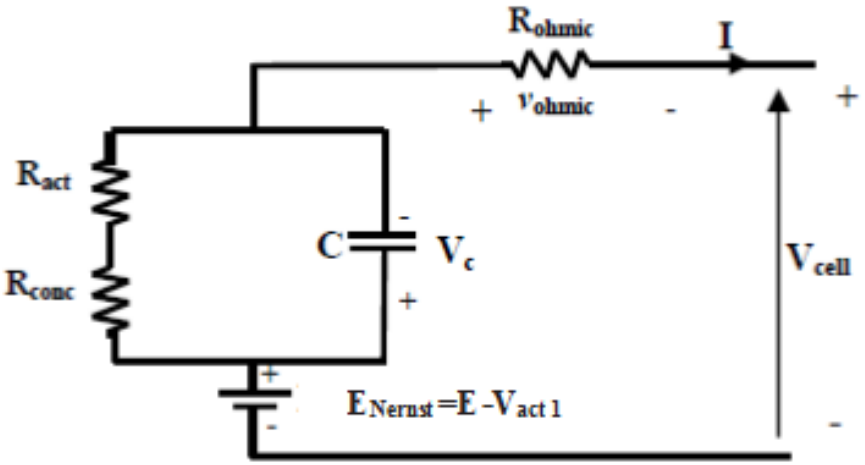

Figure 2.2 Equivalent RC circuit of charge Double Layer in the PEM Fuel Cell [41]

According to figure (2.2), the voltage across the capacitor $x_8 = V_C$ is given by following equation:

$$x_8 = V_C = \left[I_s - C\frac{dV_C}{dt}\right].(R_{act} + R_{conc}) \tag{2.40}$$

So

$$\dot{x_8} = \frac{dV_C}{dt} = \left[\frac{-1}{C(R_{act} + R_{conc})}\right].x_8 + \left[\frac{1}{C}\right].I_s \tag{2.41}$$

The capacitance C due to the effect of the double-layer charge is a function of the surface area A. The distance between the two charged layers d and the electrical permittivity ε. This capacitance is given by the following formula [40] :

$$C = \varepsilon.\frac{A}{d}$$

According of Kirchhoff's voltage law, the equation of output voltage of the PEM fuel cell V_{cell} in the equivalent circuit is written as:

$$V_{cell} = E_{Nernst} - V_O - V_C \tag{2.42}$$

Where: $V_C = V_{act2} + V_{conc}$

As indicated in this figure we can put:

$$E_{Nernst} = E - V_{act1} \tag{2.43}$$

So the output voltage V_{cell} of single cell written as following:

$$V_{cell} = E - V_{act1} - V_O - V_C \tag{2.44}$$

As mention before $V_{act1} = (a_0 + a.T)$

The output voltage V_{fc} of the fuel cell stack is become:

$$V_{fc} = n_s.E_{Nernst} - n_s.(a_0 + a.T) - n_s.V_O - n_s.V_C \tag{2.45}$$

By replacing equations (2.1), (2.4) and (2.40) into equation (2.45) and compensation of the parameters: $x_4 = T$, $x_5 = P_{H_2}$, $x_6 = P_{O_2}$ and $x_7 = P_{H_2O}$, we get [33]:

$$V_{fc} = n_s.E_0^{Cell} + \frac{n_s.R.x_4}{2.F}\ ln\left(\frac{x_5.\sqrt{x_6}}{x_7}\right) - n_s.(a_0 + a.x_4) - n_s.R_O.I_s - n_s.x_8 \tag{2.46}$$

and the output power of the stack can be given by following:

$$P_{stack} = A_s.V_{fc}.i_d \tag{2.47}$$

Hence, the output current of stack is :

$$i_{fc} = P_{stack}/V_{fc} \tag{2.48}$$

Finally, the aggregation of all equations of pressure, temperature and electrical models (2.10)-(2.47) provide a global state space model of the PEM fuel cell stack. Can set the hydrogen and oxygen pressures of the electrodes (u_a /u_c) as two inputs of the system i.e, $[u_1 , u_2] = [u_a , u_c]^t$, k= $[I_s]$ as input of disturbance, two output $[y_1 , y_2] = \left[V_{fc} , i_{fc}\right]$ as voltage and current and $[x_1, x_2, x_3, x_4, x_5, x_6, x_7, x_8] = \left[\left(m_{H_2}\right)_{net},\ \left(m_{O_2}\right)_{net},\ (m_{H2O})_{net} , T, p_{H_2} , p_{O_2}, p_{H2O} ,\ V_C\right] as$ vector state.

Hence, an overall state space representation of the PEM fuel cell is rewritten as following:

$$\begin{cases} \dot{x}_1 = -\dfrac{1}{\lambda_A}.x_1 + \dfrac{\mathrm{I}_s}{2\,.\lambda_A.\mathrm{F}} \\ \dot{x}_2 = -\dfrac{1}{\lambda_C}.x_2 + \dfrac{\mathrm{I}_s}{4.\lambda_C.F} \\ \dot{x}_3 = -\dfrac{1}{\lambda_C}.x_3 + \dfrac{\mathrm{I}_s}{2.\lambda_C.F} \\ \dot{x_4} = -\dfrac{n_s.h_s.A_s}{M_{fc}\,.C_{fc}}.\ x_4 - \dfrac{n_s\,.h_s.A_s}{M_{fc}\,.C_{fc}}.T_t - \left[\dfrac{2.n_s..E_0^{Cell}}{M_{fc}\,.C_{fc}} + \dfrac{n_s.R.x_4}{F.M_{fc}\,.C_{fc}}\ ln\left(\dfrac{x_5\sqrt{x_6}}{x_7}\right) - (V_{act} + V_O + V_{conc})\right].I_s \\ \dot{x_5} = -\dfrac{2.\alpha.R}{\beta.V_a}.x_4.x_5 + \dfrac{2.\alpha.R}{\beta.V_a}.x_4.u_{P_A} - \dfrac{R}{2\,.V_a.F}.x_4.\mathrm{I}_s \\ \dot{x_6} = -\dfrac{2.\alpha.R}{\beta.V_c}.x_4.x_6 + \dfrac{2.\alpha.R}{\beta.V_c}.x_4.u_{P_C} - \dfrac{R}{4\,.V_C.F}.x_4.\mathrm{I}_s \\ \dot{x_7} = \dfrac{4.R.\alpha}{V_c}\,.x_4 - 2.\dfrac{R.\alpha}{V_c\,.\beta}.x_4.\ x_7 + \dfrac{R}{2.V_c.F}.x_4.I_s \\ \dot{x_8} = \left[\dfrac{-1}{C(R_{act} + R_{conc})}\right].x_8 + \left[\dfrac{1}{C}\right].I_s \\ y_1 = n_s.E_0^{Cell} + \dfrac{n_s.R.x_4}{2.F}\ ln\left(\dfrac{x_5.\sqrt{x_6}}{x_7}\right) - n_s.(a_0 + a.x_4) - n_s.R_O.I_s - n_s.x_8 \\ y_2 = P_{stack}/V_{fc} \end{cases} \tag{2.49}$$

2.3 Evaluation of Mathematical Modeling

The simulation objective of PEMFC system dynamics is to obtain the voltage/current outputs data through implementation of a nonlinear state space equations (2.49) using Matlab Environment Programming. Taking the pressures $\mathrm{P_{H2}} = 2\ atm$, $\mathrm{P_{O2}} = 1\ atm$ as inputs. The basic data were obtained through the experimental work on a 500 W SR-12 PEMFC stack which is manufactured by Avista Labs.

The anode channel is supplied by pure hydrogen through manifold pressure, and the cathode side is supplied by the oxygen (air) using the SR-12's internal fan. The dimension and other characteristics of this PEMFC stack are presented in Table 2.1[32][33].

Table 2.1 The PEM Fuel Cell 500 W Model characteristics

Symbol	Description
$A_s = 3.2 \times 10^{-2} m^2$	Fuel cell area
$M_{fc} = 44$ kg	Fuel cell mass
$n_s = 48$	Number of cell
$R = 8.31$ j/(mol.K)	Gas constant
$(m_{H2O})^a_{in} = (m_{H2O})^c_{in} = 8.614 \times 10^{-5} mol/s$	Anode/ cathode water mole flow rate
$(P_{H2O})^a_{in} = (P_{H2O})^c_{in} = 30$ atm	Anode/ cathode Water partial pressure
$(P_{H2O})_{in} = 60$ atm	Partial pressure of water
$\lambda_{A,C} = 60$ s	Flow delay at anode and cathode
$\Delta G^0 = 237.2 \times 10^3$ J/mol	Gibbs free energy
$h_S = 37.5\ W/(m^2.K)$	Convective heat transfer coefficient
C = 10 F	Capacitance due to charge double layer
$C_{fc} = 500$ J/(molK)	Specific heat capacity of PEMFC stack
$R_c^0 = 0.28$	Constant in computation of$R_O(\Omega)$
$F = 96487$ C/mol	Faraday constant (96487 C/mol
$V_a = V_c = 10^{-3} m^3$	Volume of anode and cathode
$E_0^{cell} = 1.23$ V	Reference potential
T=308	Fuel cell temperature (K)
il=100 A	the current limit of PEM fuel cell
id=0.7A	the exchange current density

2.3.1 Evaluation of Mathematical Modeling for Partial Pressures Gases

When the fuel cell is under load, the hydrogen and oxygen gases diffuse through the electrode channels to a catalyst layer of cathode where the reaction sites of these gases. While the reactant water diffuses from the reaction sites to the anode side. As a result, the partial pressures of P_{H2}, P_{O2} and P_{H2O} gradient are formed along electrode channels. Assuming uniform variation of gas partial pressures (assumption2), the overall gases at the channels are considered constant. Nevertheless, in this part the effective partial pressures of all gases at the actual reaction sites inside PEM fuel cell are calculated in order to obtain the output voltage of the cell. To evaluate the effective partial pressures of hydrogen, oxygen and the water inside PEM cell fuel stack, the

dynamic equations (2.20)-(2.25)-(2.27) are simulated using Matlab Environment Programming under normal operating conditions.

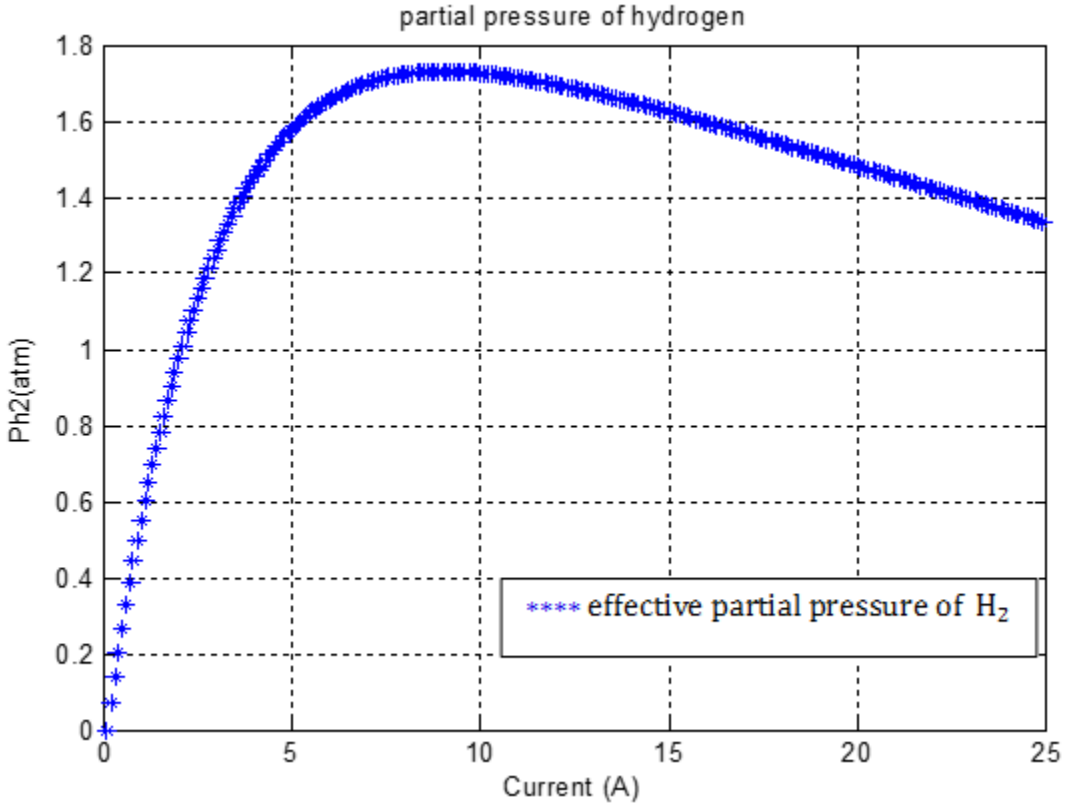

Figure 2. 3 Variation of partial pressure hydrogen with current

Figure (2.3) shows the variation of effective partial pressure of hydrogen versus the current as given in equation (2.20). Notice that, the effective partial pressures of hydrogen at reaction sites is less than those in the hydrogen flow channel , due to mass diffusion. When the effective partial pressure increases within the reaction sites, the Nernst voltage of the electrochemical reaction potential E_{Nernst} increases slightly, therefore an increase in the open-circuit output voltage $V_{O.FC}$ according to equation (2.2).

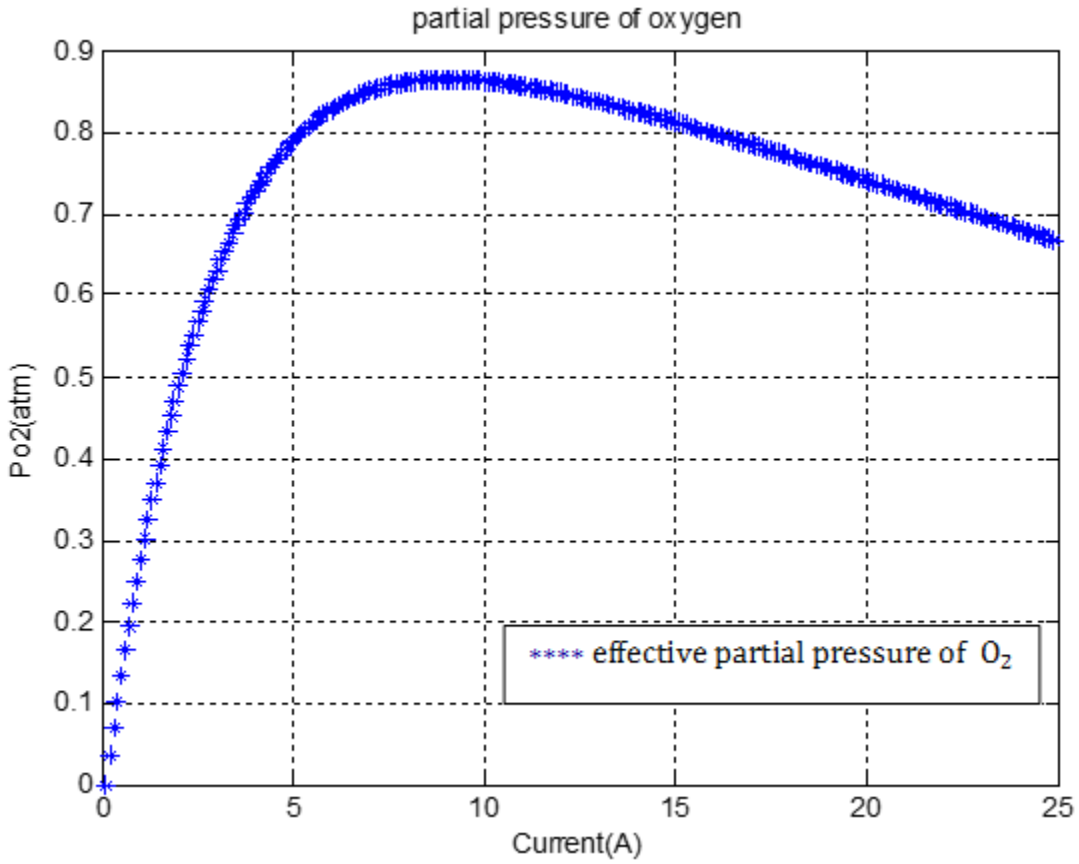

Figure 2.4 Variation of partial pressure oxygen with current

Regarding the effective partial pressure of oxygen, note that, it is identical to the hydrogen behavior as showed in figure (2.4). However, the variation effective partial pressure of oxygen is reduced to half. This is in good agreement with the behavior of the fuel cell since it takes an amount of oxygen twice less than that of hydrogen to produce the same current.

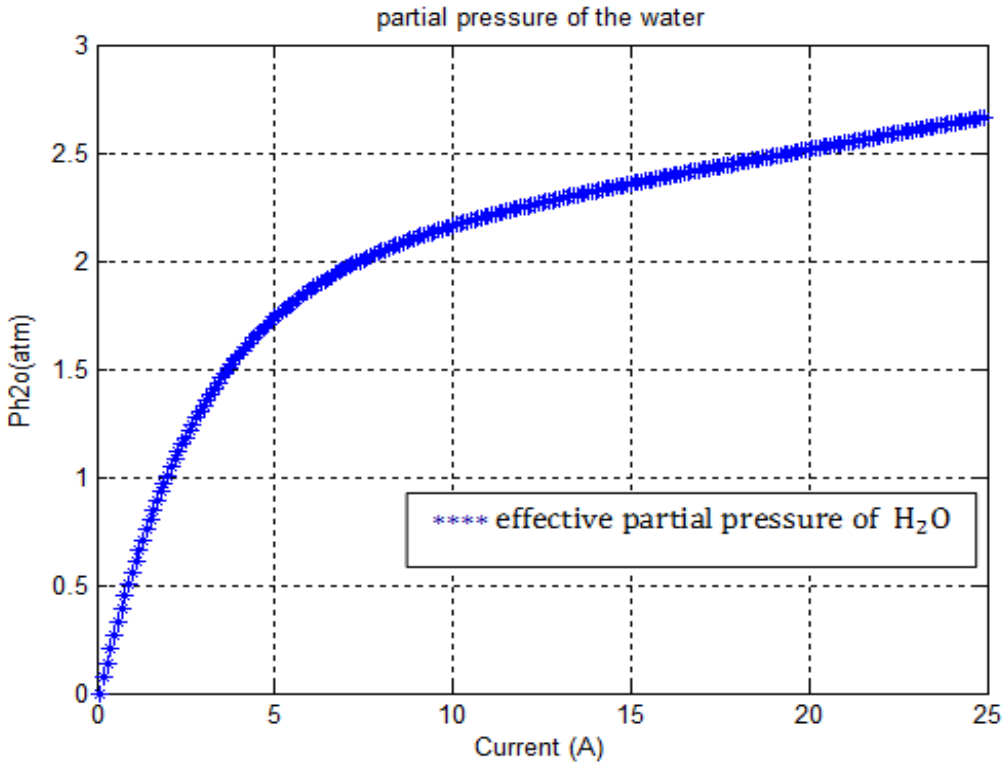

Figure 2.5 Variation of partial pressure water with current

Finally, the effective partial pressure of the water at reaction sites is higher than that in the anode channel, due to the increase in water production through chemical reaction in these sites.

In contrast, the pressure of water has the opposite effect compared to that of hydrogen as seen in figure (2.5). This result was naturally predictable since an increase in the water pressure generates a decrease in Nernst voltage of the electrochemical reaction potential E_{Nernst} and consequently a decrease in the output voltage $V_{O.FC}$.

2.3.2 V-I Characteristics of the Proton Exchange Membrane Fuel Cell

To get the V-I Characteristics of the proton exchange membrane fuel cell model, the equation (2.37) is simulated using Matlab Environment Programming, with increasing the current density from 1 to 25A in steps of 0.09. The simulation results of V-I characteristics of the fuel cell are shown in figure 2.6.

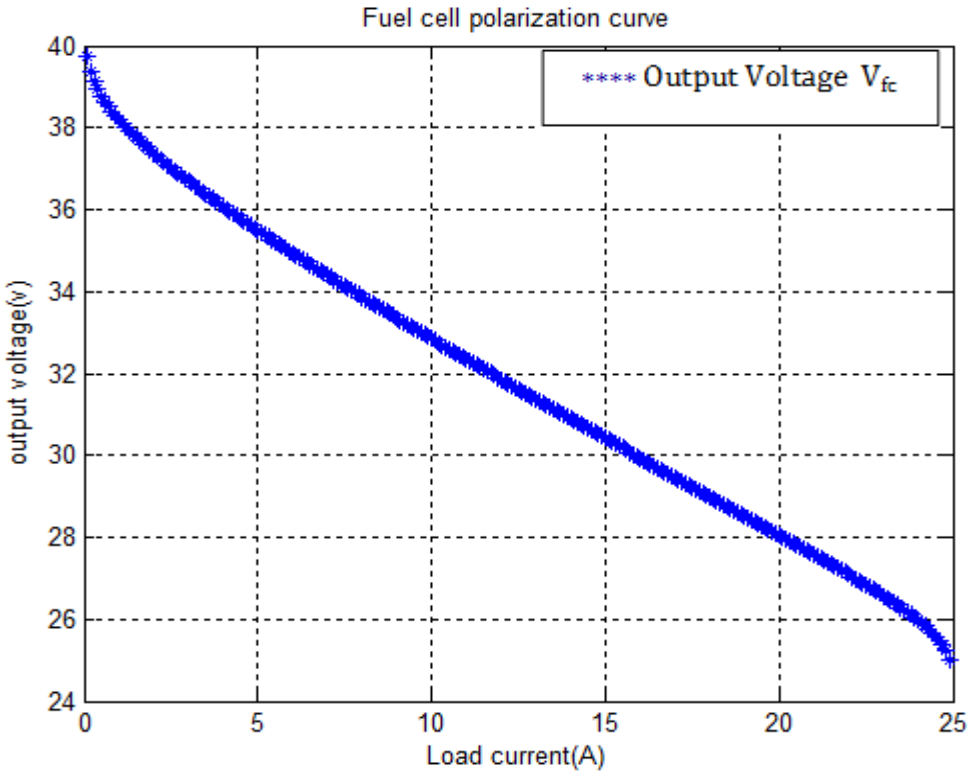

Figure 2.6 V–I characteristics curve for the PEMFC500w

The output voltage variation response of the PEMFC model is gradually decreasing from 39.75 volts to 24.98 volts according to the current variation from 1A to 25 A due to the existence of the activation, concentration losses (as nonlinear functions) at the beginning and end of the curve respectively, and the ohmic loss (as a linear function) in the middle of the curve[32].

These obtained results in figure (2.6) were validated by comparing them with experimental data of I-V polarization curve for Avista Labs SR-12 (500W) PEM fuel cell, and the Matlab/Simulink model which is obtained by M.H. Nehrir in [34]. As shown in figure (2.7), the model responses of space state Programming Matlab agree very well with both the experimental data and Simulink model.

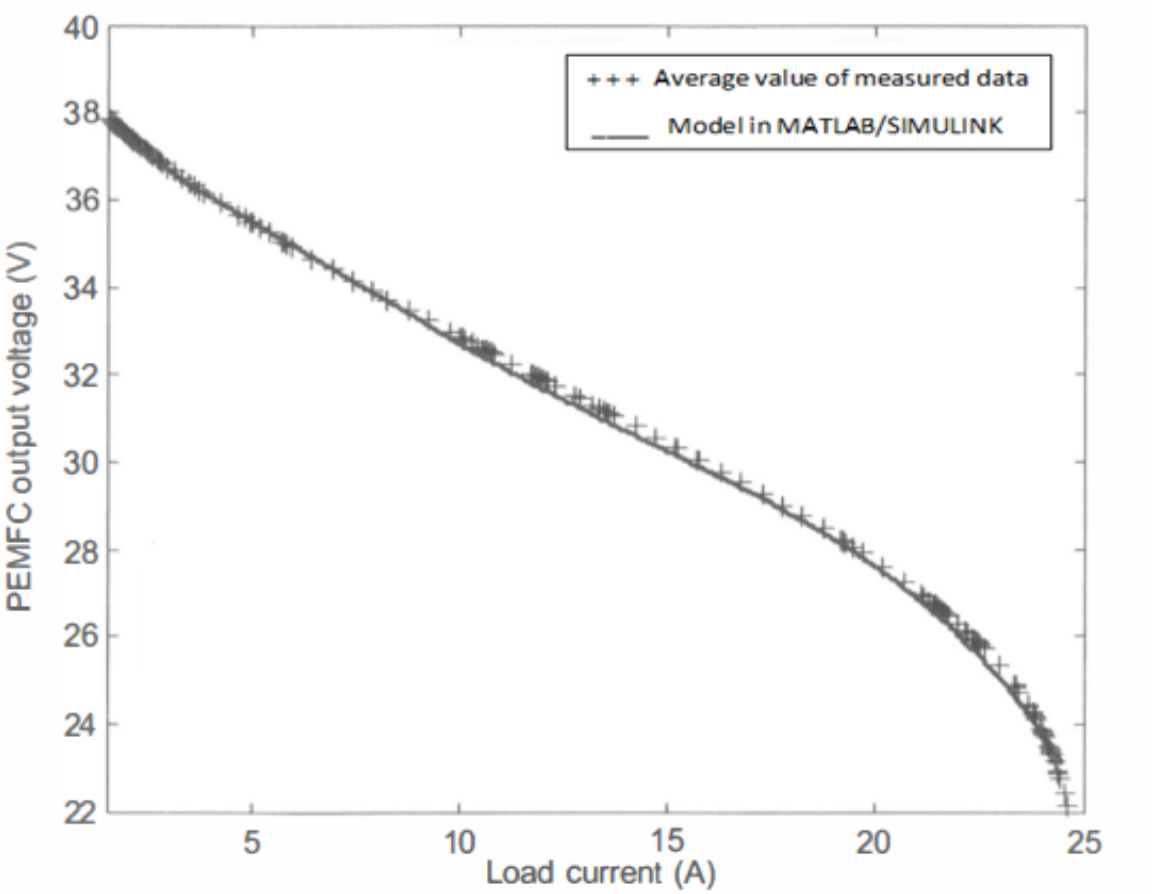

Figure 2. 7 Validation results of I-V polarization curve for the Avista Labs SR-12 (500W) fuel cell stack and Simulink model[34]

2.3.3 Evaluation of Voltage Losses

- ***Activation polarization***

Usually, the activation loss situated at the beginning of the I-V polarization curve at low current density. It is considered an over potential in electrochemical process which is derived from Tafel equation. To evaluate and plot the activation loss for a fuel cell operating at current density of 0.7A/cm^2 and an exchange current density of 10^{-7}. The Tafel equation in equation (2.3) is simulated using Matlab Environment Programming with constants $a = -3.08 \times 10^{-3} V/K$, $b = 9.724 \times 10^{-5} V/K$and $a_0 = 1.3697V$.

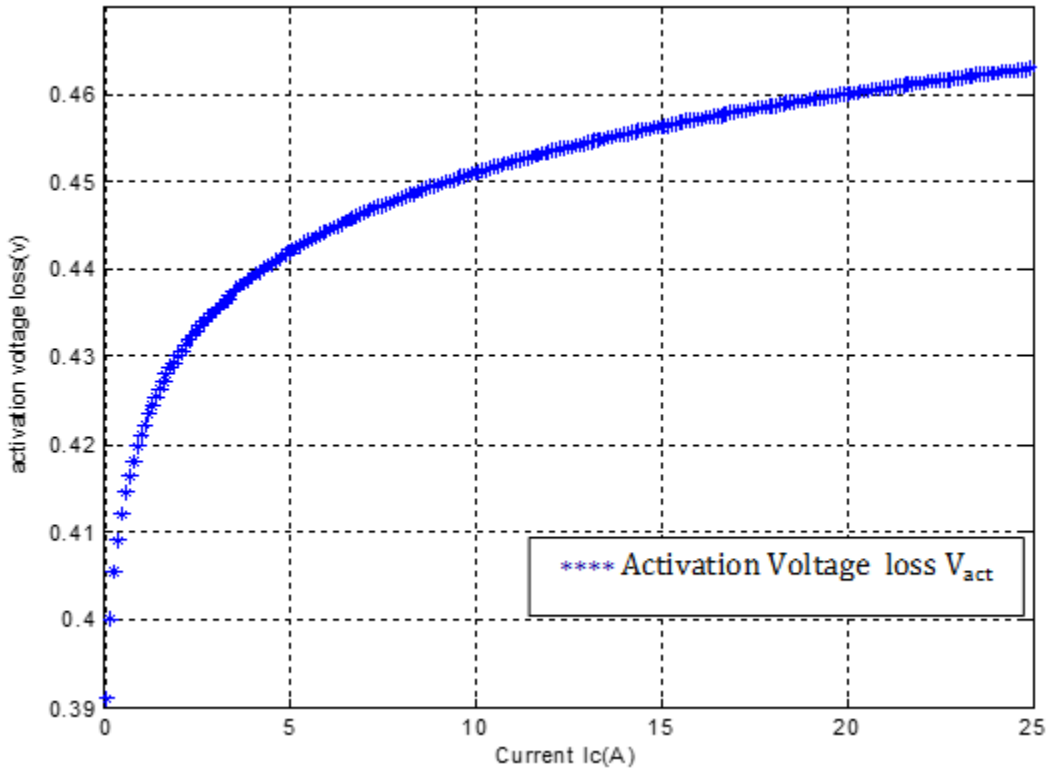

Figure 2. 8 Activation loss as a function of current

Figure (2.8) shows the responses of the activation loss to a variation in current between 1 A and 25A. The logarithmic relationship given in equation (2.3) shows that an increase in current implies a small increase in activation loss. While an increase in the exchange current density lead to the more active surface of the electrode. Hence, a decrease in the activation polarization.

- ***Ohmic polarization***

The ohmic voltage loss situated in the middle of I-V polarization curve. This loss consists of electrodes resistances (R^A, R^C) and membrane resistances (R^M). To evaluate and plot this loss, the equation (2.5) is simulated using Matlab Environment Programming for a fuel cell operating at temperature T of 308 K and current vary from 1A to 25A.

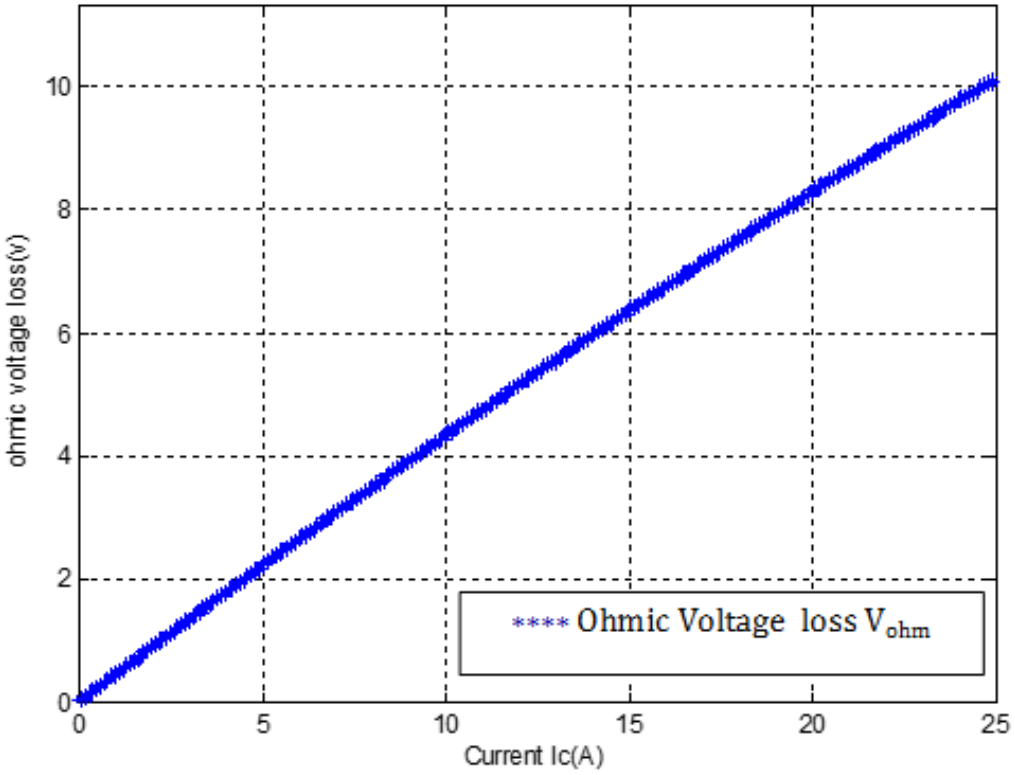

Figure 2. 9 Ohmic loss as a function of current

Note that, in figure (2.9), the ohmic loss voltage can be considered as a linear function at certain operation due to the dependence of the electrodes resistances on the current and temperature for the fuel cell stack. Where an increasing in current and temperature of the stack lead to an increasing directly in ohmic voltage loss. In order to reduce this loss either by using more conductive electrolyte for ions or this layer to be thinner.

- ***Concentration polarization***

The concentration loss situated at the end of the I-V polarization curve at height current as mentioned in figure (2.6). To evaluate this loss, equation (2.6) is simulated by Matlab Environment Programming for a fuel cell operating at current limit of 25 A, temperature T of 308 K and current varies from 1A to 25A.

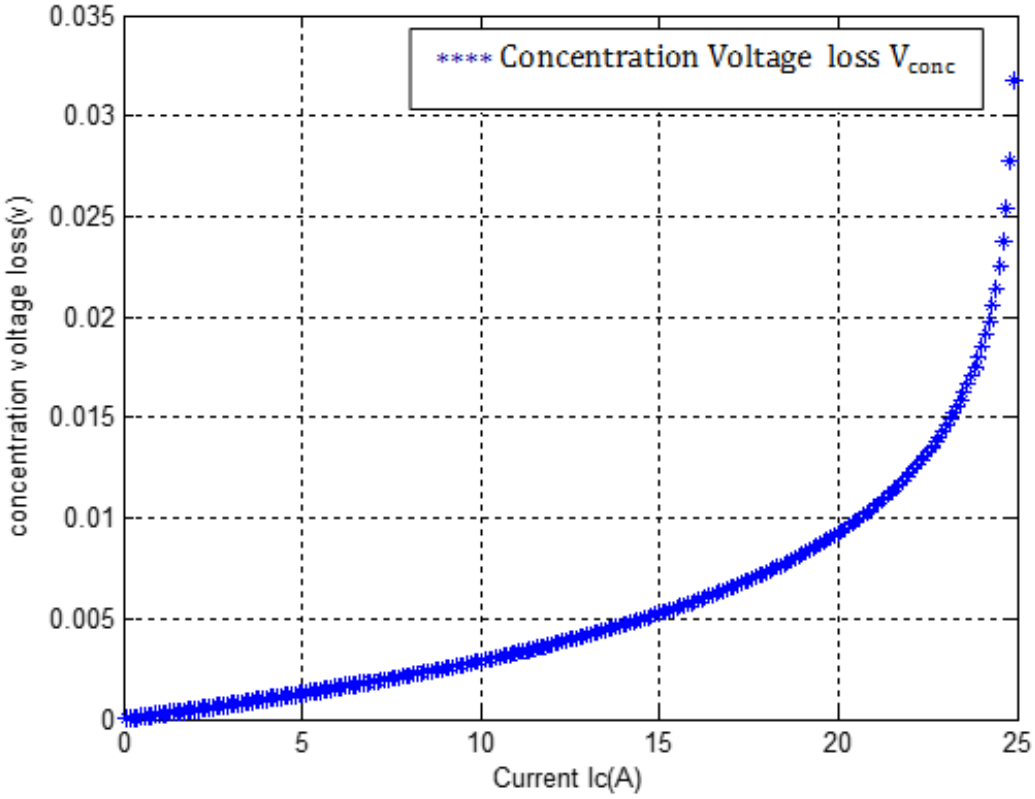

Figure 2.10 Concentration loss as a function of current

Figure (2.10) shows the concentration voltage loss as a function of current. This loss due to mass transport from electrodes channels to reaction sites. Note that, when the current densities increase, the concentration voltage loss increases due to depletion of reactant in the catalyst layer and flooding of the water in the cathode channel. At high current, the amount of liquid water produced in the cathode channel becomes greater than the amount of water that can be extracted from the gas flow channels.

2.3.4 P-I Characteristics Curve of the Proton Exchange Membrane Fuel Cell

Figure (2.11) shows the MATLAB based simulation of P-l characteristics curve for a PEMFC 500 W stack, obtained based on Matlab Environment Programming of power equation (2.47).

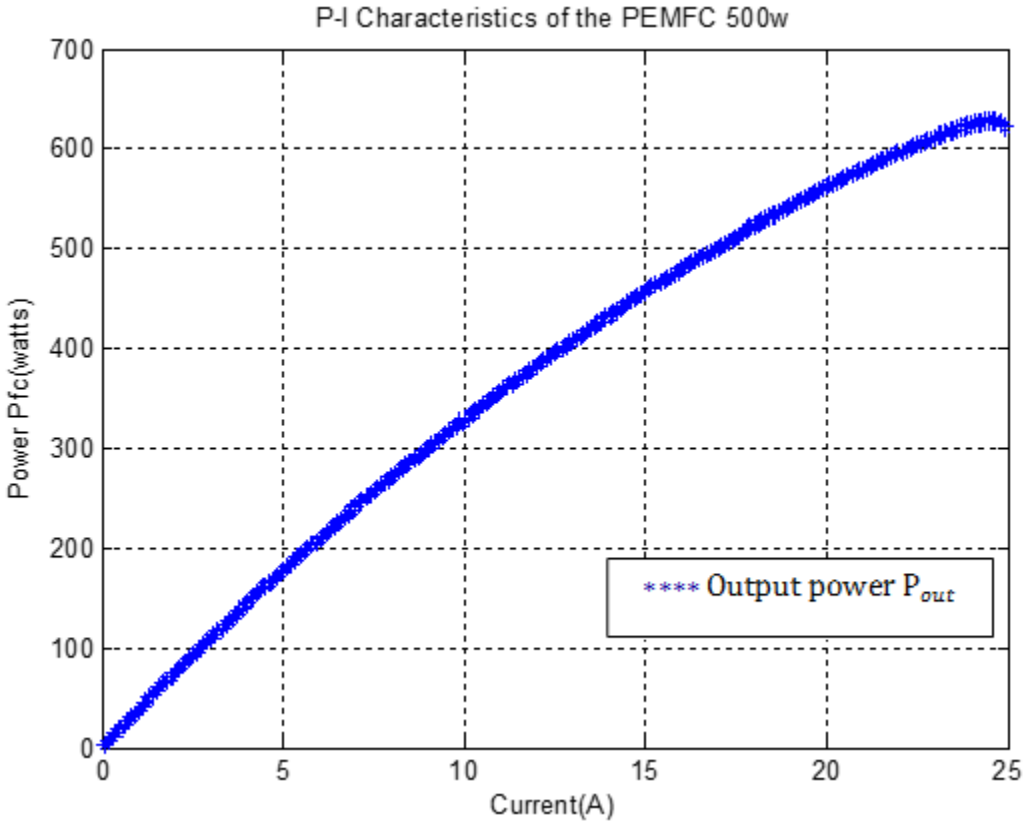

Figure 2. 11 P-I characteristics curve for the PEM fuel cell 500 w stack

Note that, the maximum output power of the 500 W fuel cell stack model 626.99W is obtained at point close to the rated current of the cell 24.6 A, where the output voltage is approximately 25.48 V. Beyond the peak of the output power curve, the fuel cell enters into the concentration region when the output voltage decreases sharply while the load current increases as mentioned in figure 2.6. As a result, the output power of fuel cell will decrease when the load current increases.

The simulation results obtained in figure (2.11) are validated with measurements data of the Avista *Labs SR-12* (500W) PEM fuel cell and the Matlab/Simulink model which is established by M.H. Nehrir at [34] for the models developed.

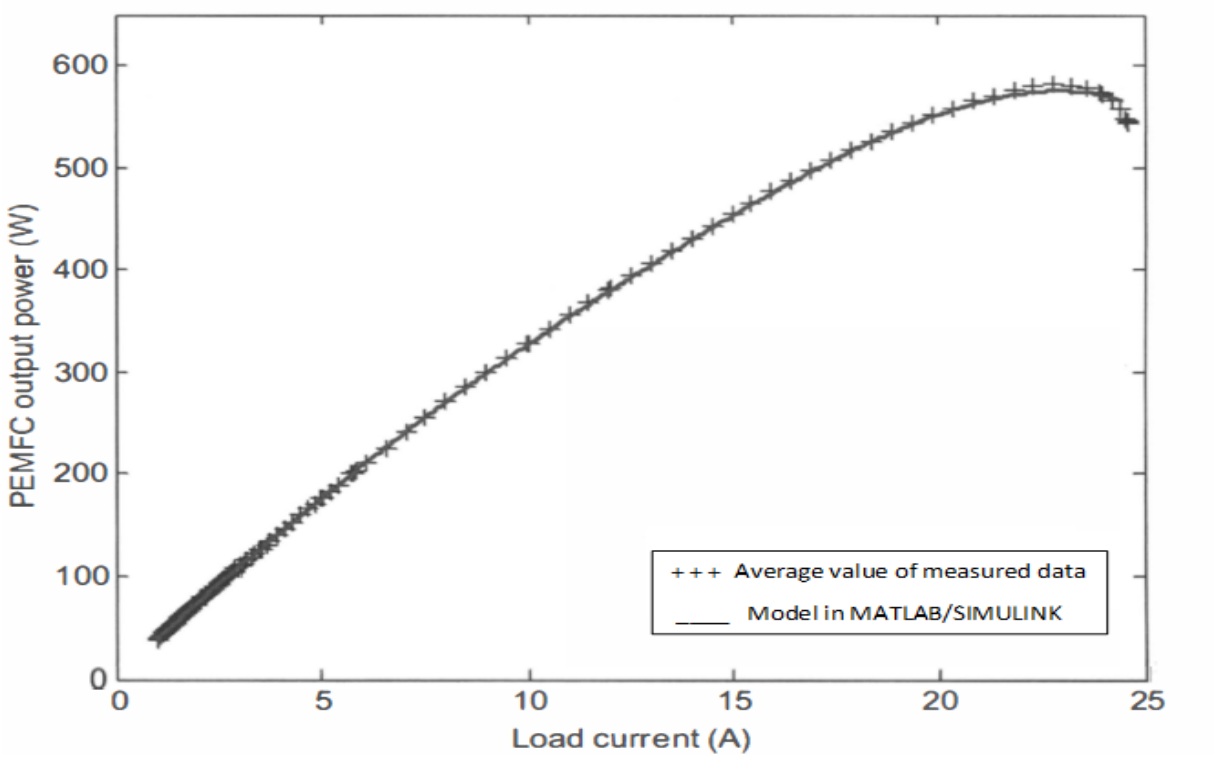

Figure 2.12 Validation results of SR -12 PEMFC and Simulink model[34]

Figure (2.12) shows a comparison of the average P-I characteristic curves for the SR -12 PEMFC stack obtained experimental measurements and the results of Matlab/Simulink model. Observe that, the model results in figure (2.11)are match close to those validation results of both measured data and Simulink models.

2.4 Conclusion

In this chapter, a nonlinear dynamic model of SR 500w PEMFC stack is suggested. which focuses on output voltage of the cell open-circuit, voltage losses which occur in them, net mole flow rate of all gases, effective partial pressures of all gases at the actual reaction sites inside PEM fuel cell, in addition the net temperature inside the fuel cell and the equivalent circuit of the cell which is formed between anode and cathode electrodes. This nonlinear model was validated through simulation of (V-I) and (P-I) polarization curves taking in account both of hydrogen and oxygen gases as inputs for the PEM fuel cell, the results of simulation have proven that are satisfying and close to the experimental data of polarization curves obtained by Avista Labs. Furthermore, voltage losses, the effective partial pressures of all gases and equivalent circuit of the fuel cell were simulated to study the dynamic behavior of the PEMFC.

Finally, the obtained $V_{fc}$and i_{fc} results through simulation will be used as outputs data for identification techniques of nonlinear PEMFC system using nonlinear autoregressive exogenous neural network (NLARX) to obtain the linear space state model in next chapter .

Chapter 3

Neural Network Nonlinear Autoregressive Exogenous Modeling of PEMFC 500W

3.1 Introduction

Based on physiochemical processes inside the PEMFC stack presented in previous chapter, the relationship between the hydrogen /oxygen inputs, stack temperature and the voltage/ current outputs is highly nonlinear. In addition, the nonlinear space model of PEMFC is quite complex. The development or simulation of this fuel cell stack require appropriate knowledge of its mathematical dynamic model. Which it's parameters is difficult to obtain using only physical laws (analytical approach). Therefore, an identification technique is required to obtain suitable mathematical model of the PEMFC stack.

The objective of this chapter is identify the linear state space model for proton exchange membrane fuel cell (PEMFC) 500W stack using neural network nonlinear autoregressive exogenous model (NN-NLARX) technique, this technique is developed and implemented by employing the system identification based on acquired set of multi inputs -multi outputs data obtained by simulation of nonlinear dynamic PEMFC stack in previous chapter . The identification procedure for space state model start with data processing, neural network nonlinear modeling, validation and linearization of the obtained nonlinear model .finally , the performance of both neural network model and space state model are investigated and shown by comparison of results.

3.2 Nonlinear Model Identification

Identification technique is an important tool in modeling field where most real systems are nonlinear processes, in which the output for these systems is a nonlinear function of the input elements .this function is represented by mathematical relations between the system's inputs (u) and outputs (y) at time (t). These mathematical relations are applied to estimate the current output from previous inputs and outputs. System identification (SI) is a process for building a mathematical model of nonlinear system dynamics from observed input-output data without detailed information about the system insights .these data are collected from experimental test of a real world system. The procedure of identification system can be outlined by followings steps in figure (3.1):

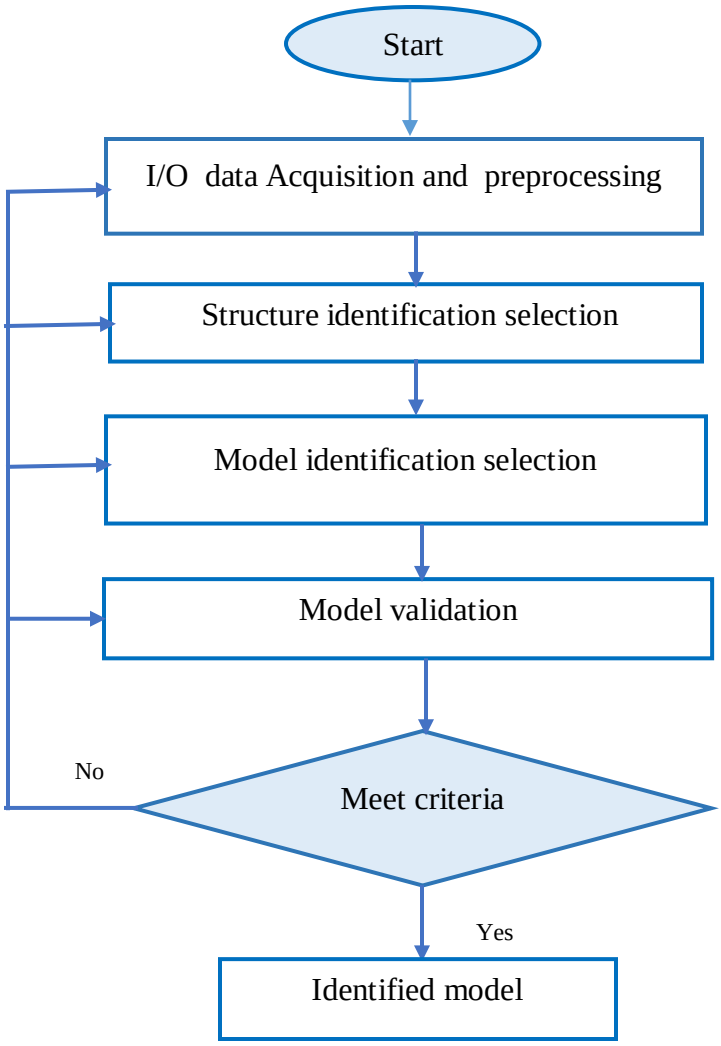

Figure 3.1 Flowchart of identification technique

Generally, in system identification, there are many structures of useful nonlinear models to describe a system dynamic, such as Hammerstein model, Wiener model, Hammerstein-Wiener model and nonlinear autoregressive exogenous model (NLARX)[42].

In this dissertation, NLRAX model has proven is the best to describe the nonlinear dynamic of PEMFC system, therefore ,the goal of NLRAX structure is to obtain the suitable mathematical model for the real PEMFC 500W system by using the I/O data , this obtained model will be useful to get a good understanding, simulation and prediction of the behavior of real PEMFC

dynamic system, especially to serve as a control mechanism to design and analysis the controller that depends on the real PEM fuel cell system model.

3.3 Nonlinear Autoregressive Exogenous (NLARX) Model

A nonlinear autoregressive exogenous (NLARX) structure is a black box model, that is an extension the linear ARX model, it is widely used in several applications as times-series modelling, multi-step ahead prediction and modelling for nonlinear dynamic systems[43]. The nonlinear ARX structure describes the nonlinear dynamic systems by using a parallel combination of nonlinear and linear blocks [44].this parallel combination is expressed in terms of variables called standard regressors $[n_a, n_b, n_k]$ as depicted in figure (3.2).

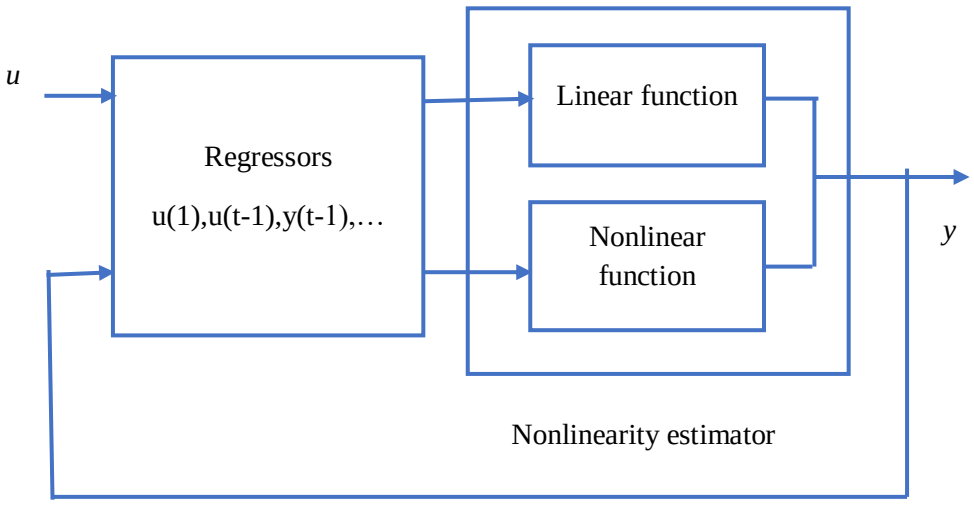

Figure 3.2 Nonlinear ARX Model Structure

The nonlinear and linear blocks can be expressed by function (f) in terms of depending on the finite number of previous inputs (u) and outputs (y), where (n_a) is the number of past output terms, (n_b) is the number of past input terms used to predict the current output and (n_k) is the delay from the input to the output (the samples number).

Hence, the predicted output of the NLARX model structure is given by following equation [42].

$$y_p(t) = f(\big(y(t-1), y(t-n_a), \dots, u(t), u(t+1), \dots, u(t-n_b), \dots, u(t-n_k-n_b+1)\big) \quad (3.1)$$

The NLARX structure enables to model the behavior of complex nonlinear systems using many flexible nonlinear estimators such as sigmoid network, wavelet network, tree partition, custom network, and neural network. In this study, a neural network estimator was chosen to model the nonlinear dynamic PEMFC system due to its high performance which was demonstrated by simulation results in the experiments part of this chapter.

3.4 Artificial Neural Network

Neural networks are intelligent computing models inspired by biological neural network of the human brain and they mimic the way biological neurons communicate with each other. Neural networks (NNs) consist of a large number of nodes (neurons) arranged in parallel layers that contain an input layer, one or more hidden layers, and an output layer. These layers are connected to each other by weighted connections, each layer receives the data from the input layer or previous layer for collecting and processing it by nonlinear activation functions then send it to the next layer or output layer of network. When the output of any individual node is higher than the specified threshold value of the activation function, that node is activated and the data are transmitted to the following layer of the network. If not, the data will not be passed to the next layer of the network.

Generally, Neural networks can be divided into two main classes: static and dynamic neural networks [43], static neural networks are feedforward neural networks, which are characterized by memoryless mapping, which means that it has not feedback elements and no delays in the input layer. Therefore, the output of static neural network depend only on the current values of the inputs for the network as shown in figure (3.3).

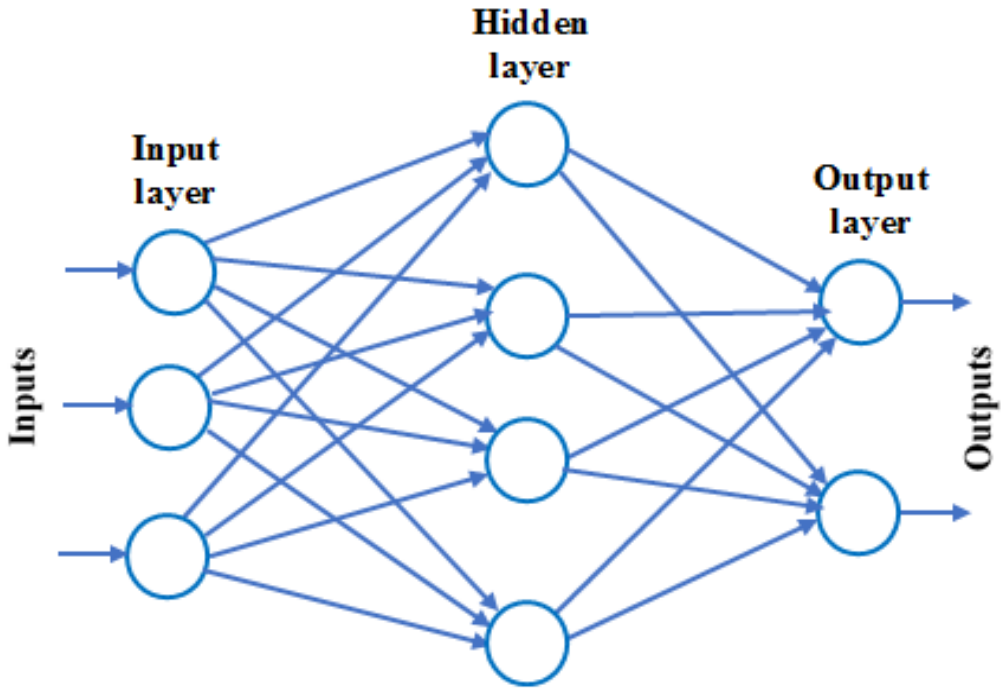

Figure 3.3 Structure of static neural network

The second class is dynamic neural network that is characterized by memory mapping between input layer and output elements of neural network, which means that, the output values from the network depend on the current input, the previous input or output values of the network. The dynamic network is divided into two types: feedforward and recurrent (or feedback) neural networks, the feedforward neural network has input delay but without feedback or recurrent connections as depicted in figure (3.4).

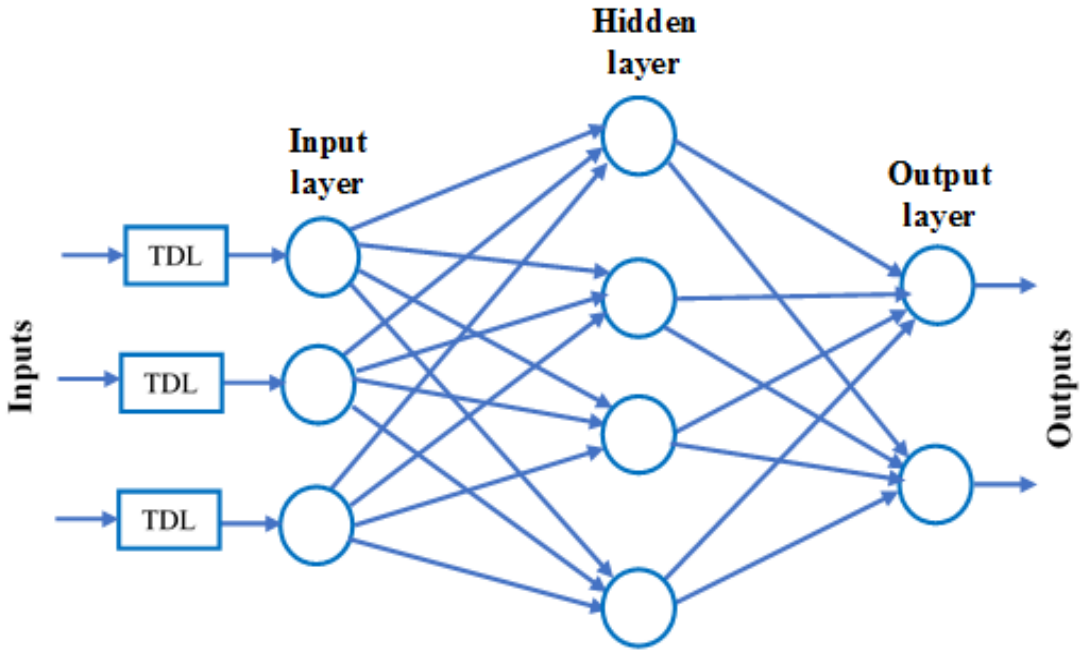

Figure 3.4 Structure of dynamic feedforward neural network with input delay

The recurrent neural network has feedback and time delays in its structure ,where the information are transmitted from the output layers to the input layers with convenient time delays as depicted in figure 3.5. These delays store the informations from previous time steps, that can be used in the current time step[33].

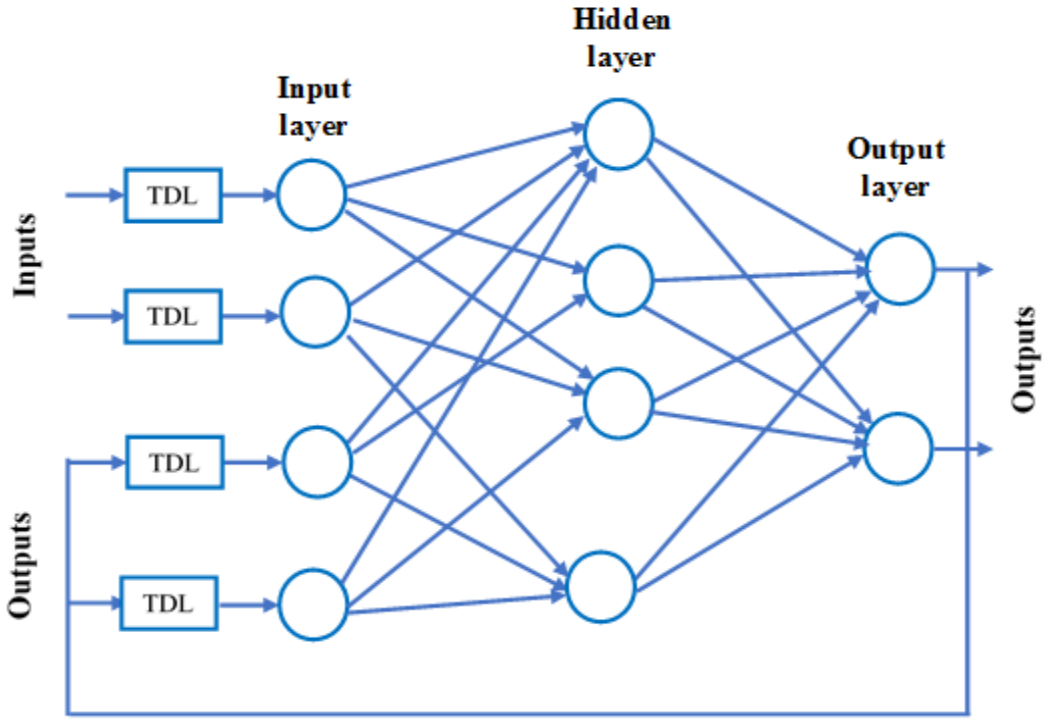

Figure 3.5 Structure of dynamic feedback neural network with time delays

To develop the nonlinear mathematical model of the proton exchange membrane fuel cell stack (PEMFC 500W), feedforward (*forward cascade modeling*) neural network is proposed as an estimator for a nonlinear autoregressive exogenous (NLARX) structure in identification technique.

3.5 The Proposed Cascade Forward Neural Network

Cascade-forward neural network (CFNN) is a class of neural networks that is similar in structure to feed-forward networks, except that, the CFNN include a weight connection from the input layer to every following hidden layers and output layer in parallel way[45], at the same time, it has connections between every previous layer toward to next layers and to output layer as shown in figure (3.6). This structure is used to estimate the nonlinear function f (equation 3.1) of the nonlinear autoregressive exogenous (NLARX) model for predicting the outputs of dynamic behavior of PEM fuel cell.

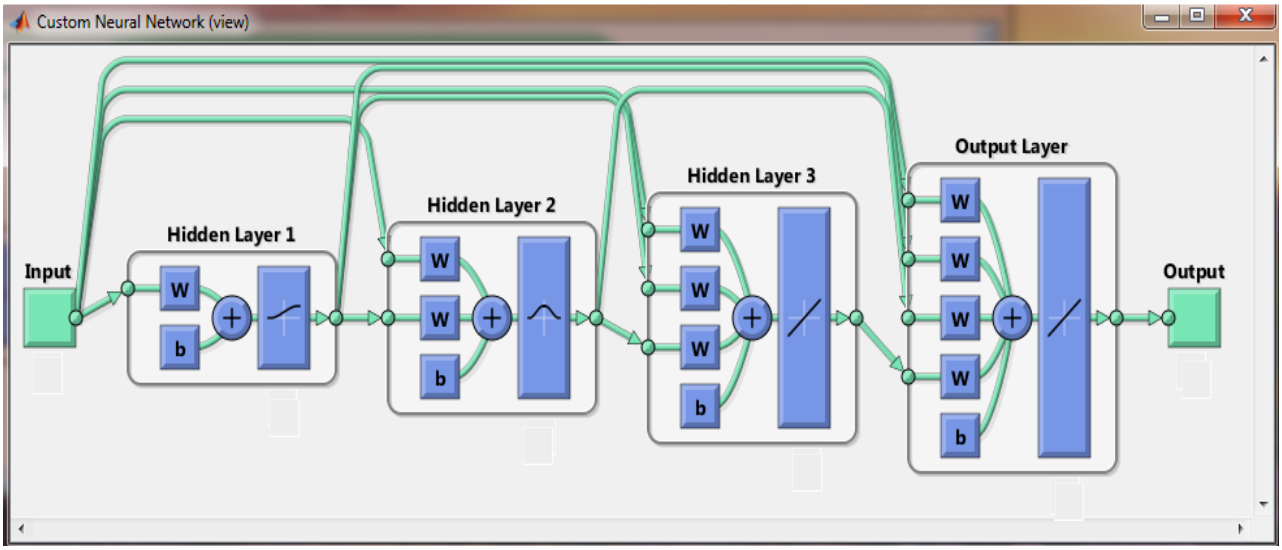

Figure 3.6 Structure of cascade-forward neural network (CFNN)

The input layer of CFNN is composed of two passive artificial neurons, and brings the initial data (u_1 , n_2) into the neural network for more processing by next layers of neural network. While, the output layer (y_{out}) consists of one active neuron with pure linear function "*purelin (.)*" as an activation function.

The hidden layers of a cascade-forward neural network composed of three layers , the first one has two neurons with a log-sigmoid function "*logsig(.)*" as an activation function, the second layer has a radial basis function "*radbas(.)*" as an activation function in their nodes and the third hidden layer has two neurons with a pure linear function "*purelin(.)*" as an activation function .

Hence, the outputs of the cascade-forward neural network (CFNN) are calculated by following:

- The output of the first hidden layer with "*logsig(.)*":

$$a_{h11} = logsig(n_{h11}) = \frac{1}{1+e^{-n_{h11}}} \tag{3.2}$$

$$a_{h12} = logsig(n_{h12}) = \frac{1}{1+e^{-n_{h12}}} \tag{3.3}$$

Where:

$$n_{h11} = W_{11}^{(1)}.u_1 + W_{21}^{(1)}.u_2 + b_1^{(1)} \quad (3.4)$$

$$n_{h12} = W_{12}^{(1)}.u_1 + W_{22}^{(1)}.u_2 + b_2^{(1)} \quad (3.5)$$

$W_{11}^{(1)}, W_{21}^{(1)}, W_{12}^{(1)}, W_{22}^{(1)}$ are the weighted connections from inputs to first hidden layer, $b_1^{(1)}$ and $b_2^{(1)}$ are bias. The outputs of this layer is then fed to the second hidden layer.

- The output of the second hidden layer with "*radbas(.)*" function:

$$\begin{aligned} a_{h21} &= radbas(n_{h21}) = e^{-(n_{h21})^2} \\ a_{h22} &= radbas(n_{h22}) = e^{-(n_{h22})^2} \\ &\vdots \\ a_{h2k} &= radbas(n_{h2k}) = e^{-(n_{h2k})^2} \end{aligned} \quad (3.6)$$

Where:

$$\begin{aligned} n_{h21} &= \left[\left\|W_{11}^{(2)} - a_{h11}\right\| + \left\|W_{21}^{(2)} - a_{h12}\right\| + \left\|W_{c11}^{(1)} - u_1\right\| + \left\|W_{c21}^{(1)} - u_2\right\|\right].b_1^{(2)} \\ n_{h22} &= \left[\left\|W_{12}^{(2)} - a_{h11}\right\| + \left\|W_{22}^{(2)} - a_{h12}\right\| + \left\|W_{c12}^{(1)} - u_1\right\| + \left\|W_{c22}^{(1)} - u_2\right\|\right].b_2^{(2)} \\ &\vdots \\ n_{h2k} &= \left[\left\|W_{1k}^{(2)} - a_{h11}\right\| + \left\|W_{2k}^{(2)} - a_{h12}\right\| + \left\|W_{c1k}^{(1)} - u_1\right\| + \left\|W_{c2k}^{(1)} - u_2\right\|\right].b_k^{(2)} \end{aligned} \quad (3.7)$$

$W_{11}^{(2)}, W_{21}^{(2)}, W_{12}^{(2)}, W_{22}^{(2)}, \ldots, W_{1k}^{(2)}, W_{2k}^{(2)}$ are the weighted connections from the first hidden layer to the second hidden layer , $W_{c11}^{(1)}, W_{c21}^{(1)}, W_{c12}^{(1)}, W_{c22}^{(1)}$,…, $W_{c1k}^{(1)}, W_{c2k}^{(1)}$ are the weighted connections from inputs to second hidden layer, $b_1^{(2)}$, $b_2^{(2)}$,…, $b_k^{(2)}$ are bias of the second hidden layer. The outputs of this layer is fed to the third hidden layer.

- The output of the third hidden layer with "*purelin(.)*" function :

$$a_{h31} = purelin(n_{h31}) \quad (3.8)$$

$$a_{h32} = purelin(n_{h32}) \quad (3.9)$$

Where:

$$n_{h31} = W_{c11}^{(2)}.u_1 + W_{c21}^{(2)}.u_2 + W_{h11}^{(1)}.a_{h11} + W_{h21}^{(1)}.a_{h12} + W_{h11}^{(2)}.a_{h21} + W_{h21}^{(2)}.a_{h22} + \cdots + W_{hk1}^{(2)}.a_{h2k} + b_1^{(3)} \quad (3.10)$$

$$n_{h32} = W_{c12}^{(2)}.u_1 + W_{c22}^{(2)}.u_2 + W_{h12}^{(1)}.a_{h11} + W_{h22}^{(1)}.a_{h12} + W_{h12}^{(2)}.a_{h21} + W_{h22}^{(2)}.a_{h22} + \cdots + W_{hk2}^{(2)}.a_{h2k} + b_2^{(3)} \quad (3.11)$$

$W_{c11}^{(2)}$, $W_{c21}^{(2)}$, $W_{c12}^{(2)}$, $W_{c22}^{(2)}$ are the weighted connections from inputs to third hidden layer, $W_{h11}^{(1)}, W_{h21}^{(1)}, W_{h12}^{(1)}, W_{h22}^{(1)}$ are the weighted connections from the first hidden layer to third hidden layer, $W_{h11}^{(2)}, W_{h21}^{(2)},\ldots, W_{hk1}^{(2)}$ and $W_{h12}^{(2)}, W_{h22}^{(2)}$,…, $W_{hk2}^{(2)}$ are the weighted connections from the second hidden layer to third hidden layer, $b_1^{(3)}$, $b_2^{(3)}$ are bias of the third hidden layer.

Hence, the output y_{out} of the cascade-forward neural network are given by following equations:

$$y_{out} = purelin(n_{out}) \quad (3.12)$$

$$n_{out} = W_{c11}^{(3)}.u_1 + W_{c21}^{(3)}.u_2 + W_{h11}^{(2)}.a_{h11} + W_{h21}^{(2)}.a_{h12} + W_{11}^{(3)}.a_{h31} + W_{21}^{(3)}.a_{h32} + W_{h11}^{(3)}.a_{h21} + W_{h21}^{(3)}.a_{h22} + \cdots + W_{hk1}^{(3)}.a_{h2k} + b_1^{(4)} \quad (3.14)$$

$W_{c11}^{(3)}$, $W_{c21}^{(3)}$ are the weighted connections from inputs to output layer, $W_{h11}^{(2)}, W_{h21}^{(2)}$ are the weighted connections from the first hidden layer to output layer, $W_{h11}^{(3)}, W_{h21}^{(3)},\ldots.$, $W_{hk1}^{(3)}$ are the weighted connections from the second hidden layer to output layer , $W_{11}^{(2)}, W_{21}^{(2)}$ are the weighted connections from the third hidden layer to output layer and $b_1^{(4)}$ is a bias of the output layer. The cascade-forward neural network (CFNN) is stored as a nonlinearity estimator for estimating nonlinear ARX to derive a mathematical model of the PEMFC 500w stack based on input-output data.

3.6 Neural Network Nonlinear Autoregressive Exogenous Model Identification

The feedforward neural network is one of the most popular neural network structures can be used in estimating the nonlinear autoregressive exogenous structure especially in the identification of a nonlinear system. The neural network version of nonlinear ARX model structure is denoted as NN-LARX as shown in figure (3.7), with assume the input delay $n_k = 1$:

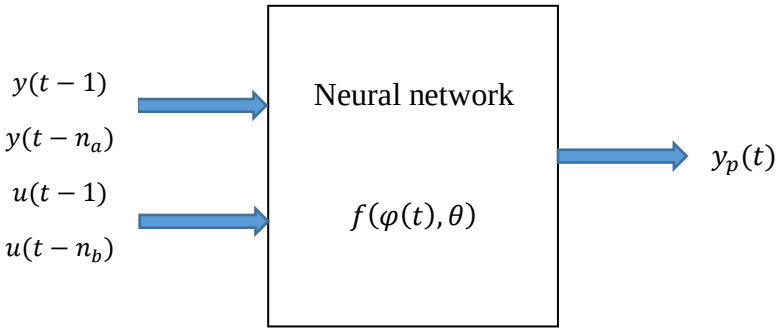

Figure 3. 7 NN-NLARX model structure

The predicted output for one-step-ahead prediction of the NN-NLARX model structure is given by following equation:

$$y_p(t/\theta) = f(\varphi(t),\theta) \tag{3.14}$$

Where, $\varphi(t)$ is the regression vector, θ is unknown parameters vector, f nonlinear function which is realized by the neural network and y_p is the predicted output based on the unknown parameter vector θ.

In this work, the prediction error method (PEM) is used to evaluate the performance of the network training algorithm (or estimated model) , the PEM is defined by following equation :

$$\varepsilon(t,\theta) = y(t) - y_p\,(t/\theta) \tag{3.15}$$

$y(t)$ is the observed output of the system.

The loss function (L_N) is a common method used in system identification to minimize the prediction error equation (3.15).This function can be written as follows:

$$L_N(\theta, Z^N) = \frac{1}{N}\sum_{t=1}^{N}\left(y(t) - y_p\,(t/\theta)\right)^2 \quad (3.16)$$

Where Z^N refers to the training data set

3.7 Model Validation

The model validation is step which involves verifying whether the model accurately represents the studied system using the comparison between the measured data and predicted outputs data of the system until the best model is reached. Based on this work, we will use some criterions such as the mean square error (MSE), the best fit to the estimation and validation data (fit %) and the final prediction error (FPE) [46][47]:

3.7.1 Mean Square Error

The mean square error criterion (MSE) is often used for model validation, is a measure in a single positive number of how well the model output fits the measured data, it is given by [48]:

$$MSE = \frac{1}{N}\sum_{t=1}^{N}\left(y(t) - y_p\,(t)\right)^2 \quad (3.17)$$

3.7.2 Best Fit Criterion

The fit percentage (fit %) is a statistical measure of how well a predicted output matches with the measured output. The percentage of fit was used as criterion for selecting both of best nonlinear and linear models to represent the studied system. The best fit is given by [1]:

$$Best\ fit(\%) = \left(1 - \frac{|y - y_p|}{|y - \bar{y}|}\right) \times 100 \quad (3.18)$$

Where: y is a measured output, y_p represents the predicted output and $\bar{y}$ is the mean value of the measured output.

3.7.3 Final Prediction Error

The final prediction error (FPE) evaluates quality of the model, where the model is tested on a new data set, the most accurate model has the smallest FPE. The equation of FPE is given by the following equation[46]:

$$FPE = L_N(\theta, Z^N)\left(\frac{1+\frac{n}{N}}{1-\frac{n}{N}}\right) \tag{3.19}$$

Where: $L_N(\theta, Z^N)$ is the loss function of the studied system, n is the total number of estimated data and N is the length of data record.

3.8 Result and Analysis

The objective of this section is to identify a linear MIMO discrete time state space model for the PEMFC 500w stack as following representation:

$$\Sigma_{\mathrm{N}}: \begin{cases} x_N(k+1) = A_N x(k) + B_N u(k) + K_N e(k) \\ y(k) = C_N x(k) + Du(k) + e(k) \\ x(o) = x_N \end{cases} \tag{3.20}$$

$A_N \in \mathbb{R}^{\mathrm{N}\times\mathrm{N}}$ state matrix, $B_N \in \mathbb{R}^{\mathrm{N}\times\mathrm{m}}$ input matrix, $C_N \in \mathbb{R}^{\mathrm{p}\times\mathrm{N}}$ output matrix and $K_N \in \mathbb{R}^{\mathrm{N}\times\mathrm{m}}$ disturbance matrix. $x(k) \in \mathbb{R}^{\mathrm{N}}$ represent the state vector , the model's inputs $[u_1, u_2] = [u_a, u_c]^t$ are hydrogen and oxygen pressures, k= $[I_s]$ is input of disturbance matrix and the model's outputs $[y_1, y_2] = [V_{fc}, i_{fc}]$ are voltage and current.

The outputs of this linear model should be close as possible to measured output data of the nonlinear PEMFC 500W model. That can be achieved by estimating the parameters of matrices ($A_N, B_N, C_N, D, K_N, x_N$), and validating this model by comparing their outputs to the nonlinear model outputs. To accomplish the linear model, the NN-NLARX structure is performed using following steps:

3.8.1 Preparing and Preprocessing of the Data

The first step in identification technique is gathering the inputs-outputs data from simulating the nonlinear dynamical model of the PEMFC stack developed and validated in previous chapter. The simulation is carried out using programming matlab with four input-output data at different values of u_a , u_c , V_{fc} and i_{fc} , these data are used as training data sets for NN-NLRAX modelling . Each set consists of 500 data samples of each input variable. The values utilized for the input variables are: u_a is varied from 0.5 atm to 2 atm, u_c is varied from 0.25 atm to 1 atm, V_{fc} is varied from 39.75 volts to 24.98 volts and i_{fc} is varied from 0.2A to 25A. Overall, 2000 data points are used to train the model for the PEM fuel cell's outputs voltage/current.

All these measured data need to be preprocessing before start the identification process, where it collect the input and the output in one object at sampling time of $T_s = 0.2\ s$. Then, remove the means or detrending values from measured data and split the detrended data (or processed data) into estimation (ze) and validation data (zv).

3.8.2 Neural Network Estimation of PEMFC 500W Stack

The most important parameters used to create the nonlinearities (f) of the NN-NLRAX structure are time sampling $[T_s]$, standard regressors corresponding to the orders $[n_a, n_b, n_k]$ and hidden layers size for neural network $[h_1, h_2, h_3]$. The Levenberg-Marquardt back propagation algorithm is used for training, which is performed in the neural network toolbox of MATLAB. Table (3.1) shows the effect of the standard regressors and the number of units in the hidden layers on models fit for estimation data (ze) and validation data (zv) of the eighteen for NN-NLRAX models.

Table 3. 1 Effect of the number of units in the hidden layers and the regressors on ze and zv of NN-NLRAX models

Regressors	Hidden layers [2 4 2]		Hidden layers [2 5 2]		Hidden layers [2 6 2]	
	Model Fit(%)		Model Fit(%)		Model Fit(%)	
	ze $\begin{pmatrix} y_1\% \\ y_2\% \end{pmatrix}$	zv$\begin{pmatrix} y_1\% \\ y_2\% \end{pmatrix}$	ze $\begin{pmatrix} y_1\% \\ y_2\% \end{pmatrix}$	zv$\begin{pmatrix} y_1\% \\ y_2\% \end{pmatrix}$	ze $\begin{pmatrix} y_1\% \\ y_2\% \end{pmatrix}$	zv$\begin{pmatrix} y_1\% \\ y_2\% \end{pmatrix}$
na=[2 2, 2 2] nb=[2 2, 2 2] nk=[1 1, 1 1]	100% 100%	79.87% 99.87%	100% 100%	77.07% 99.92%	100% 100%	77.08% 99.82%
na=[2 0, 2 0] nb=[0 2, 0 2] nk=[1 1, 1 1]	100% 100%	79.87% 99.87%	100% 100%	77.07% 99.92%	100% 100%	77.08% 99.82%
na=[2 0, 2 0] nb=[2 2, 0 0] nk=[1 1, 1 1]	99.97% 99.97%	76.94% 98.82%	99.99% 99.98%	76.89% 98.88%	100% 100%	76.87% 98.93%
na=[2 2, 2 2] nb=[2 2, 0 0] nk=[1 1, 1 1]	52.17% 53.23%	-23.7% 9.29%	100% 100%	76.84% 99.93%	88.7% 35%	50.95% -274%
na=[1 2, 1 2] nb=[2 2, 0 0] nk=[1 1, 1 1]	99.98% 100%	76.74% 99.86%	99.9% 100%	76.91% 99.89%	-1613% $-1.83e+004\%$	-1026% $-1.3e+004\%$
na=[1 2, 1 2] nb=[0 2, 1 2] nk=[1 1, 1 1]	-131% 79.1%	$-7.8e+010\%$ $-2.9e+009\%$	99.9% 100%	77.08% 99.79%	99.9% 100%	77.02% 99.99%

The best fit of estimation data and validation data for 1^{st}, 2^{sd} and 3^{th} models with different numbers of units in the hidden layers and different regressors are more accurate than 4^{th}, 5^{th} and 6^{th} models , where these percentage fits are ranging from 99.9%-100% for estimation data and 76.8%-99.9% for validation data. Note that, the models with hidden layer [2 5 2] at different regressors have a good fit compared with other models. Table (3.2) shows the loss function results for nonlinear regressors using NN-NLARX with different hidden layers of nonlinearity estimator (cascade-

forward neural network). And the table (3.3) shows the mean square error (MSE) performance for training of each neural network model.

Table 3. 2 Loss function for NLRAX structures with neural network estimator

Regressors	Loss Function (L_N)		
	Hidden layers [2 4 2]	Hidden layers [2 5 2]	Hidden layers [2 6 2]
na=[2 2, 2 2] nb=[2 2, 2 2] nk=[1 1, 1 1]	8.8199e-024	2.8463e-026	1.2516e-027
na=[2 0, 2 0] nb=[0 2, 0 2] nk=[1 1, 1 1]	3.6166e-023	3.1415e-028	1.2714e-021
na=[2 0, 2 0] nb=[2 2, 0 0] nk=[1 1, 1 1]	2.7788e-018	5.5713e-019	1.3939e-021
na=[2 2, 2 2] nb=[2 2, 0 0] nk=[1 1, 1 1]	2.0132e-022	2.6781e-028	1.2648e-022
na=[1 2, 1 2] nb=[2 2, 0 0] nk=[1 1, 1 1]	1.1935e-024	1.5523e-023	4.0859e-023
na=[1 2, 1 2] nb=[0 2, 1 2] nk=[1 1, 1 1]	1.4162e-024	1.1796e-023	4.9611e-025

Table 3. 3 MSE performance for model structures with neural network estimator

Regressors	Mean square error (MSE)		
	Hidden layers [2 4 2]	Hidden layers [2 5 2]	Hidden layers [2 6 2]
na=[2 2, 2 2] nb=[2 2, 2 2] nk=[1 1, 1 1]	2.4478e-012	1.506e-014	3.9885e-015
na=[2 0, 2 0] nb=[0 2, 0 2] nk=[1 1, 1 1]	2.4029e-014	8.701e-017	8.005e-011
na=[2 0, 2 0] nb=[2 2, 0 0] nk=[1 1, 1 1]	2.2745e-010	6.7991e-009	2.137e-010
na=[2 2, 2 2] nb=[2 2, 0 0] nk=[1 1, 1 1]	2.4029e-014	8.701e-017	8.005e-011
na=[1 2, 1 2] nb=[2 2, 0 0] nk=[1 1, 1 1]	7.828e-015	4.5741e-015	4.2932e-013
na=[1 2, 1 2] nb=[0 2, 1 2] nk=[1 1, 1 1]	4.8497e-015	2.837e-014	3.289e-015

From observation results of both tables , the model which has the smallest value of loss function (L_N) of about 2.6781e-028 has regressors ([2 2, 2 2],[2 2, 0 0], [1 1, 1 1]) and at hidden layers size [2 5 2]. Whilemean, the models which have the smallest value of MSE of about 8.701e-017 has regressors (([2 0, 2 0],[0 2, 0 2], [1 1, 1 1]) and ([2 2, 2 2],[2 2, 0 0], [1 1, 1 1]) at hidden layers size [2 5 2].

In order to know which regressions and hidden layers are suitable for obtaining the best linear model of the PEMFC stack, the six examples of NN-NLRAX models are linearized and presented in the next step.

3.8.3 NN-NLRAX Model Linearization

By using system SI toolbox in MATLAB, *linapp* command is used to generate the best linear approximation of a NN-NLRAX structure of PEMFC 500W model for a given input signal

technique[42], this command determines the structurally model similar to the original nonlinear PEMFC model and delivers the best fit between a linear model and the corresponding simulated response of the nonlinear model. Table (3.4) shows the best fit for estimation data (ze) and validation data (zv) of the six examples for estimated linear ARX models with different standard regressors and the number of units in the hidden layers.

Table 3. 4 Effect of the number of units in the hidden layers and the regressors on ze and zv for identified linear ARX models

Regressors	Hidden layers [2 4 2]		Hidden layers [2 5 2]		Hidden layers [2 6 2]	
	Model Fit(%)		Model Fit(%)		Model Fit(%)	
	ze $\begin{pmatrix} y_{l1}\% \\ y_{l2}\% \end{pmatrix}$	zv$\begin{pmatrix} y_{l1}\% \\ y_{l2}\% \end{pmatrix}$	ze $\begin{pmatrix} y_{l1}\% \\ y_{l2}\% \end{pmatrix}$	zv$\begin{pmatrix} y_{l1}\% \\ y_{l2}\% \end{pmatrix}$	ze $\begin{pmatrix} y_{l1}\% \\ y_{l2}\% \end{pmatrix}$	zv$\begin{pmatrix} y_{l1}\% \\ y_{l2}\% \end{pmatrix}$
na=[2 2, 2 2] nb=[2 2, 2 2] nk=[1 1, 1 1]	79.98% 98.52%	55.19% 97.71%	94.11% 99.88%	87.32% 99.93%	84.23% 98.89%	84.19% 99.22%
na=[2 0, 2 0] nb=[0 2, 0 2] nk=[1 1, 1 1]	93% 99.72%	88.05% 99.91%	26.4% 99.84%	−97.79% 99.53%	0.861% 95.11%	−100.9% 88.12%
na=[2 0, 2 0] nb=[2 2, 0 0] nk=[1 1, 1 1]	92.86% 97.22%	88.41% 97.12%	92.6% 96.92%	88.4% 95.24%	93.73% 94.69%	87.19% 95.02%
na=[2 2, 2 2] nb=[2 2, 0 0] nk=[1 1, 1 1]	$-9.18e+005\%$ $-1.65e+006\%$	−1964% −2618%	45.46% 20.68%	32.63% 87.94%	−26.38% −691.2%	12.12% −340.7%
na=[1 2, 1 2] nb=[2 2, 0 0] nk=[1 1, 1 1]	−214% 64.63%	−266.3% 89.28%	−13.11% −23.86%	−101.8% −27.89%	$-4.031e+008\%$ $-4.51e+009\%$	−2217% $-2.66e+004\%$
na=[1 2, 1 2] nb=[0 2, 1 2] nk=[1 1, 1 1]	$-6.99e+29\%$ $-2.59e+28\%$	$-5.42e+010\%$ $-2.01e+009\%$	46.75% 99.91%	84.67% 99.99%	93.13% 99.77%	88.42% 99.89%

Note that, the best fit of estimation data and validation data for models at regressors ([2 0, 2 0], [2 2, 0 0],[1 1,1 1]) with different numbers of units in the hidden layers are more accurate than other

models , where these percentage fits are ranging from 92.6%-97.2% for estimation data and 87.1%-97.1% for validation data. Table 3.5 shows both of the loss function L_N and final prediction error FPE results for estimated parameter using ARX models from estimation data (ze)

Table 3. 5 L_N and FPE results for estimated using ARX from data set

Regressors	Hidden layers [2 4 2]		Hidden layers [2 5 2]		Hidden layers [2 6 2]	
	L_N	FPE	L_N	FPE	L_N	FPE
na=[2 2, 2 2] nb=[2 2, 2 2] nk=[1 1, 1 1]	3.14997e-007	3.41877e-007	7.89975e-008	8.5738e-008	1.4940e-008	1.6215e-008
na=[2 0, 2 0] nb=[0 2, 0 2] nk=[1 1, 1 1]	2.06131e-007	2.14926e-007	4.50597e-008	4.69e-008	1.0425e-005	1.0679e-005
na=[2 0, 2 0] nb=[2 2, 0 0] nk=[1 1, 1 1]	2.52083e-007	2.62839e-007	5.6797e-007	5.9220e-007	3.7879e-007	3.9495e-007
na=[2 2, 2 2] nb=[2 2, 0 0] nk=[1 1, 1 1]	6.13873e-007	6.53161e-007	1.48369e-008	1.5786e-008	8.2196e-007	8.7456e-007
na=[1 2, 1 2] nb=[2 2, 0 0] nk=[1 1, 1 1]	2.42554e-008	2.5549e-008	1.90345e-007	2.0049e-007	9.2660e-006	9.7602e-006
na=[1 2, 1 2] nb=[0 2, 1 2] nk=[1 1, 1 1]	8.01107e+045	8.48105e+045	4.63208e-009	4.9038e-009	2.6004e-007	2.7529e-007

It can be seen that, the selected models with hidden layers [2 5 2] have best loss function L_N and FPE values. Where, the smallest value of loss function is 1.48369e-008 which is given by model at regressors ([2 2, 2 2], [2 2, 0 0], [1 1, 1 1]) , and the smallest value of FPE is 4.9038e-009 which is given by model at regressors ([1 2, 1 2], [0 2, 1 2], [1 1, 1 1]). Figures (3.8)-(3.9)-(3.10) show predicted outputs results of optimized nonlinear (nlsys) and linear (sys1) models for estimation (ze2) and validation data (zv2) at regressors ([2 0, 2 0], [2 2, 0 0], [1 1, 1 1]) with different hidden layers [2 4 2], [2 5 2] and [2 6 2] respectively.

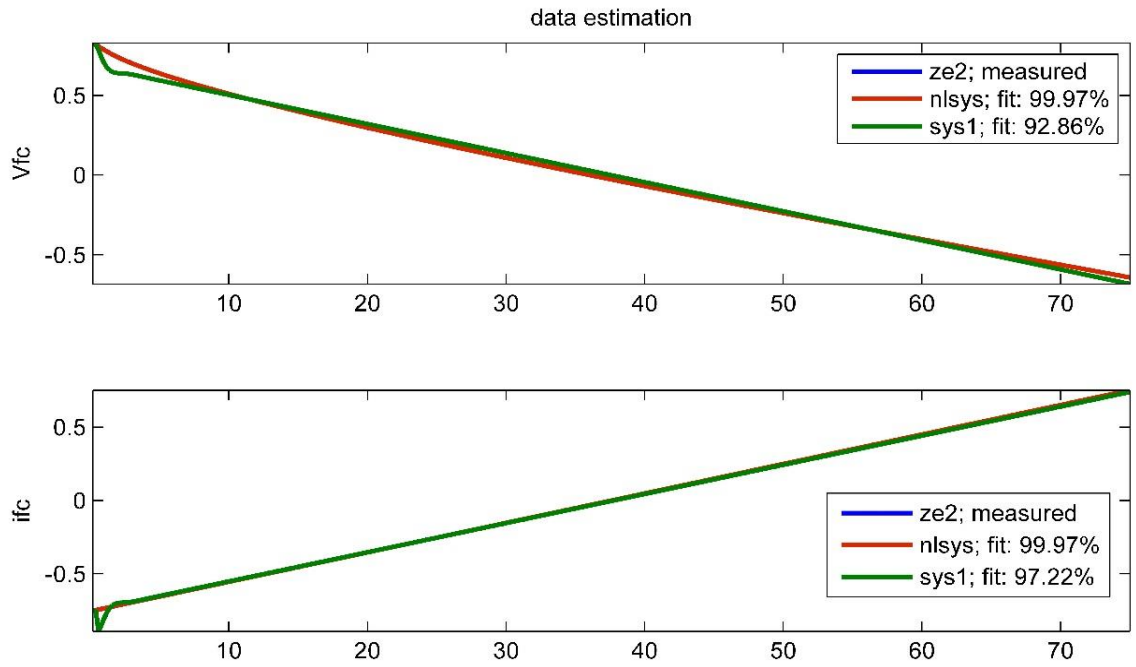

(a) Data estimation

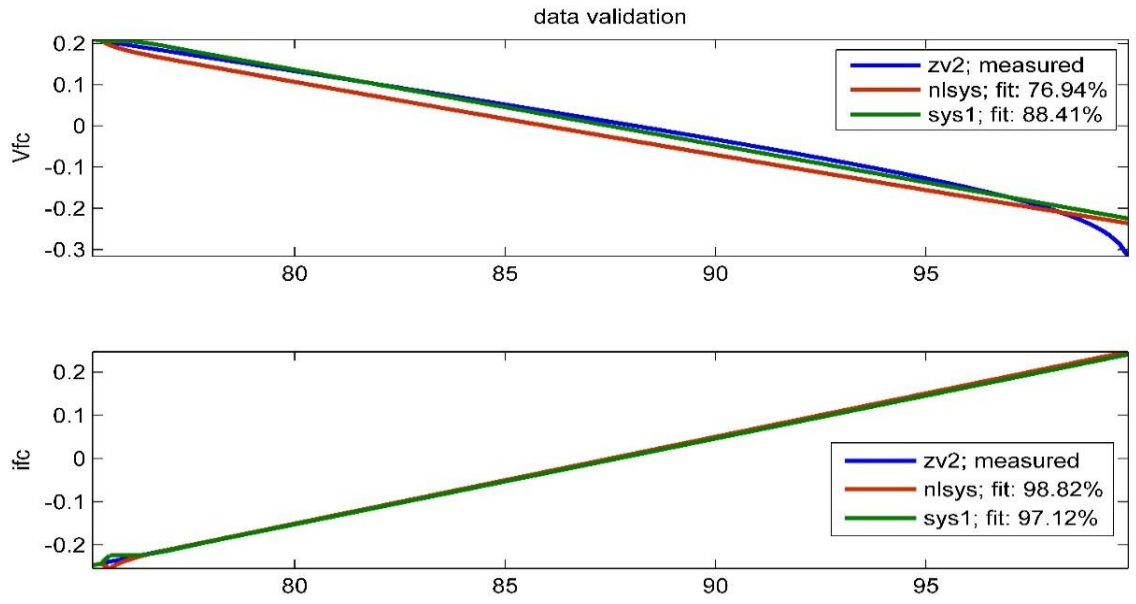

(b) Data validation

Figure 3.8 (a) Data estimation , (b) Data validation of predicted outputs model for ([2 0, 2 0], [2 2, 0 0], [1 1, 1 1] at [2 4 2].

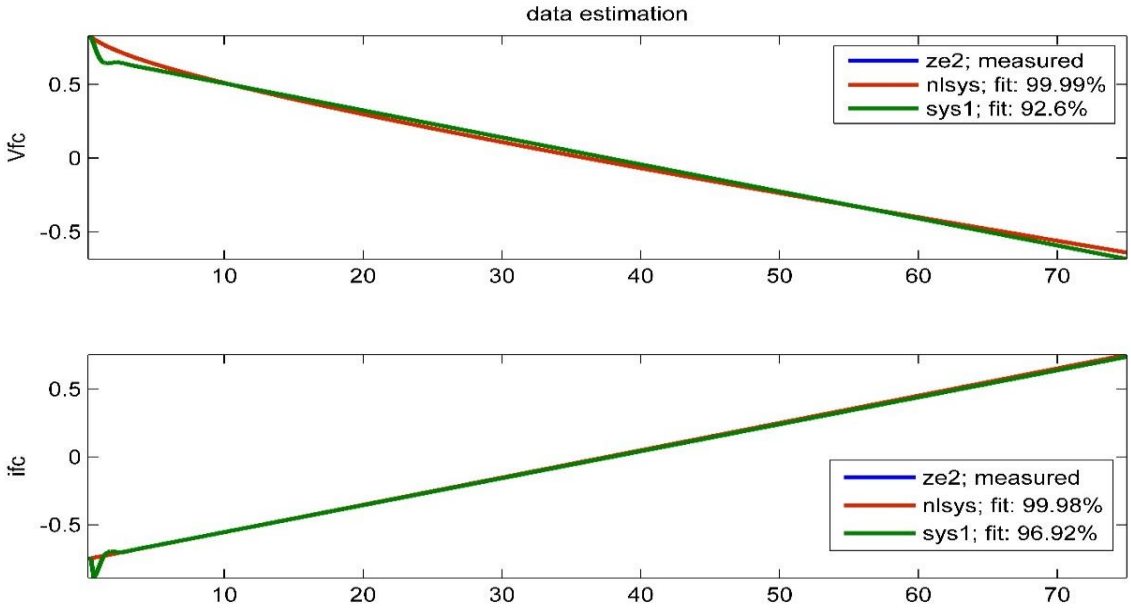

(a) Data estimation

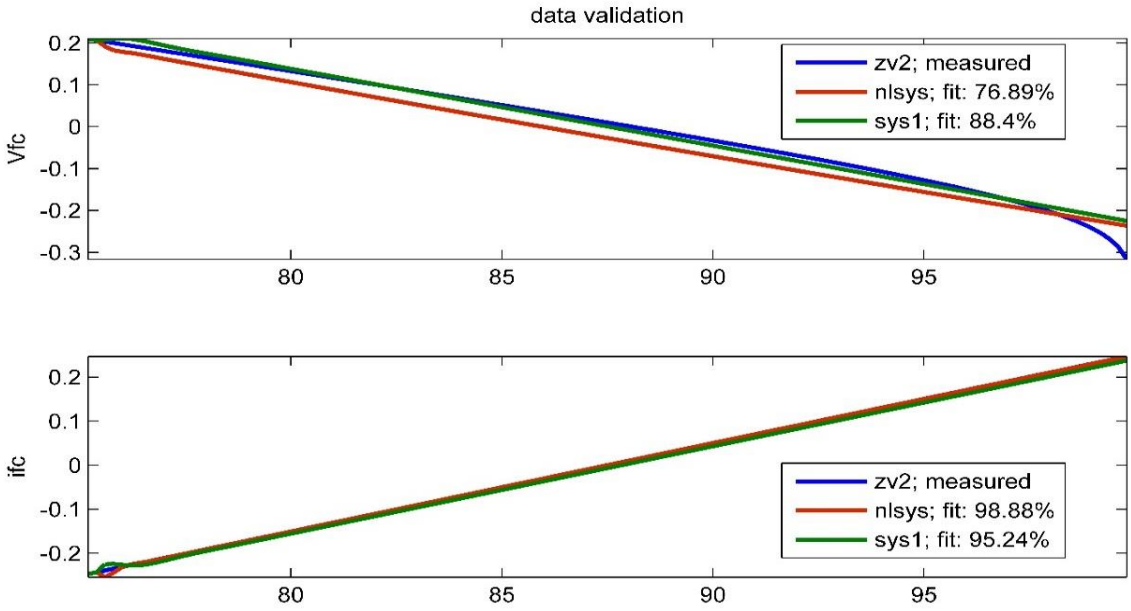

(b) Data validation

Figure 3.9 (a) Data estimation , (b) Data validation of predicted outputs model for ([2 0, 2 0], [2 2, 0 0], [1 1, 1 1] at [2 5 2].

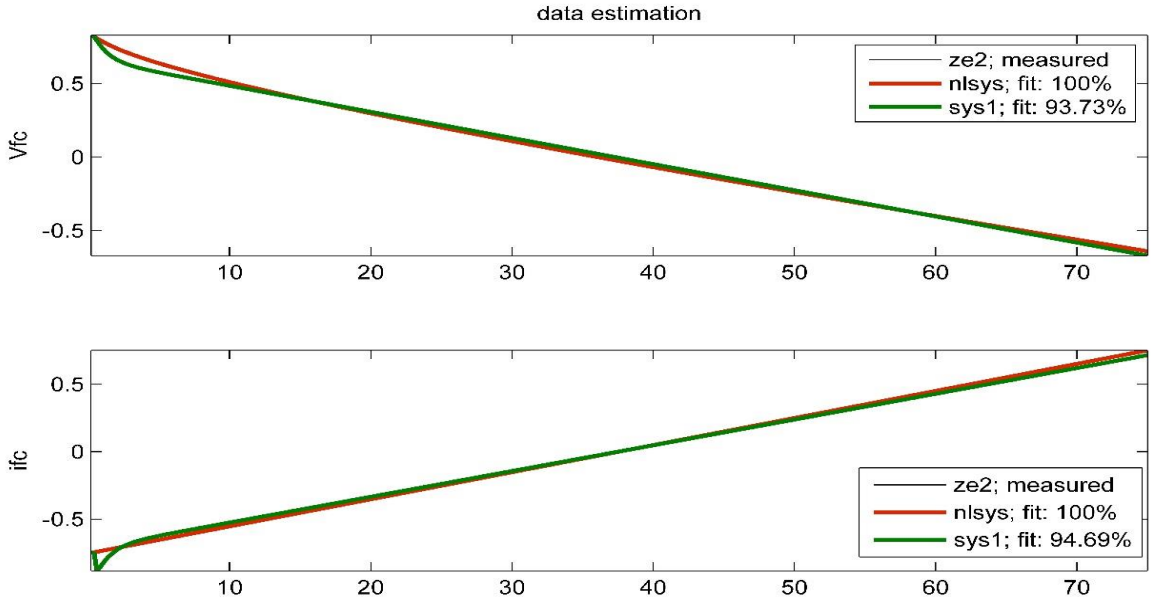

(a) Data estimation

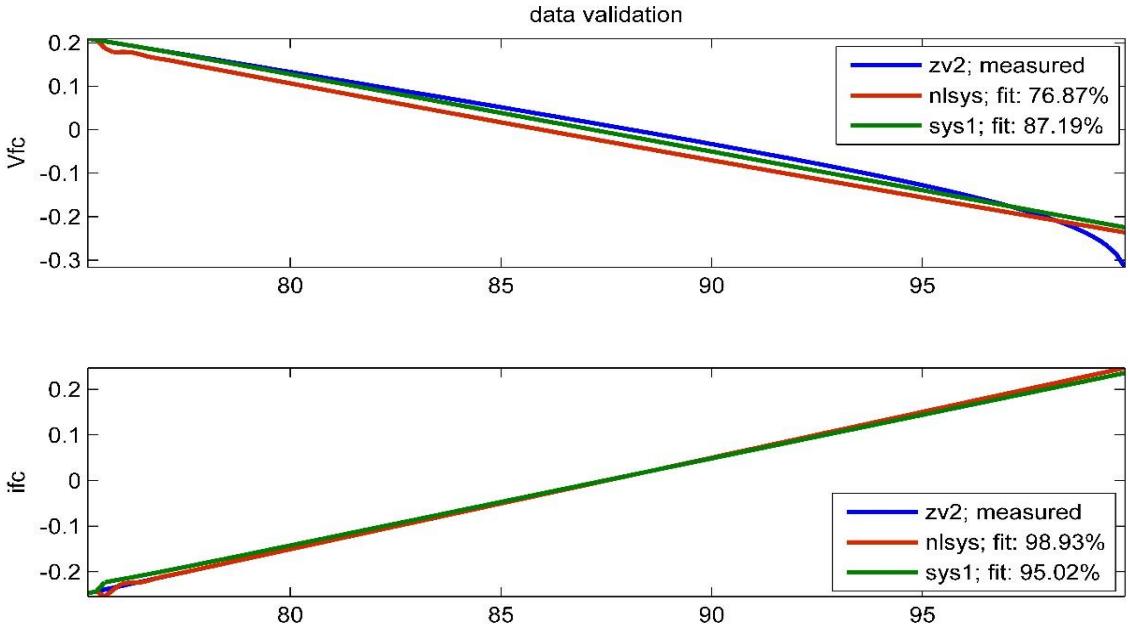

(b) Data validation

Figure 3.10 (a) Data estimation, (b) Data validation of predicted outputs model for ([2 0, 2 0], [2 2, 0 0], [1 1, 1 1] at [2 6 2].

Note that, the data estimation and data validation for both linear and nonlinear models of all previous figures are close much to set data of the initial PEMFC model. Where the percentage fits of estimation data are ranging from 99.9%-100% for nonlinear models and 92.6%-97.22% for linear models, for validation data the percentage fits are ranging from 76.87%-98.93% for nonlinear models and 87.19%-97%for linear models.

To find out which linear model is closest to the nonlinear PEMFC model , the step responses of three models were traced with different hidden layers [2 4 2], [2 5 2], [2 6 2] at regressors ([2 0, 2 0], [2 2, 0 0], [1 1, 1 1]) as shown in following figures .

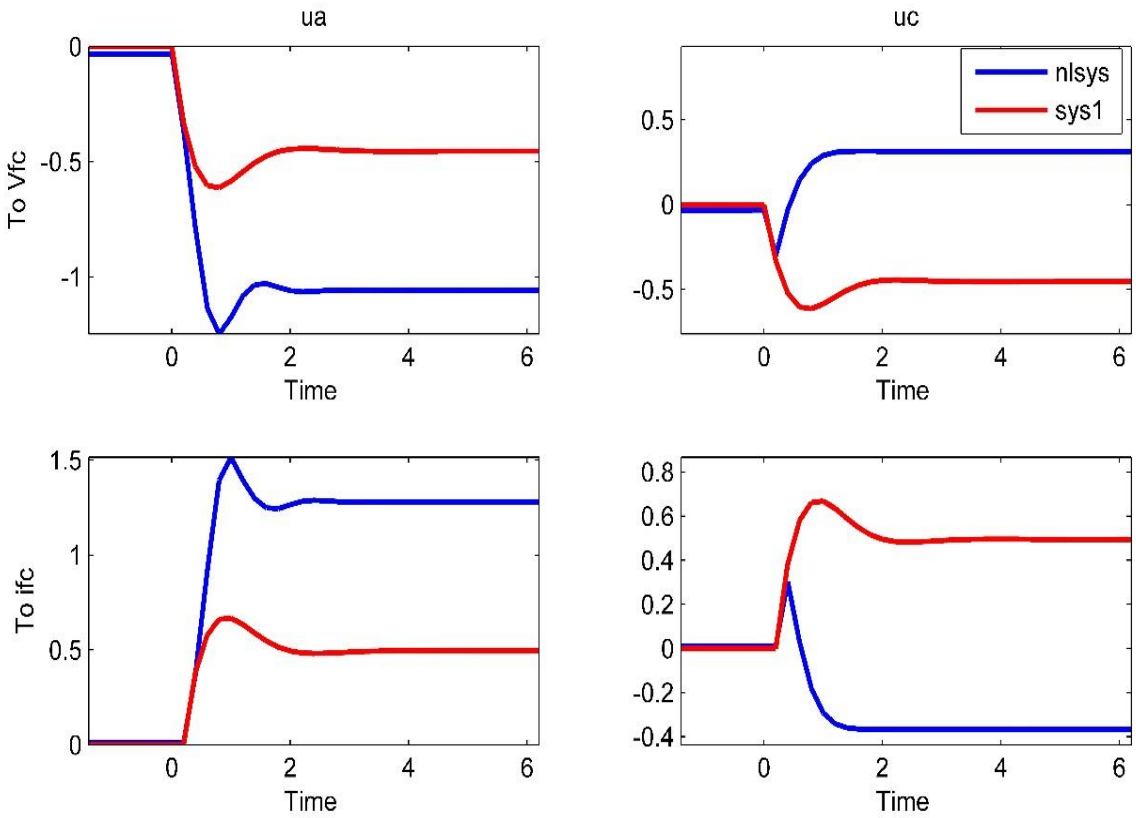

Figure 3.11 Step responses of linear and nonlinear models with hidden layers [2 4 2]

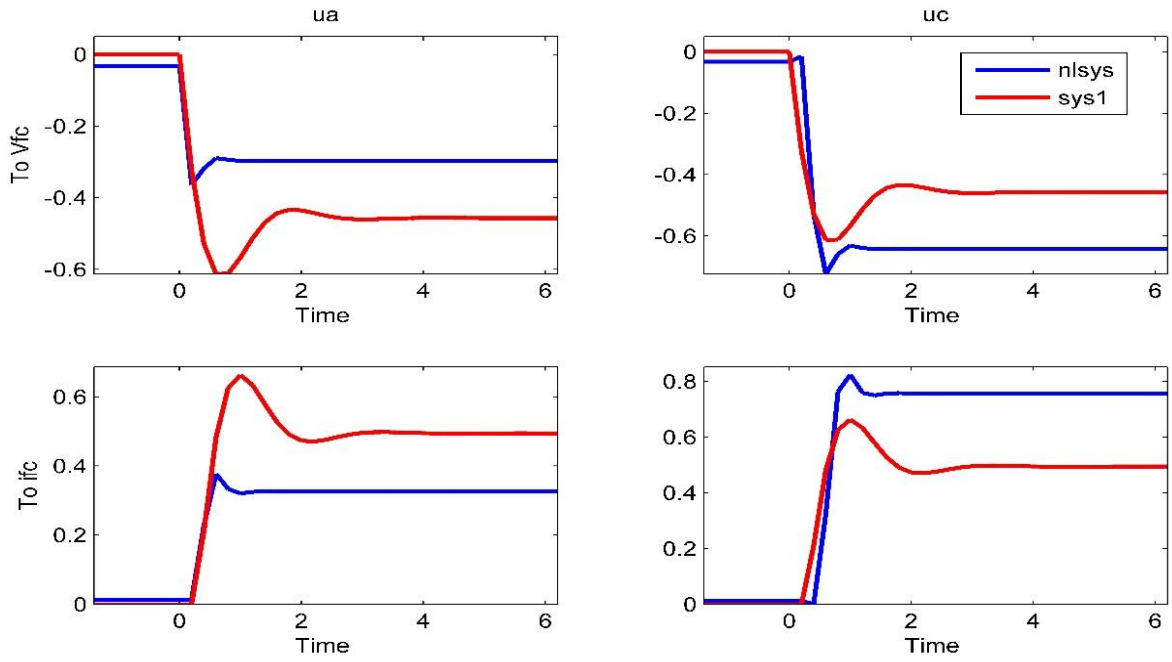

Figure 3.12 Step responses of linear and nonlinear models with hidden layers [2 5 2]

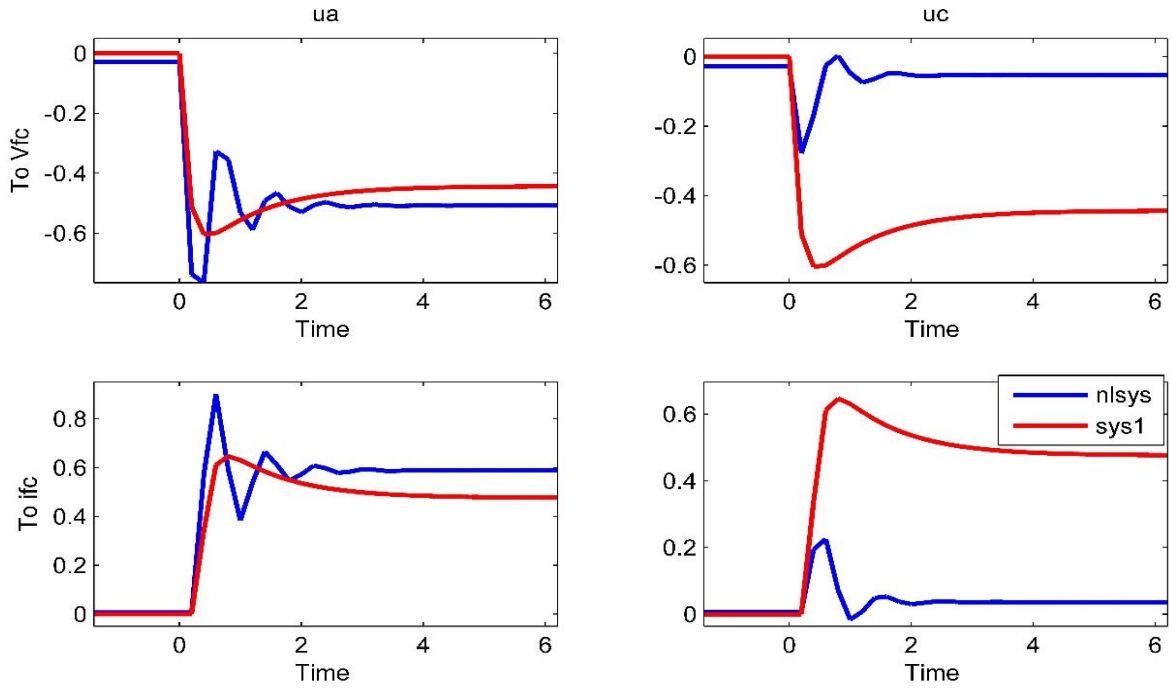

Figure 3.13 Step responses of linear and nonlinear models with hidden layers [2 6 2]

From the figure (3.12), the step response of the linear PEMFC model with layer size [2 5 2] is very close to the nonlinear model compared with the step responses of models [2 4 2] and [2 6 2] in figures (3.11)-(3.13).Hence, accordingly of equation (3.20), the values of the space state matrices (A_N, B_N, C_N,D, K_N , x_N) for the linear PEMFC 500W model with layer size [2 5 2] at regressors ([2 0, 2 0], [2 2, 0 0], [1 1, 1 1]) are given by following:

A_N = [1.2291 0 -0.5141 0 -0.3237 -0.3237 0.1935 0.1935
-0.6438 0 -0.4385 0 -0 0 0 0
1 0 0 0 0 0 0 0
0 1 0 0 -0 0 0 0
0 0 0 0 0 0 0 0
0 0 0 0 0 0 0 0
0 0 0 0 1 0 0 0
0 0 0 0 0 1 0 0]

$B_N = [0 \quad 0; 0 \quad 0; 0 \quad 0; 0 \quad 0; 1 \quad 0; 0 \quad 1; 0 \quad 0; 0 \quad 0]^t$

C_N = [1.2291 0 -0.5141 0 -0.3237 -0.3237 0.1935 0.1935
-0.6438 0 -0.4385 0 0.0000 0.0000 -0.0000 -0.0000]

D =1.0e-016 *[0.8327 0.2776; -0.2776 -0.0694]

K_N =1.0e-015 *[0.0264 -0.0402; -0.0402 0.2147;0.0333 -0.1451; -0.0397 0.1644;
0 0; 0 0; 0 0; 0 0]^t

x_N =[0; 0; 0; 0; 0; 0; 0; 0]^t

Eigenvalues:$\lambda_1 = 0,\ \lambda_2 = 0, \lambda_{3,4} = 0.6146 \pm 0.3693\, i, \lambda_5 = 0\ , \lambda_6 = 0\ , \lambda_7 = 0\ , \lambda_8 = 0$

Note that, the neural network of the selected model with three hidden layers [2 5 2] has satisfying results of percentage fit, loss function and finale prediction error for both linear and nonlinear

models which are compared with data set of PEMFC 500W stack. For the regressors of the linear and nonlinear models, the selected model with the regressors([2 0, 2 0], [2 2, 0 0], [1 1, 1 1]) shows a high similarity to the original nonlinear model and delivers the best fit between a given data set and the corresponding simulated step responses of the nonlinear model. Finally, the linear state space model for PEMFC stack is obtained in order to reduce it in last chapter of this dissertation .

3.9 Conclusion

In this chapter, a nonlinear autoregressive exogenous (NLARX) model of a PEMFC 500-W is developed using a cascade-forward neural network. This model shows that, the nonlinear dynamics of the PEM fuel cell can be effectively modeled using three hidden layers neural network. This neural network was trained using the data set which were generated by implementing the nonlinear state space model of the PEM fuel cell using Matlab Environment Programming .then, the obtained model was linearized to get the linear space state matrices of the PEM fuel cell. Based on the percentage of models fit, the result shows that, the linear and nonlinear models have a nearly similar trend of outputs data of the PEMFC stack. Overall, the NN-NLRAX and ARX structures with neural network estimator are capable in representing the PEMFC stack under tests. In conclusion, the results of the best ARX and NN-NLARX models are given by regressors na =[2 0,2 0] , nb = [2 2,0 0], and nk = [1 1,1 1] and three hidden layers [2 5 2], where, the best fit of the nonlinear model is given by : $y_1 = 99.99\ \%$, $y_2 = 99.99\%$ for estimation data and $y_1 = 76.89\%$, $y_2 = 98.88\%$ for validation data , the loss function is 5.5713e-019 and MSE performance for nonlinear model structures with neural network estimator is 6.7991e-009. For the linear model, the best fit is given by : $y_1 = 92.6\%$, $y_2 = 96.92\%$ for estimation data and $y_1 = 88.4\%$, $y_2 = 95.24\%$ for validation data, the loss function is 5.6797e-007 and the final prediction error FPE is 5.9220e-007.

Chapter 4

Model Order Reduction Literature

Chapter 4 Model Order Reduction Literature

4.1 Introduction

Nowadays, simulation or computational science has become an important part in the technological world, due to the increasing interest of engineers and designers for realistic simulations of real systems such as telecommunication systems, civil engineering, aerospace engineering, chemical reactors, mechanical and Micro-Electro-Mechanical Systems (MEMS), that through set up virtual design environments for a variety of problem classes in order to ease the work of those designers and engineers. To achieve the accurate and viable simulation, a modeling process is required first to understand and analyze the real behaviors of these systems.

To realize an accurate model, it is necessary to express the behavior of the real systems with an ordinary or partial differential equations. The more complex systems is and the more accurate the models is, the higher order of the corresponding differential equations should be. To model a physical behavior with a good accuracy, a high order differential equation is unavoidable. As a result, complex large scale systems require high order models to represent them well. These high models are used to solve an engineering problem that is a time consuming task or may lead to difficulties finding a satisfactory result. In the control engineering fields, designing a controller for a complex systems is difficult and if we are able to find a solution using a modern control technique like robust control, the controller would have an order the same as the original system posing difficulties in controller implementation. Simulation and analysis of a high order models is also difficult or even impossible[49].

To solve all preceding difficulties in both areas of simulation and design of controllers, a low order model must be found to approximate the high order original model figure (4.1). For simulation task, the reduced order model is achieved directly after the modeling step, while in controller design, reducing the original system can be done before designing or simultaneously with controller design where the reduction is done on the controller by considering the performance of the closed loop system [49].

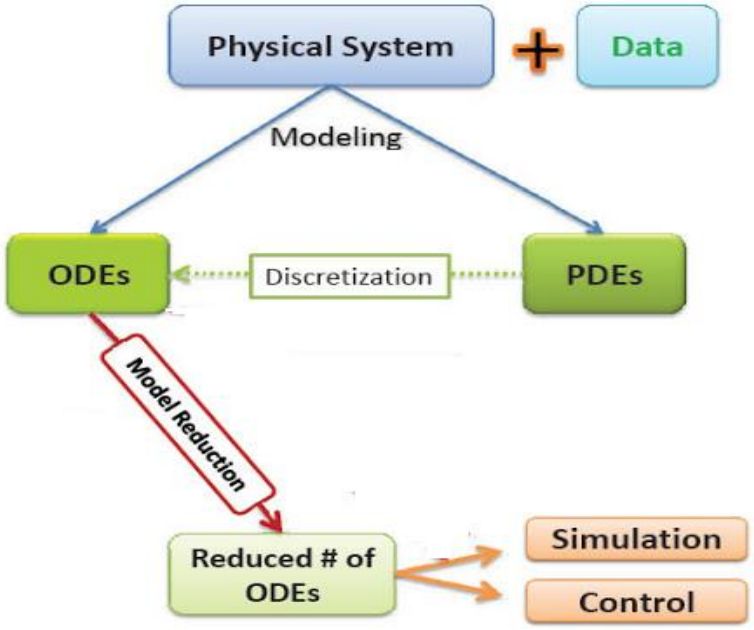

Figure 4.1 Overall picture of model order reduction

4.2 Model Order Reduction

Model order reduction (MOR) was developed in the field of systems and control literature, which studies the properties of dynamical systems in order to reduce their complexity (or simplification), while preserving their input-output behavior as much as possible. Such reduction is necessary in order to perform simulations within an acceptable time interval and limited capacity of storage with reliable results.

The MOR techniques attempt to capture the essential features of an original structure. Which means that in an early stage of the reduction process, the most basic characteristics of the original system must already be present in the reduced model. At a certain moment the process of reduction is stopped. At that point all necessary properties of the original model must be captured with sufficient precision. All of this has to be done automatically[2].

The advantages of low order models can be summarize in the following properties:

1. ***Simple simulation*:** usually the simulation of order reduced model shows adequately the important dynamics of the original system, leading to control the complex systems in real time in addition to their implementation in simple hardware.
2. ***Simplicity of design and control*:** in designing the large-scale systems feedback, the high order control laws become in complex feedback structures leading to difficulties in controller implementation therefore these structures should be simplified by reduced models in order to form the low order control laws.
3. ***Lower computational*:** the computational requirements on reduced models will be much lower since computation time and complexity than on complex models.

To put the model reduction in a mathematical context, we need to understand that many models developed in computational science consist of a system of differential equations (partial and/or ordinary), supplemented with boundary conditions. For example, in electromagnetic systems (EM) the Maxwell equations are needed, and in computational fluid dynamics (CFD) the equations of Navier-Stokes are used. These dynamics equations can be expressed and gathered in form algebraic as following [50]:

$$\Sigma_{\mathrm{N}} = \begin{cases} \dot{x_N}(t) = f_N(x_N, u) \\ y = h_N(x_N, u) \end{cases} \tag{4.1}$$

Where: N is the order of original system or number of state, $x \in \mathbb{R}^N$ is the state, $u \in \mathbb{R}^m$is the input, $y \in \mathbb{R}^p$ is the output or set observations, f describes the dynamics of Σ_{N} and h describes the way in which the observations are derived from the input and state.

The aim of MOR is reducing the order of system N, while preserving the character of the input-output relations. In another meaning, a dynamical system must be found as following representation:

$$\Sigma_{\mathrm{n}} = \begin{cases} \dot{x_n}(t) = f_n(x_n, u) \\ y = h_n(x_n, u) \end{cases} \tag{4.2}$$

If the functions f_N , h_N , $f_n$and h_n are linear operators as special case, so Σ_{N} and Σ_{n} are represented by linear dynamic systems in continuous time as following:

$$\Sigma_{\mathrm{N}}:\begin{cases}\dot{x_N}(t) = A_N x(t) + B_N u(t)\\ y(t) = C_N x(t) + Du(t)\end{cases} \quad (4.3)$$

With transfer function:

$$G_N(s) = C_N(sI_N - A_N)^{-1} B_N + D \quad (4.4)$$

For the discrete time system, Σ_{N} becomes:

$$\Sigma_{\mathrm{N}}:\begin{cases}x_N(k+1) = A_N x(k) + B_N u(k)\\ y(k) = C_N x(k) + Du(k)\end{cases} \quad (4.5)$$

The transfer function $G_N(z)$ is given by:

$$G_N(z) = C_N(zI_N - A_N)^{-1} B_N + D \quad (4.6)$$

Where $A_N \in \mathbb{R}^{\mathrm{N\times N}}$ is the state matrix, $B_N \in \mathbb{R}^{\mathrm{N\times m}}$ and $C_N \in \mathbb{R}^{\mathrm{p\times N}}$ are input, output matrices respectively. The reduced-order model in continuous time is given by:

$$\Sigma_{\mathrm{n}}:\begin{cases}\dot{x_n}(t) = A_n x_n(t) + B_n u\,(t)\\ y_n(t) = C_n x_n(t) + Du(t)\end{cases} \quad (4.7)$$

Its transfer function:

$$G_n(s) = C_n(sI_n - A_n)^{-1} B_n + D \quad (4.8)$$

The reduced-order model in discrete time is given by following:

$$\Sigma_{\mathrm{n}}:\begin{cases}x_n(k+1) = A_n x_n(k) + B_n u(k)\\ y_n(k) = C_n x_n(k) + Du(k)\end{cases} \quad (4.9)$$

Its transfer function:

$$G_n(z) = C_n(zI_n - A_n)^{-1} B_n + D \quad (4.10)$$

Where $x_n \in \mathbb{R}^n$, $A_n \in \mathbb{R}^{\mathrm{n\times n}}$, $B_n \in \mathbb{R}^{\mathrm{n\times m}}$ and $C_n \in \mathbb{R}^{\mathrm{p\times n}}$ and n is the order of the reduced model (or number of states), it should be smaller than the order of the original system, i.e. $n \ll N$. With the input/output behavior of the original complex system is approximated by the input/output the reduced system behavior. The quality of this approximation could be measured by the closeness of the transfer functions [51]i.e.

$$\|G_N - G_n\| < \varepsilon \quad (4.11)$$

For a given accuracy ε and a suitable norm.

In order to evaluate the quality of the reduced order model, the following conditions should be satisfied [2]:

- The approximation error should be small i.e. the existence of a global error bound.
- Preservation of properties of the original system, such as stability and passivity.
- The procedure of reduction is to be computationally efficient.

There are several approaches for model order reduction can be found in control theory. In this chapter, some classical methods for linear and nonlinear systems are reviewed briefly, some approaches for optimal model reduction, in addition to meta-heuristic techniques.

4.3 Classical methods

4.3.1 Model order reduction for linear systems

Model reduction methods for linear systems are quite well-advanced and a variety of techniques can be found in control literature and numerical mathematics. Especially for linear time-invariant (LTI) systems. these methods can be divided in two main classes: those based on gramians such as balanced truncation method which is presented by Moore in 1981[52], the optimal Hankel norm approximation which is proposed by Glover in 1984[53] and the singular perturbation approximation that is appeared by Lui in 1989 [54]. This class of reduction focused on the approximation of input-output behavior of complex systems by others lower order models with preservation the main properties of original system like stability, controllability, observability and the existence of a computable error bound. The main disadvantages of this class is high computation cost of extracting the reduced models, associated with expensive solution of Lyapunov equations, and applicability of truncated balancing realization method for more complex systems is limited [55].

The second class based on Krylov subspace approaches which are considered as numerically robust algorithms for generating reduced order model through construction the projection bases (subspace) using moment matching techniques, where the transfer function of the reduced system approximates well the original transfer function around a specified moments, there are many of Krylov-based MOR methods have been developed in the field of numerical

mathematics, including approaches based on Lanczos algorithm such as Asymptotic waveform evaluation [56] and Padé Approximation [57] proposed by Gallivan in 1995, another approach based on Arnoldi algorithm instead of those of Lanczos was published by Odabasioglu in 1997[58] .The last type of Krylov-based approximation method is tangential interpolation which is proposed by K. Gallivan in 2004[59], this technique applied instead Lanczos or Arnoldi algorithms for complex MIMO systems. In general, the main disadvantages of those methods are, no guarantees maintain the stability or passivity of the original system, in addition loss the provable of error bounds for the generated reduced models.

4.3.2 Model Order Reduction For Nonlinear Systems

Although the theory of model order reduction for nonlinear systems is limited compared to linear case, but there are many approaches can be found in the literature includes:

Balanced truncation as an extension for nonlinear systems which was presented by Scherpen in 1993 [60] and later it was developed by Fujimoto and Scherpen through finding the relation between the procedure of nonlinear balancing and the nonlinear Hankel operator[61]. In 2002 Lall developed a balancing using empirical gramians method by combine the balanced truncation and proper orthogonal decomposition [62]. The main drawback of these techniques applied to the nonlinear case is that they generally inadequately address the problem of efficient representation of the nonlinearity in the reduced order model. In addition, the cost of evaluating the projected nonlinear operator often remains very high, which severely reduces performance of the corresponding reduced order models [55].

There are other approaches for nonlinear MOR based on linearization (Taylor expansion)[63] or based on Volterra (functional) series expansion [64] of system's nonlinearity. Where the linear part or some of the nonlinear parts in these expansions are employed for construction the Krylov projection to get the reduced order model. The main drawback of those methods is that they generate models valid only locally around the initial operating point of the nonlinear system. This is a result of an inherently local nature of approximation of the nonlinearity by Taylor or Volterra expansion series, and limits application of the discussed MOR methods to weakly nonlinear systems. Also, the trajectory piece-wise linear method (TPWL) which proposed by

Rewiénski in 2003 [55], this approach approximates the nonlinear system by many linear systems piece-wisely at linearization points selected along a relevant trajectory. Each of the linear system is reduced by projection based linear order reduction method or moment matching techniques [65].However, again, no results provable on the existence of error bounds.

4.4 Optimal Model Reduction

The term optimality appeared in 1970 when Wilson used an H_2norm to generate a reduced model which was optimal. This norm was used to minimize the error between the output vector of original model and the reduced one [66] .Lately, different optimal MOR approaches were developed in the context of generating the approximate model based on L_1 norm,H_2 norm and H_∞ norm for complex systems. In this section, all these prominent norms are presented to quantify the size of the approximation error.

4.4.1 Signal Norms

In the control system, using the L_p-norm concept is to quantify measurements of signals size. Due to the existence of the different concepts of signals sizes, there are many kinds of norms that can be defined for these signals. Generally, the mathematical the norm of signal $y(t)$ is defined by following:

$$\|y\|_p = \left(\int_0^\infty |y(t)|^p \, dt\right)^{1/p} \tag{4.12}$$

If $p = 1$, therefore the L_1-norm of a signal $y(t)$ is given by:

$$\|y\|_1 = \int_0^\infty |y(t)| \, dt \tag{4.13}$$

If $p = 2$, The L_2 norm of signal $y(t)$ in equation (4.12) becomes:

$$\|y\|_2 = \left(\int_0^\infty |y(t)|^2 \, dt\right)^{1/2} \tag{4.14}$$

If $p = \infty$, the L_∞ norm of signal $y(t)$ is the maximum of its absolute value:

$$\|y\|_\infty = \max_{t\in\mathbb{R}} |y(t)| \tag{4.15}$$

For y(k) is signal valued infinite sequences, , the mathematical norms are defined as following:

$$\|y\|_p = \left(\sum_k \|y(k)\|^p\right)^{1/p} \tag{4.16}$$

If $p = 1$, therefore the L_1-norm of a sequences $y(k)$ is given by:

$$\|y\|_1 = \sum_k |y(k)| \tag{4.17}$$

If $p = 2$, the L_2 norm of signal $y(k)$ in equation (4.16) becomes:

$$\|y\|_2 = (\sum_k |y(t)|^2)^{1/2} \tag{4.18}$$

If $p = \infty$, the L_∞ norm of signal $y(k)$ is the maximum of its absolute value:

$$\|y\|_\infty = \max_{t\in\mathbb{R}} |y(k)| \tag{4.19}$$

4.4.2 System Norms

System norms are important tools in the system theory, they as measures the size of the systems, for comparing and analyzing. In this section, the system is represented by a transfer function which be defined on frequency domain $\mathbb{C}_\alpha^+ = \{s \in \mathbb{C}: \Re(s) > \alpha\}, \alpha \in \mathbb{R}$ for continuous-time systems, or on $\mathbb{D}_a^+ = \{z \in \mathbb{C} : |z| > a\}, a \in \mathbb{R}_+$ for discrete-time systems.

4.4.2.1 H_2 Norm

The transfer function of the continuous-time system G(s) is considered as analytic function in the open right-half of the complex plane $\mathbb{C}$. (Where $\mathbb{C} = \{s \in \mathbb{C}: \Re(s) > 0\}$ [67]. So, the H_2 norm is define by:

$$\|G\|_{H_2} = \left(\frac{1}{2\pi}\int_{-\infty}^{+\infty} \text{trace}\,[G(j\omega)]^*\,[G(j\omega)]d\omega\right)^{1/2} \tag{4.20}$$

Where: $[G(j\omega)]^*$ is a complex conjugation and transposition of G(jω)

If the analytic function G (z) $\in \mathbb{D}$ (with discrete-time system) where $\mathbb{D} = \{z \in \mathbb{C}: |z| < 1\}$ for $z = e^{i\theta}$, $\theta \in [0, 2\pi]$. So, the H_2 norm of G (z) is define by:

$$\|G\|_{H_2} = \left(\frac{1}{2\pi}\int_0^{2\pi} trace\left[G(e^{i\theta})\right]^*\left[G(e^{i\theta})\right]d\theta\right)^{1/2} \tag{4.21}$$

Literature

For the continuous/discrete-time MIMO system, The transfer function G is a ($p \times m$)-dimensional matrix-valued function with components G_{ij} , $= 1, \dots, p$, $j = 1, \dots, m$:

$$G(.) = \begin{pmatrix} G_{11} & \cdots & G_{1m} \\ \vdots & \ddots & \vdots \\ G_{p1} & \cdots & G_{pm} \end{pmatrix} \tag{4.22}$$

Each G_{ij} is represented as a SISO transfer function, hence the H_2 norm of matrix-valued function G can be interpreted as the energy of the impulse response (the sum of the energies of the impulse responses associated with each transfer G_{ij} in this case),so the H_2 norm of G is given by:

$$\|G\|_{H_2}^2 = \sum_{i=1}^{m} \sum_{j=1}^{l} \|G_{ij}\|_{H_2}^2 \tag{4.23}$$

To calculate H_2 norm of state space representation of continuous-time system (4.3), the controllability and observability grammians ($\mathcal{P}_c, \mathcal{Q}_c$) are used as the unique symmetric positive definite solutions of the following Lyapunov equations[51]:

$$A\mathcal{P}_c + \mathcal{P}_c A^* + BB^* = 0 \tag{4.24}$$

$$A^*\mathcal{Q}_c + \mathcal{Q}_c A + C^*C = 0 \tag{4.25}$$

Where:

$$\mathcal{P}_c = \int_0^\infty e^{At} BB^* e^{A^* t}\, dt \tag{4.26}$$

$$\mathcal{Q}_c = \int_0^\infty e^{A^* t} C^*C\, e^{At} dt \tag{4.27}$$

The H_2 norm of continuous-time system G(s) is given by following:

$$\|G(s)\|_{H_2} = \sqrt{trace(C\mathcal{P}_c C^T)} = \sqrt{trace(B^T \mathcal{Q}_c B)} \tag{4.28}$$

For the discrete-time system, the H_2 norm of state space representation (4.5) used the controllability and observability grammians ($\mathcal{P}_d$, $\mathcal{Q}_d$) as the unique symmetric positive definite solutions of the following Stein equations[51]:

$$A\mathcal{P}_d A^* + BB^* = \mathcal{P}_d \quad (4.29)$$

$$A^*\mathcal{Q}_d A + C^*C = \mathcal{Q}_d \quad (4.30)$$

Where:

$$\mathcal{P}_d = \sum_{j=0}^{\infty} A^j BB^* (A^*)^j \quad (4.31)$$

$$\mathcal{Q}_d = \sum_{j=0}^{\infty} (A^j)^* C^*CA^j \quad (4.32)$$

The H_2 norm of discrete -time system G(z) is given by following:

$$\|G(z)\|_{H_2} = \sqrt{trace(C\mathcal{P}_d C^T)} = \sqrt{trace(B^T\mathcal{Q}_d B)} \quad (4.33)$$

4.4.2.2 H_∞ Norm

We can define the H_∞ as a space of rational functions of a complex variable which are analytic in the close right half plane in $\mathbb{C}$. (Where $\mathbb{C} = \{s \in \mathbb{C}: \Re(s) > 0\}$. So, the H_∞ norm of continuous-time system $G(s)$ defined on this space(i. e. $G(s) \in H_\infty$) is represented by following:

$$\|G(s)\|_{H_\infty} = \max_{\omega \in \mathbb{R}} |G(j\omega)| \quad (4.34)$$

$|G(s)|$ is the gain of system frequency response

For MIMO system H_∞ norm is given by:

$$\|G(s)\|_{H_\infty} = \max_{\omega \in \mathbb{R}} \sigma_{max}(G(j\omega)) \quad (4.35)$$

Where σ_{max} denotes the largest singular value of G(s).

For a discrete-time system G (z) ($z = e^{j\theta}$), the H_∞ norm be:

$$\|G(z)\|_{H_\infty} = \max_{\theta \in [0,2\pi]} \left|G\left(e^{j\theta}\right)\right| \quad (4.36)$$

For MIMO system:

$$\|G(z)\|_{H_\infty} = \max_{\theta \in [0,2\pi]} \sigma_{max}\left(G\left(e^{j\theta}\right)\right) \quad (4.37)$$

To calculate H_∞ norm of state space representations (4.3) or (4.5), the $2n \times 2n$ Hamiltonian matrix is defined as following [68]:

$$H = \begin{bmatrix} A & BB' \\ -C'C & -A' \end{bmatrix} \tag{4.38}$$

According to the theorem in [68], $\|G(z)\|_{H_\infty} < 1$ if the matrix H do not have eigenvalues on the imaginary axis, this theorem suggests following steps to compute the H_∞ of the system G:

1. Select a positive number γ.
2. Test if $\|G(z)\|_{H_\infty} < \gamma$ by calculating the eigenvalues of the appropriate matrix.
3. Increase or decrease γ accordingly and repeat step 2.

4.4.2.3 L_1 Norm

For a linear time invariant system G with input u and output y, where $u(.), y(.) \in L_\infty on[0, \infty)$ and G is an operator mapping $G: L_\infty \rightarrow L_\infty$ .so, the L_1 norm of transfer function G is given by:

$$\|G\|_{L_1} = \sup_{u \in L_\infty} \frac{\|y\|_{L\infty}}{\|u\|_{L\infty}} = \sup_{u \in L_\infty} \left(\frac{\sup \|y\|_2}{\sup \|u\|_2} \right) \tag{4.39}$$

Thus $\|G\|_{L_1}$ is the maximum peak-to-peak gain of G.

4.4.3 H_2 Norm Model Reduction

The optimization problem of minimizing the H_2-norm of the error between the original system and reduced-order model has been an interest subject for researches over the past decades. This problem can be mentioned as follows:

Given a stable complex system (4.3) of dimension N with transfer function G. Create a reduced-order model (4.5) of a fixed dimension n that minimizing the H_2 norm of the reduction error. The minimization problem is considered as following:

$$\text{Minimizing} \qquad \mathcal{J}(G_n) = \|G - G_n\|_{H_2}^2 \tag{4.40}$$

With respect to the variable of optimization $G_n(A_n, B_n, C_n)$

The most common approaches to address this problem are based on projection spaces such as Wilson and Hyland-Bernstein conditions [66] [69], they constructed the projection matrices by observability and reachability gramians to derive H_2 reduced models. In 1999, Yang .et [70] presented an H_2 optimal model reduction for a given multivariable complex system using orthogonal projections. In 2006, Gugercin.et [71] developed an iterative rational Krylov algorithm for finding an optimal H_2 norm model reduction using interpolation based first-order necessary condition. In 2010 Caleb.et[72] applied this algorithm on unstable dynamic system for H_2 optimal model reduction, where this reduced model were hermite interpolants to the original model at the mirror images of stable and unstable the model reduction poles, the results have been illustrated a good performance of proposed method compared to balanced truncation. In 2007 Christopher.et [73] proposed a Krylov-based minimization for H_2 optimal model reduction method using Galerkin projection process for stable SISO linear dynamical system. In 2008 P. Van Doorena .et [74] used tangential interpolation conditions to derive H_2optimal model reduction for MIMO systems, this approach approximate a matrix rational transfer function G(s) of high order by another matrix rational transfer function $\hat{G}(s)$ of much smaller order. A. Bunse-Gerstner .et [75] proposed A MIMO Iterative Rational Interpolation Algorithm (MIRIAm) for discrete-time MIMO system to find a reduced order model which minimizes H_2 norm of approximation error between the original system and the reduced model.

4.4.4 H_∞ Norm Model Reduction

The H_∞ norm recently appeared as very important tool in different optimal control, filtering and model order reduction problems, it is attested by a vast amount of researches published in the last decade. The $\|.\|_{H_\infty}$ is widely accepted to be the most suitable measure for approximation error for robustness considerations [76]. The optimal H_∞ model reduction problem is defined below:
Given a transfer function $G_N \in H_\infty$ with degree N, find the transfer function $G_n \in H_\infty$ with degree n which solves the following problem:

$$\min_{G_n \in H_\infty} \|G_N - G_n\|_{H_\infty} \qquad (4.41)$$

The first method contributed towards the solution of the H_∞ approximation problem is started with Kavarangğlu and Bettayeb[77] in 1993, they showed that problem (4.41) can be converted into an optimal Hankel norm approximation problem, the H_∞ norm model reduction method was compared with a Hankel norm model reduction problem through examples and they found that, the H∞ approximation method could be much better compared to the Hankel norm approximation. In 1995, D.Kavarangğlu et.al [78] studied the problem of constant L∞ approximation of complex rational matrix functions for unstable systems. They presented a suboptimal computational scheme based on balanced realization. Where an H∞ norm error bound for these systems is obtained. Also, they treated the problem of rational L∞ norm approximation of mutli-variable systems, these simultaneous mutli-variable systems are approximated using rational matrix function which is obtained by LMI based iterative algorithm for the computation the L∞ norm approximation[79]. In 1996, they developed LMI based computational schemes for H∞ model reduction problem in [80]. In 2004 Y. Ebihara .et [81] used a LMIs technique to analyze the lower bounds of H∞ norm of error between the original LTI system and the reduced model. They proved that the error problem basically being convex, accordingly, the optimal reduced-order models were obtained via LMI optimization. In 2008, Lixian.et [82] investigated the problem of H∞ model reduction for switched linear discrete-time systems with poly-topic uncertainties. A reduced-order switched model is constructed for a given robustly stable switched system,

4.4.5 L_1 Norm Model Reduction

For L_1 model order reduction, the impulse response of discrete time systems is focused. Where, the lower order model is defined as the impulse response which approximates the impulse response of original system in the sense of the L_1 norm [83]. The problem of optimal L_1 model reduction for discrete time systems can defined as following:

$$\|e(k)\|_{L_1} = \sum_{k=0}^{\infty} |y(k) - y_n(k)| \tag{4.42}$$

Where:

$$y(k) = u(k) \circledast h(k) = \sum_{i=-\infty}^{\infty} u(i)h(k-i) \tag{4.43}$$

$$y_n(k) = u(k) \circledast h_n(k) = \sum_{i=-\infty}^{\infty} u(i)h_n(k-i) \tag{4.44}$$

$e(k)$ is the impulse response difference between the original system and the reduced model, $y(k)$ denote the output described by the convolution sum of input $u(k)$ and the impulse response of the original system $h(k)$. $y_n(k)$ denotes the output of reduced model described by the convolution sum of input $u(k)$ and impulse response of the reduced order model $h_n(k)$.

The approach which contributes to the solution of problem (4.42) is developed by El-Attar et al.[83]. They reduced the linear SISO continues time system by minimizing the L_1 norm of the error between the impulse responses of the original system and the impulse response of the low-order model. In 1998, Sebakhy et al. [84] used hybrid approach based on L1, L2 and L∞ Norms to reduce the order of the discrete time system. In 2005, Li et al. [85] investigated the problem of robust L1 model reduction for uncertain stochastic systems with state delay.

4.5 Meta-Heuristic Techniques for Model Reduction

Recently, many researchers used meta-heuristic techniques as an optimal problem solvers for model order reduction instead of the previously mentioned analytical optimization techniques due to their versatility and ability to search the global optimization, most of these techniques has been done using Genetic Algorithms (GA) and Particle Swarm Optimization (PSO) or both of them. In 1996, Tan et al.[86] proposed a Boltzmann learning enhanced GA algorithm for solving L∞ identification and model reduction for robust control applications. They used GA technique to obtain the 2nd and 3rd order discrete nominal models for the 4th order discrete plant of an industrial heat exchanger. In 2007, H. Dua et.al [87] proposed a constrained H_2 approximation method for multiple input–output delay systems by using a genetic algorithm (GA). The best parameters of reduced order model was obtained by repeating the genetic operations on the population incorporated a parameter search space expansion scheme. In 2020, M. Juneja et al.[88] presented a reduced order model of autonomous AC microgrid considering state perturbation based on PSO algorithm. This algorithm was implemented to minimize the error between the order complex microgrid system and their reduced order approximant with retaining dominant poles of the original system. In 2009, R. Izzeldin Salim et al. [89] presented

an optimal model reduction using genetic algorithm and particle swarm optimization. It used GA and PSO algorithms to minimize the hybrid (L_1, H_2, H_∞) norms between reduced order models and the original models. both of approaches were tested and compared to results obtained by other researchers in the area as well as they were compared to one another in order to determine which of the two algorithms yields better results . The comparison results were based on temporal response, frequency response, steady state values, initial values, H_2 norm, H_∞ norm and L_1 norm and found that, PSO was faster in comparison to the GA technique that due to their simplicity of the computations, in addition, PSO outperformed the GA in the norm sense by leading to better norms.

4.6 Conclusion

In next chapter, the new meta heuristic methods called artificial ecosystem-based optimization (AEO) and Manta Ray Foraging Optimization (MRFO) algorithms are presented to find the optimal reduced model for linear PEMFC models. These algorithms are used to minimize the error between reduced order models and their counterparts of the 8th order linear PEMFC model which was obtained via linearization technique in previous chapter. The performances of both temporal and frequency analysis will be considered in this work. Also, the error criteria of optimal model reduction problems is considered to study both of hybrids of (H_2, H_∞) and o (L_1, H_2, H_∞) to obtain a better compromised reduced models.

Chapter 5

Meta-Heuristic Algorithms

Chapter 5 Meta-Heuristic Algorithms

5.1 Introduction

Meta-heuristic algorithms have become popular and powerful tools to obtain the optimum solution of real engineering design optimization problems. These algorithms mimic the behaviors of natural phenomena or living organisms for various problems in the real world. The popularity of these techniques drives from the following raisons:

1- Simplicity: Meta heuristics have mathematical models or main theories inspired from evolutionary concepts, physical phenomena or animals behaviors, this simplicity allows computer scientists to simulate different natural concepts easier and to solve real-world problems.

2- Flexibility: the Meta heuristic algorithms can be seen as a black box, able to offer outputs set from inputs set for a given problem. Furthermore, one can apply these meta-heuristics to different problems with modification in the structure and parameters of these algorithms to obtain satisfactory solutions.

3- Randomness: the stochastic nature of meta-heuristics allows to explore the entire search area extensively and avoid them to trap into local optima when solving real problems

4- Derivation-free mechanisms: meta-heuristic algorithms start with random solutions, and there is no need to calculate the derivative of search spaces to find the optimum. This makes meta-heuristics highly suitable for real problems with expensive or unknown derivative information [90].

Because of these advantages, the application of meta-heuristics can be found in various domains of sciences and industries. In this section, a new nature and bio-inspired optimization techniques named artificial ecosystem-based optimization (AEO) and Manta Ray Foraging Optimization (MRFO) are presented as optimization algorithms to achieve the objectives for this dissertation.

5.2 Artificial Ecosystem-Based Optimization (AEO)

An ecosystem can be defined as a community or group of organisms live and react with each other in a specific environment. These organisms can be divided into non-biotic and biotic elements. Non-biotic components contain sunlight, air and water. While the biotic constituents contain all living elements. These living elements in turn are divided into three categories:

1) Producers: represented by any type of green plant that gets its energy directly through the photosynthesis operation. During photosynthesis, water and carbon dioxide react together in the existence of sunlight to produce glucose and oxygen. Plants use this sugar to make roots, wood, leaves and fruits. Generally, producers provide essential food energy for herbivore and omnivore consumers.
2) Consumers: categorized into herbivores, carnivores, and omnivores, where the herbivores eat just producers (or plants), the carnivores eat only other animals whereas omnivores eat both producers and other animals.
3) Decomposers: are organisms called bacteria and fungi that feed on died living organisms and convert the residues into minerals and carbon dioxide that again absorbed from the soil by the producers and so the cycle repeats.

All these categories (producers, consumers and decomposers) are interacted with each other to compose a food chain. This chain shows who feeds whom in an ecosystem, where each organism needs to get food energy from another one to achieve the nutrients movement, in addition it displays the connected pathway the various energy levels of feeding can follow through an ecosystem. The food web consists of many overlapping and interconnected food chains, this web shows various ways of food chains interconnecting among them. In addition, it arranges living organisms depending on their energy level.

Figure (5.1) shows the energy flow in an ecosystem on earth, where the energy flows between living organisms from high energy (producers) towards the living organisms with low energy (decomposers). From figure (5.1), it can be noted that, organism with higher energy is found at the top of food web while the lower energy organism is located at the bottom of the food web. On the other hand, the consumers are considered the most complex among different organisms. Usually, the ecosystem develops this energy transfer mechanism as a strategy to keep the species stability and to maintain the ecological balance over a long term.

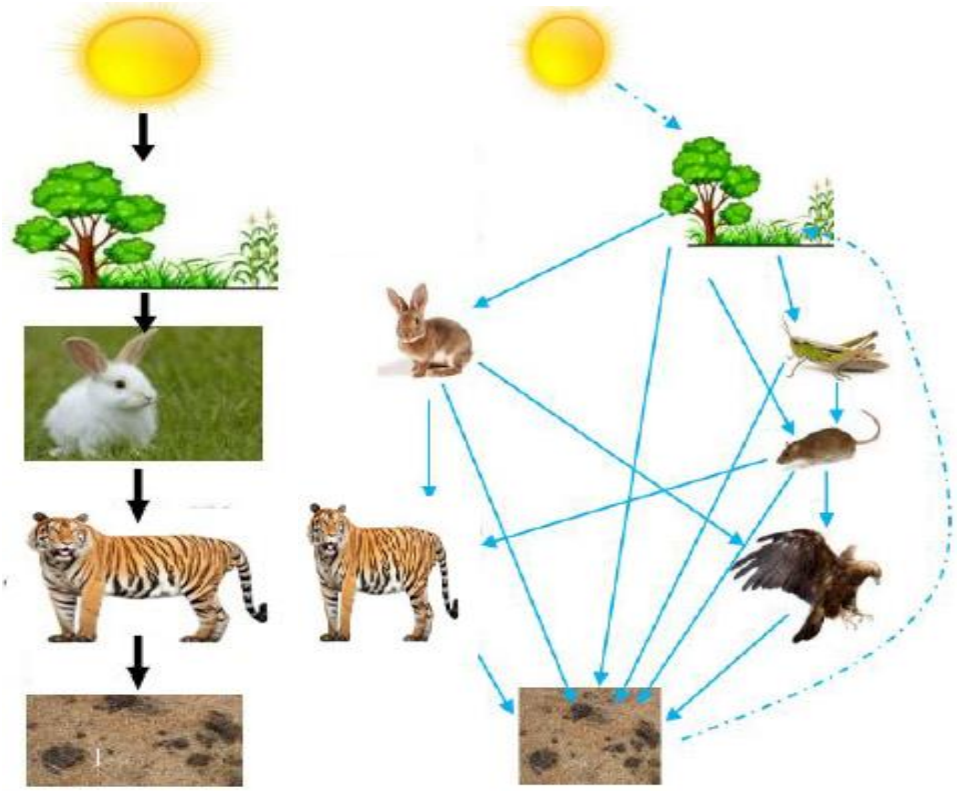

(a) (b)

Figure 5.1 Flow energy in an ecosystem; (a) food chain, (b) food web

According to the former discussion, Weiguo Zhao has developed a novel artificial ecosystem-inspired optimization algorithm in 2019 [91] , that works with three operators, including production, consumption, and decomposition. Generally, the AEO operation proposes the following rules to search the best solution:

1- There is only one producer and only one decomposer as individuals in a population.

2- The other population individuals are consumers including a carnivore, a herbivore, or an omnivore with the same probability.

3- In a population, the level of energy of each individual is evaluated by its function fitness value. Figure (5.2) represents an ecosystem in AEO. In this ecosystem, all individuals are sorted in descending order of the function fitness value [91], where the black arrows represent the energy flow. The worst individual x_1 (producer) has the highest energy level while the best

individual x_n (decomposer) has the lowest energy level. The other individuals are consumers, for example: x_2 ,x_3 are herbivores, x_5 , x_6 omnivores and x_4 ,x_7 are carnivores.

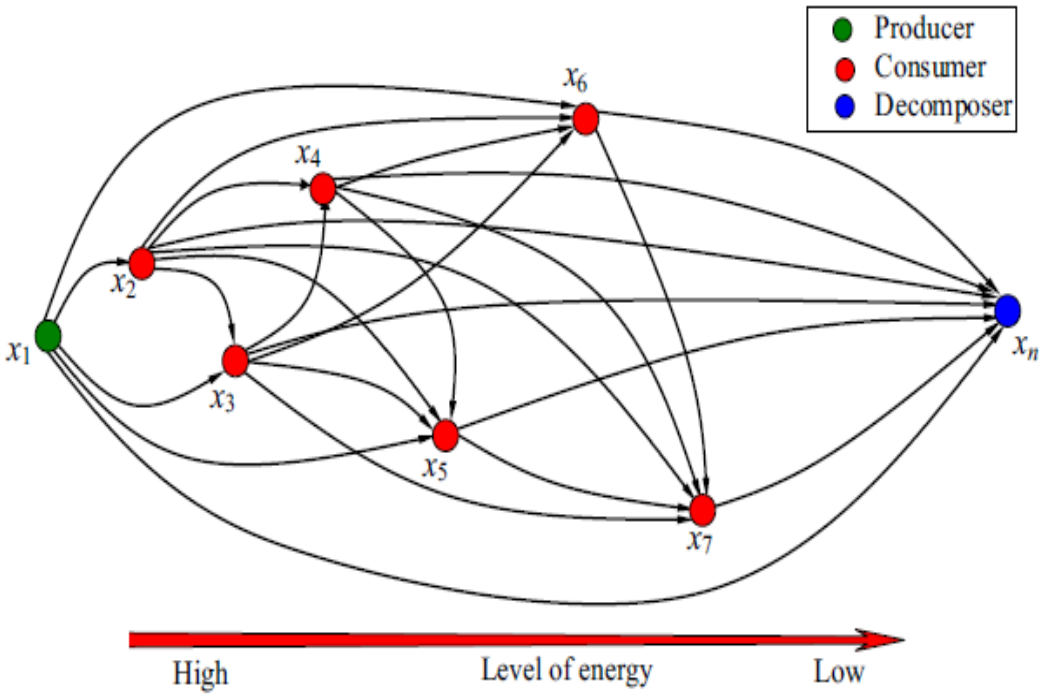

Figure 5.2 An ecosystem in AEO technique [91]

a) Production

In AEO, the producer with the high energy level (lowest fitness) is updated based on the low and upper limits of search space and the decomposer (the best individual). Consequently, the other individuals such as herbivore and omnivore in the population will update their positions in various regions. The production operator allows AEO to generate randomly a new individual (producer) between the best one (x_n) and a randomly generated individual in the search space (x_{rand})[92]. The mathematical model of the production operator is given by following [91]:

$$x_1(t+1) = (1-\alpha).x_n(t) + \alpha.x_{rand}(t) \quad (5.1)$$

$$\alpha = \left(1 - \frac{t}{MaxIter}\right) r_1 \quad (5.2)$$

$$x_{rand} = r(U-L) + L \quad (5.3)$$

Where n is the population size, α coefficient of linear weight, x_{rand} is an individual position, $r_1 \in [0,1]$ is a random number, $MaxIter$ is the maximal number of iterations, $r \in [0,1]$ is a random vector *L* and *U* are the lower and upper limits, respectively.

b) Consumption

In AEO, all the consumers start to perform consumption operator after the production operator is accomplished. In this operation each consumer can get the food energy from another consumer with lower fitness or from a producer or both. In this operator, the mechanism of food searching of many animals is imitated by Levy flight technique that used for improving the exploration phase in many nature-inspired algorithms and finding their optimization performance. The consumption factor C which has the feature of the Levy flight is given by following:

$$C = 0.5 \frac{v_1}{|v_2|} \tag{5.4}$$

$$v_1 \sim N(0,1) \quad , \quad v_2 \sim N(0,1) \tag{5.5}$$

N is normal distribution with mean of 0 and deviation of 1.

The consumption factor can assist each consumer to hunt the food with various consumers types adopting different hunting strategies.

Herbivore: If a consumer is randomly selected as an herbivore, i.e. It eats only the produce, the mathematical model of the consumption behavior is presented by the following equation[91]:

$$x_i(t+1) = x_i(t) + C.\left(x_i(t) - x_1(t)\right),\ i \in [2, \cdots, n] \tag{5.6}$$

Carnivore: when the consumer is randomly selected as a carnivore, it can only eat randomly a consumer with the lowest fitness value. So, the mathematical modeling the consumption behavior of a carnivore is expressed as follows:

$$\begin{cases} x_i(t+1) = x_i(t) + C.\left(x_i(t) - x_j(t)\right),\ i \in [3, \cdots, n] \\ j = randi([2 \quad i-1]) \end{cases} \tag{5.7}$$

Omnivore: when the consumer is randomly taken as an omnivore, it can eat other consumer with the lowest fitness value and eat the producer or both. The mathematical formulation of the consumption behavior of an omnivore can be expressed as follows:

$$\begin{cases} x_i(t+1) = x_i(t) + C.\left(r_2.(x_i(t) - x_j(t)) + (1 - r_2) - \left(x_i(t) - x_j(t)\right), i \in [3, \cdots, n] \\ j = randi([2 \quad i-1]) \end{cases} \tag{5.8}$$

Where: $r_2 \in [0,1]$ is a random number.

c) Decomposition

The third operator is decomposition which plays a necessary role in the ecosystem, providing essential minerals for the growth of the product (plants). During this operation, the decomposer will decay chemically the residues of individual in the population after the death, to mathematically express this behavior, the decomposition process uses D as the factor of decomposition, e and h are the coefficients of the weight. Hence, the individual position (x_i) in a population can be updated by the position of the decomposer (x_n) via these parameters D, e, and h. It allows the next position of each individual to spread around the best individual (the decomposer), showing the exploitation to some extent. equation of the decomposition behavior is given as follows [91]:

$$x_i(t+1) = x_n(t) + D.\left(e.x_n(t) - h.x_i(t)\right), \; i = 1, \cdots, n \tag{5.9}$$

$$\mathrm{D} = 3.u \qquad u \sim N(0,1) \tag{5.10}$$

$$e = r_3.randi([1 \;\; 2]) - 1 \tag{5.11}$$

$$h = 2.r_3 - 1 \tag{5.12}$$

At the beginning of the AEO, an initial population is generated randomly. For each iteration, the first individual (producer) update their position based on (5.1). For the other individuals (consumers), they have the same probability to select among equations (5.6), (5.7) or Eq. (5.8) in order to update their positions, regarding the kind of the consumer when the individual do not obtain a higher fitness value, then such individual position will be updated based on (5.9). All the updates will continue until the AEO algorithm reaches the end criterion. Finally, the optimal solution of the best individual will be found. Figure (5.3) depicts the AEO framework in the flow-chart and the pseudo code of AEO algorithm is given by following [91]:

1. Initialize a set of an ecosystem population X_i(solutions) and calculate the fitness Fit_i and the best solution X_{best}.
2. While the stop criterion is not satisfied do
    //Production//
    2.1 For individual X_1, update its solution, using equation (5.1)
    //Consumption//
    2.2 For individual X_i (i=2... n),
        // Herbivore //
        If rand <1/3 then update its solution, using equation (5.6)
        // Carnivore //
        Else if $1/3 \leq \text{rand} \leq 2/3$ then update its solution, using equation (5.7)
        // Omnivore //
        Else update its solution, using equation (5.8)
        End if
    End if
    Calculate the fitness of each individual.
    2.3 Update the best solution found so far X_{best}
    // Decomposition//
    Update the position of each individual, using equation (5.9)
3. Calculate the fitness of each individual.
4. Update the best solution found so far X_{best}

End While.

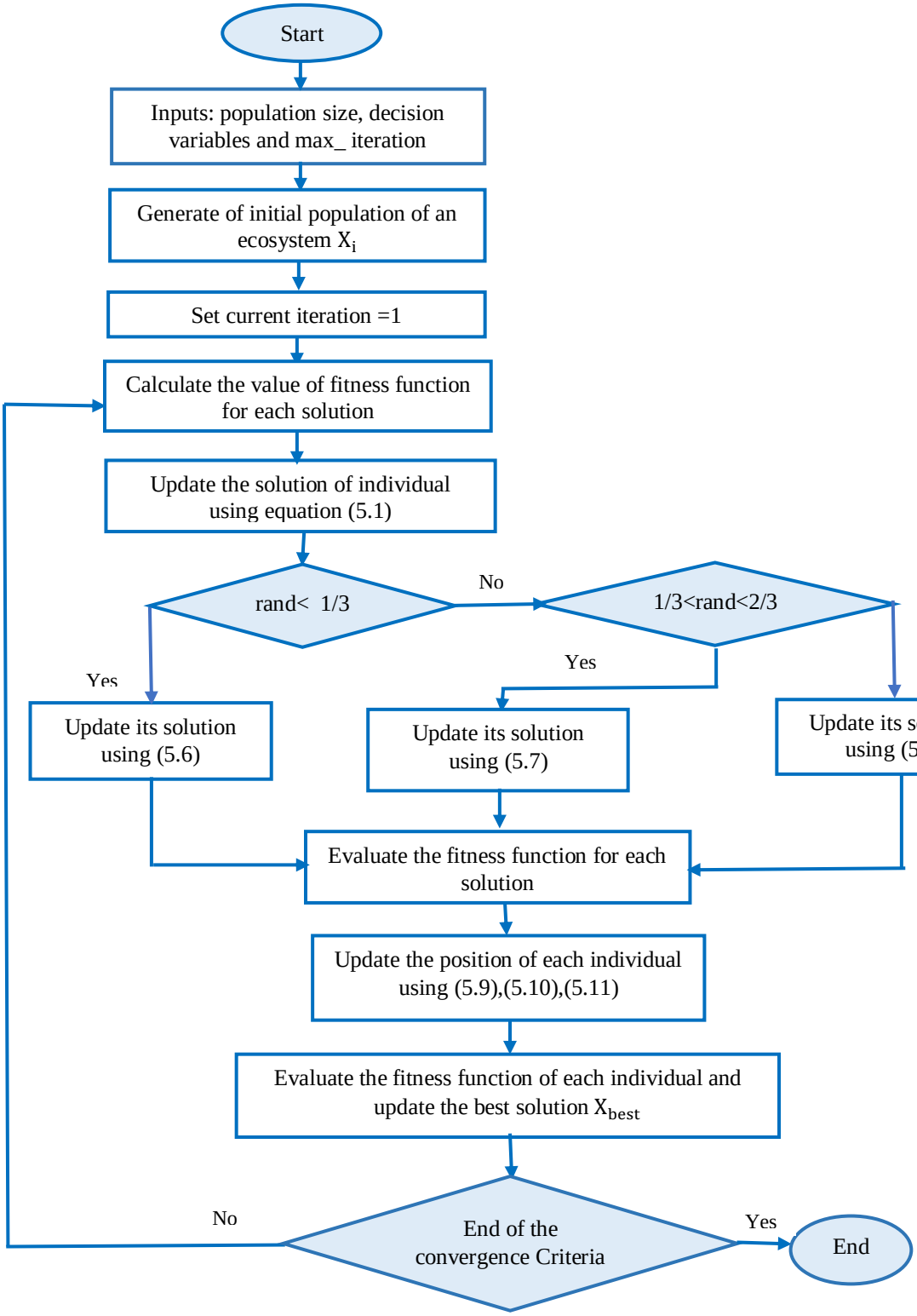

Figure 5.3 Flowchart of AEO algorithm

5.2.1 Application of AEO Algorithm

With application of AEO algorithm, the AEO is performed by three energy transfer strategies in an ecosystem involving production, consumption, and decomposition, these strategies can effectively enhance the ability of AEO to find the best individual ($\sum_n$) for minimizing optimal both hybrids (L_1, H_2, H_∞) norms and (H_2, H_∞) norms. Hence, the AEO steps which used to reduce the order of the PEMFC 500W model were presented as follows:

Step 1: Read the matrices of space state of the discrete linear PEMFC system ($A_N, B_N, C_N, D, K_N, X_N$), dimension of the system N= 8, dimension of the reduced order model n=3 and time sampling $T_s = 0.2s$.

Step 2: Determine the dimension of the problem: Dim = $n^2 + 2 * n + 2 * n + 2 * n + nu * ny + n$ (where $nu = 2$, $ny = 2$ are number of the inputs and outputs of the PEMFC model respectively).

Step 3: Determine the size of population (nPop = 100) and maximum number of iterations (MaxIter =2000)

Step 4: Determine randomly the vector of population position by upper and lower limits of search space (Up = 1, Low = -1).

Step 5: Determine the position of each individual (solution) by using equation (5.3).

Step 6: Optimize the desired objective function (equation 6.2) by generate randomly the reduced-order models as population X_i(solution), calculate the fitness Fit_i of each individual and the best solution X_{Best} found so far using the AEO operators as following:

***Step 7*:** calculate the individual X_1 using production operator (equation 5.1), this operator assists AEO algorithm to update the position of each individual (solution) from randomly generated position to the best one with the iteration number. Hence, the updated solution will guide other candidates to perform consumation operator during the process of consumation. The production behavior contributes highly between the balancing exploratory search and exploitative search.

***Step8*:** calculate the individuals $X_i(i = 2, \dots, nPop)$ by using consumation operator, in this behavior, each individual is selected randomly as an herbivore, a carnivore, or an omnivore with the same probability. In herbivore process, the individual solution is updated using the solution which generated by the production operator (equation 5.6). In carnivore process, the individual

solution is updated by the selected individual randomly with higher level of the energy (equation 5.7). In omnivore operator, the individual solution is updated by both the solution of the production operator and the selected solution with higher level of the energy (equation 5.8). The consumation operator can improve the exploration process in the AEO algorithm, and reach to the global optimum without falling into the trap of local optimum.

***Step 9*:** calculate the individual X_{nPop} by using decomposition operator, in this process, the individuals are updated by the best solution in the population using three parameters D, e, and h (equation 5.9), this operator can improve the AEO exploration.

***Step 10*:** Calculate the fitness of each individual and update the best solution found so far X_{Best}.

Step11: Repeat steps 7-10 until stop the MaxIter of the convergence reached.

Step12: Report the optimal results with $\sum_n(A_n, B_n, C_n, D, K_n, x_n)$

5.3 Manta Ray Foraging Optimization (MRFO) Algorithm

Manta rays are one of the largest known marine creatures, usually they live in tropical zones of Indian ocean or in subtropical zones of south pacific. They have a flat body from top to bottom and a two of pectoral fins and a pair of vertical lobes in front of their huge, terminal mouths, they can reach 5.5 m to 7 m in width. They swim elegantly and freely as birds fly. Figure (5.4) shows a foraging manta ray and their physical structure [93].

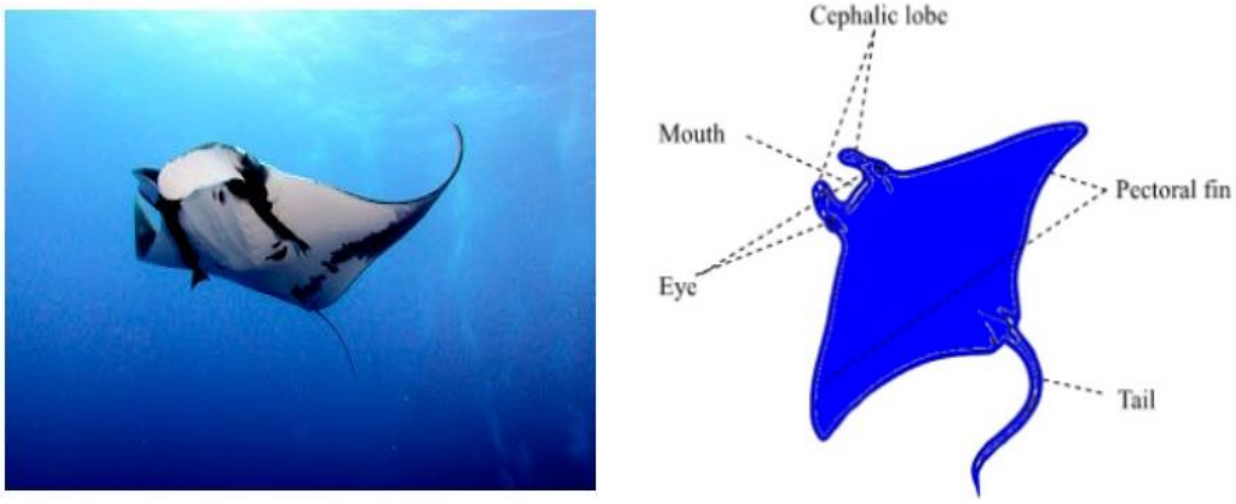

(a) (b)

Figure 5.4 (a) A foraging manta ray, (b) manta ray structure

Manta rays feed on plankton without sharp teeth, they funnel the water and food into their mouths using horn-shaped cephalic lobes. Then the food is filtered from the water by gill rakers [93]. Every day, manta rays eat a large quantity of plankton that can reach about 5 kg per an individual. This plankton is formed by the tides or change of seasons that leads to not evenly dispersed or regularly concentrated in some specific areas of ocean. Interestingly, manta rays are always good to find plentiful plankton. The most intriguing thing about manta rays is their foraging behaviors, and they may travel alone or in groups of up to 50, but foraging is often observed in groups. These creatures have developed a variety of wonderful, and intelligent foraging strategies. These strategies include chain, cyclone, and somersault foraging:

1) Chain foraging: when a group of manta rays start to search for food, they line up, one behind another, forming an orderly line and move forward to the food, the paths of feeding extending to several hundred meters depending on concentration and distribution of plankton. The manta rays keep their line formed around the food and each of them updates its position slightly above or below in the foreground. Consequently, the plankton that missed by previous manta rays will be picked up by another manta which is behind them.
2) Cyclone foraging: this foraging strategy is used when the concentration of plankton is very high in a limited area, group of manta rays gather together in spiral way to generate a spiraling vortex in the eye of the cyclone and the filtered water moves up towards the surface. This pulls the plankton into their open mouths.
3) Somersault foraging: it is the one of the most beautiful scenery that can be provided by nature. When there is an extremely concentration of plankton in the water, the manta rays do a reverse somersault in the water, spinning around the plankton to improve feeding process. It's a wonderfully elegant display.

According to the intelligent foraging behaviors of these creatures, W. Zhao [93] has developed a new bio-inspired Manta Ray Foraging Optimization (MRFO) in 2020. This algorithm is modeled mathematically by three feeding strategies including chain foraging, cyclone foraging and somersault foraging to find a global optimization. The mathematical models are given by the following:

a) Chain Foraging

In MRFO, manta rays can determine the plankton position and swim directly towards it, where the best position is that which includes the higher concentration of plankton. Manta rays line up head-to-tail to make a feeding chain, each individual updates its position by the best food location so far and move towards it. The strategy of chain foraging is modeled by following equation[94] :

$$x_i^d(t+1) = \begin{cases} x_i^d(t) + r.\left(x_{best.}^d(t) - x_i^d(t)\right) + a.\left(x_{best}^d(t) - x_i^d(t)\right) & i = 1 \\ x_i^d(t) + r.\left(x_{i-1}^d(t) - x_i^d(t)\right) + a.\left(x_{best}^d(t) - x_i^d(t)\right) & i = 2, \dots, N \end{cases} \quad (5.13)$$

$$a = 2.r\sqrt{|\log(r)|} \quad (5.14)$$

x_i^d is the i^{th} individual position in the d^{th}dimension, x_{best}^d is the high concentration of the food, x_{i-1}^d is the position update of the $(i-1)^{th}$ current individual at x_{best}^d , a is the weight coefficient and $r \in [0,1]$ is a random vector. Figure (5.5) shows the chain foraging strategy, where the update of the i^{th} individual position is determined by the best position of the food x_{best} and the position $x_{i-1}(t)$ of the $(i-1)^{th}$ current individual.

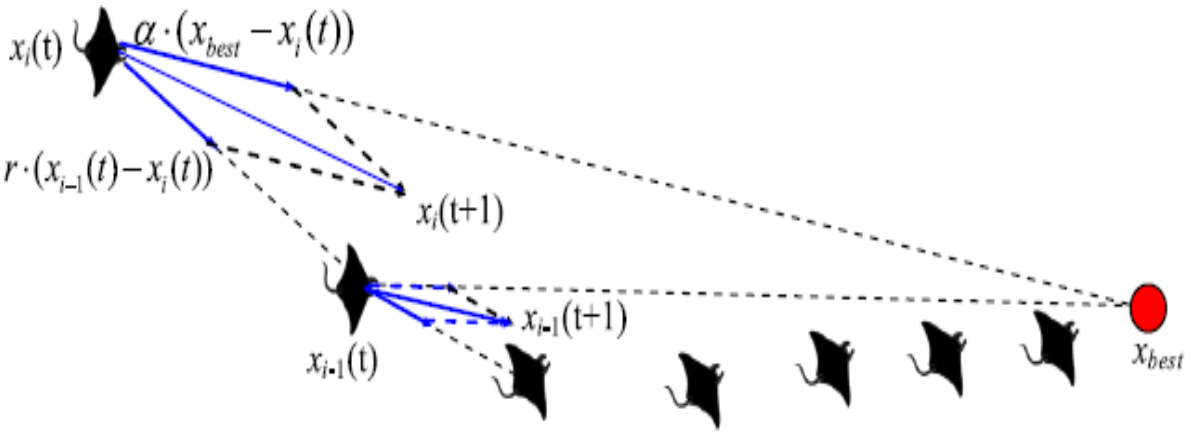

Figure 5.5 Chain foraging strategy

b) Cyclone Foraging

In the cyclone foraging strategy, the manta rays determine the plankton position in deep water. They will do a long foraging chain and swim towards the food by a spiral way. However, in this movement each individual manta moved based on position of food and the position of the one in front. Figure (5.6) depicts the cyclone foraging behavior in a 2-D space. This spiral movement can be given by mathematical equation as following [93]:

$$\begin{cases} X_i(t+1) = X_{best} + r.\left(X_{i-1}(t) - X_i(t)\right) + e^{bw}.\cos(2\pi w).\left(X_{best} - X_i(t)\right) \\ Y_i(t+1) = Y_{best} + r.\left(Y_{i-1}(t) - Y_i(t)\right) + e^{bw}.\sin(2\pi w).\left(Y_{best} - Y_i(t)\right) \end{cases} \quad (5.15)$$

Where *w* is a random number in [0, 1].

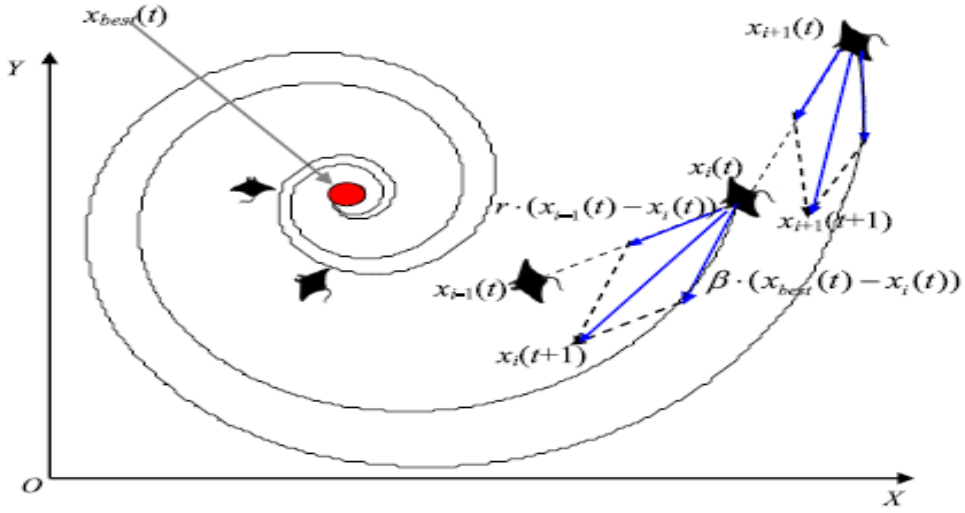

Figure 5.6 Cyclone foraging strategy in a 2-D space

The spiral movement formula in n-D space can be given by a mathematical equation as follows[93]:

$$x_i^d(t+1) = \begin{cases} x_{best}^d + r.\left(x_{best}^d(t) - x_i^d(t)\right) + b.\left(x_{best}^d(t) - x_i^d(t)\right) & i = 1 \\ x_{best}^d + r.\left(x_{i-1}^d(t) - x_i^d(t)\right) + b.\left(x_{best}^d(t) - x_i^d(t)\right) & i = 2, \dots, N \end{cases} \quad (5.16)$$

$$b = 2e^{\frac{r1(T-t+1)}{T}}.\sin(2\pi r_1) \tag{5.17}$$

Where: b is the weight coefficient, T is the iterations number, and r_1 is the rand number in [0, 1].

The cyclone foraging behavior focuses mainly on exploration and exploitation through updating position of each individual which enables MRFO to achieve a comprehensive global search by improving the global best position. The mathematical equation of this spiral movement is given by the following [94]:

$$x_i^d(t+1) = \begin{cases} x_{rand}^d + r.\left(x_{rand}^d - x_i^d(t)\right) + b.\left(x_{rand}^d - x_i^d(t)\right) & i = 1 \\ x_{rand}^d + r.\left(x_{i-1}^d(t) - x_i^d(t)\right) + b.\left(x_{rand}^d - x_i^d(t)\right) & i = 2, \dots, N \end{cases} \tag{5.18}$$

$$x_{rand}^d = L + r.(U - L) \tag{5.19}$$

Where x_{rand}^d is a random position, L, U are the lower and upper limits of the d^{th} dimension.

c) Somersault Foraging

In the somersault foraging behavior, each individual tends to swim around the food and somersault to a new position. Then, it updates their site about the best position. The mathematical model can be represented by following [94]:

$$x_i^d(t+1) = x_i^d(t) + S.\left(r_2 . x_{best}^d - r_3 . x_i^d(t)\right) \quad i = 1, \dots, N \tag{5.20}$$

S is the somersault factor, r_2 and r_3 are random numbers in range$[0,1]$.

This type of foraging is an individual feeding behavior, where each individual swims between their current position and their new position, circling around the best defined position so far. After few iterations, the distance between the individual position and the best position is reduced so far and all individuals gradually approach to the best solution in the search space. Figure (5.7) shows the draw of somersault foraging strategy.

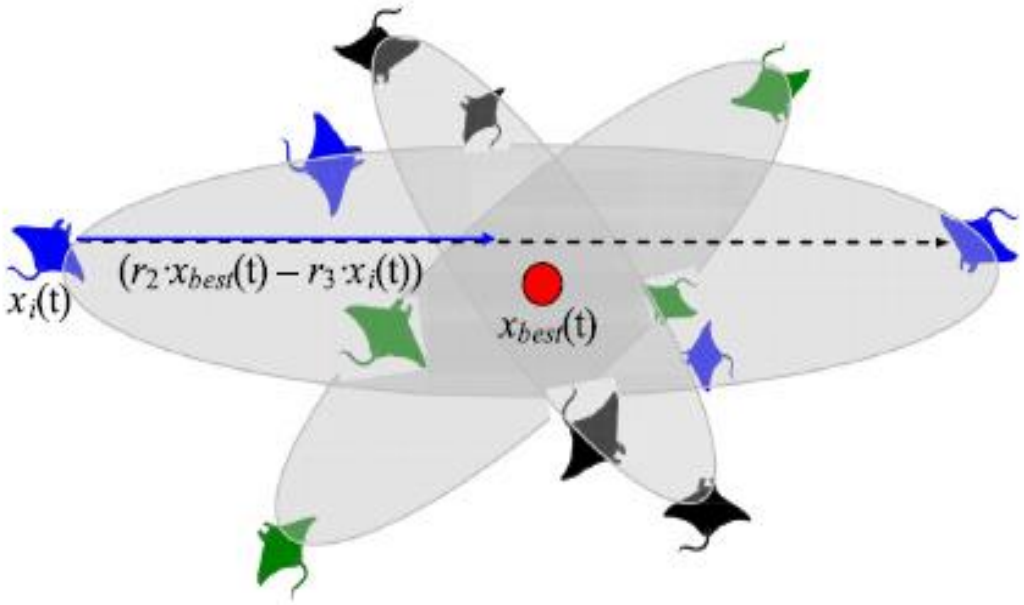

Figure 5.7 Somersault foraging strategy

Figure (5.8) depicts the MRFO framework in the flow-chart and the pseudo code of MRFO algorithm is given in the following [93]:

1. Initialize a set of population N (candidate solutions), the iteration number T and define x_u, x_l as the upper and lower limits of problem space
2. Determine the position of each manta ray:

$$x_i(t) = x_l + rand.(x_u - x_l) \quad for \quad i = 1, \dots, N$$

3. Determine the fitness of each individual $f_i = f(x_i)$
4. Determine the best solution found so far x_{best}
5. While stop criterion is not satisfied do

for i=1 to N do

5.1 If rand > 0.5 then // cyclone foraging

If t/T < rand then $x_{rand} = x_l + rand.(x_u - x_l)$,using equation (5.18)

Else update location using equation (5.16)
End if

5.2 Else rand< 0.5 // Chain foraging
update location using Equation (5.13)
End if

If $f(x_i(t+1)) < f(x_{best})$ then // calculate the fitness of each individual

$$x_{best} = x_i(t+1)$$

5.3 Else // Somersault foraging

For i=1 to N do using equation (5.20)

Then $x_{best} = x_i(t+1)$

End for

End while

Return

The best solution found so far x_{best}

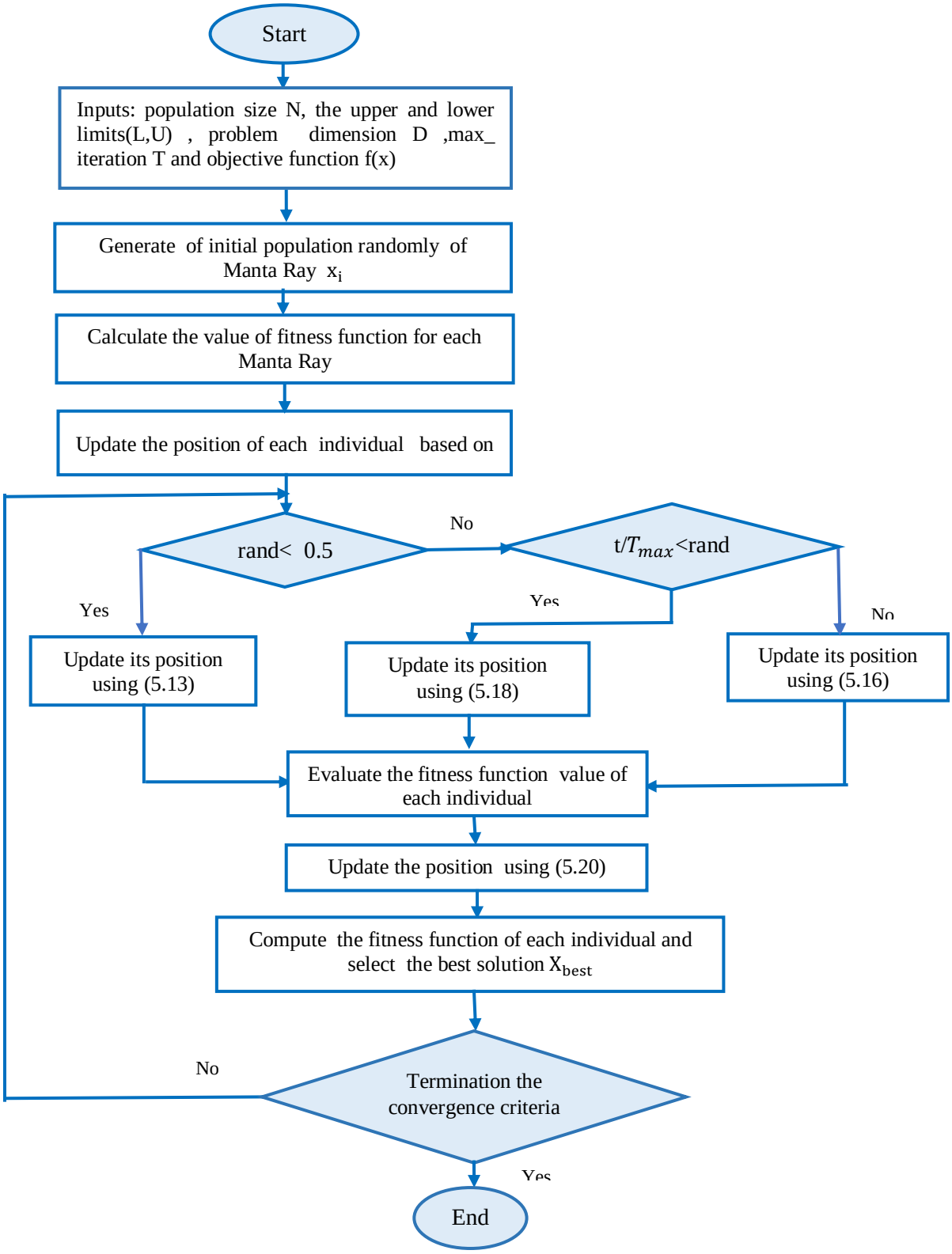

Figure 5.8 Flowchart of MRFO algorithm

5.3.1 Application of MRFO Algorithm

With application of MRFO algorithm, the MRFO is proceeded by three manta rays foraging strategies :chain foraging, cyclone foraging and somersault foraging, these strategies can effectively enhance the ability of MRFO to find the best individual ($\sum_n$) for minimizing optimal the hybrid (L_1, H_2, H_∞) norms. The MRFO steps which used to reduce the order of the PEMFC 500W model were presented as follows:

Step 1: Read the matrices of space state of the PEMFC system ($A_N, B_N, C_N, D, K_N, X_N$) , dimension of the system N= 8 dimension of the reduced order model n=3 and time sampling $T_s = 0.2s$.

Step 2: Determine the dimension of the problem Dim = $n^2 + 2 * n + 2 * n + 2 * n + nu * ny + n$

Step 3: Determine the size of population (nPop = 100) and maximum number of iterations (MaxIter =2000)

Step 4: Determine randomly the vector of population position by upper and lower limits of search space (Up = 1, Low = -1).

Step 5: Determine the position of each individual (each solution) by using equation (5.19).

Step 6: Optimize the desired objective function (equation 6.2) by generate randomly the reduced-order models as population X_i(solution), calculate the fitness Fit_i of each individual and the best solution X_{Best} found so far using the MRFO operators in following steps:

Step 7: update the position of each individual X_i at each iteration with respect to both the reference position and the one in front of it. The best position obtained so far or a random position generated in the search space is selected as the reference position based on the value of t/T . When $r < t/T$ a random position randomly produced in the search space is selected as a reference position for the exploration (equation 5.16). When $t/T < r < 0.5$, the current best solution is selected as a reference position for the exploitation (equation 5.18).

Step 8: update the position of each individual X_i depending on the one which in front of it and the current global best solution. When $0.5 < r$, MRFO can convert between the cyclone foraging behavior and the chain foraging behavior (equation 5.13). The value of t/T encourages MRFO to cross from exploratory search to exploitative search smoothly, and with the value of r (rand number), MRFO can covert between the chain foraging and the cyclone foraging.

Step 9: the individuals X_i update their own positions with respect to the best position found so far (equation 5.20).

***Step 10*:** Calculate the fitness of each individual and update the best solution found so far X_{Best}.

Step11: Repeat steps 7-10 until stop the MaxIter of the convergence reached

Step12: Report the optimal results with $\sum_n(A_n, B_n, C_n, D, K_n, x_n)$.

5.4 Conclusion

In this chapter, the artificial ecosystem-based optimization (AEO) and Manta Ray Foraging Optimization (MRFO) algorithms were presented as new optimization approaches. They are considered as powerful tools for many applications in different engineering areas, they have an ability to find the optimum solution of real-world problems. In the next chapter, both AEO, MRFO algorithms are implemented in Matlab Environment Programming to find the optimal model reduction of MIMO complex linear PEMFC SR-12 500W system by minimizing both of hybrids (H_2 , H_∞) and (L_1 ,H_2 , H_∞) norms between full PEMFC model and order reduction model.

Chapter 6

Hybrid (L_1 ,H_2 , H_∞) Norms For Optimal Order Reduction of PEMFC 500W Model

6.1 Introduction

The objective of this chapter is to reduce order for a complex linear PEMFC SR-12 500W model resulting from the optimal technique based on the hybrid (L_1, H_2, H_∞) and hybrid (H_2, H_∞) norms ,these hybrids have been implemented by Artificial Ecosystem Optimization (AEO) and Manta Rays Foraging Optimization (MRFO) algorithms using Matlab Environment , Programming, both algorithms are compared with standard technique called balanced truncation (BT) (annex A) [52], the compared results have been validated by the temporal and frequency responses of reduced models and original PEMFC 500w model.

6.2 Statement of Problem

The goal of optimal MOR is obtaining the state space of reduced-order model for PEMFC stack that is able to represent the original model:

$$\sum_{\mathrm{n}}: \begin{cases} x_n(k+1) = A_n x(k) + B_n u(k) + K_n e(k) \\ y(k) = C_n x(k) + Du(k) + e(k) \\ x(o) = x_n \end{cases} \tag{6.1}$$

Where: $A_n \in \mathbb{R}^{n\times n}$, $B_n \in \mathbb{R}^{n\times m}$, $K_n \in \mathbb{R}^{n\times m}$, $C_n \in \mathbb{R}^{p\times n}$ and $n \ll N$,

In this thesis, the problem of PEMFC500w model reduction is investigated by AEO and MRFO Algorithms using minimization both of hybrid (L_1 , H_2, H_∞) and (H_2, H_∞) norms for the errors between full PEMFC model and reduced order models, this minimization problem is considered as following:

$$\text{Minimizing} \qquad E(\sum_{\mathrm{n}}) = \left\| \sum_{\mathrm{N}} - \sum_{\mathrm{n}} \right\| \tag{6.2}$$

With respect to the variable of optimization $\sum_{\mathrm{n}}(A_n, B_n, C_n, D, K_n, x_n)$

The two different hybrid (L_1 , H_2, H_∞) and (H_2, H_∞) norms reduction approaches to obtain the optimal reduced-order models for PEMFC system are given by following [89]:

$$\|E\|_{(L_1, H_2, H_\infty)} = a\,\|E\|_{L_1} + b\|E\|_{H_2} + c\|E\|_{H_\infty} \tag{6.3}$$

$$\|E\|_{(H_2,H_\infty)} = a\|E\|_{H_2} + b\|E\|_{H_\infty} \quad (6.4)$$

a, b and c are constants

With taken $a = b = c = 1$

H_2 and H_∞ norms are defined as following:

$$\|E\|_{H_2} = \left\{\frac{1}{2\pi}\sum_1^\infty |E(k)|^2\right\}^{1/2} \quad (6.5)$$

$$\|E\|_{H_\infty} = \max|E(k)| \quad (6.6)$$

The L_1 norm is given by:

$$\|E\|_{L1} = \sum_0^\infty |e(k)| \quad (6.7)$$

$e(k)$ is the impulse response difference between the original model and the reduced model:

$$e(k) = y_N(k) - y_n(k) \quad (6.8)$$

6.3 Numerical Results

The obtained state space model of PEMFC SR-12 500W stack is composed by eight stats ,tow inputs and two outputs e.g. N=8, m = p = 2 , with disturbance coefficients matrix K, initial state vector x_0 and sample time T_s = 0.2. Hence, the matrices of this space state model are given by following:

A_N = [1.2291 0 -0.5141 0 -0.3237 -0.3237 0.1935 0.1935
-0.6438 0 -0.4385 0 -0 0 0 0
1 0 0 0 0 0 0 0
0 1 0 0 -0 0 0 0
0 0 0 0 0 0 0 0
0 0 0 0 0 0 0 0
0 0 0 0 1 0 0 0
0 0 0 0 0 1 0 0]

$B_N = [0 \quad 0;0 \quad 0;0 \quad 0;0 \quad 0;1 \quad 0;0 \quad 1;0 \quad 0;0 \quad 0]^t$

C_N = [1.2291 0 -0.5141 0 -0.3237 -0.3237 0.1935 0.1935
-0.6438 0 -0.4385 0 0.0000 0.0000 -0.0000 -0.0000]

D =1.0e-016 ∗[0.8327 0.2776; -0.2776 -0.0694]

K_N =1.0e-015∗ [0.0264 -0.0402; -0.0402 0.2147;0.0333 -0.1451; -0.0397 0.1644;
0 0; 0 0; 0 0; 0 0]^t

x_N =[0; 0; 0; 0; 0; 0; 0; 0]^t

Eigenvalues:$\lambda_1 = 0,\ \lambda_2 = 0, \lambda_{3,4} = 0.6146 \pm 0.3693\, i, \lambda_5 = 0\ , \lambda_6 = 0\ , \lambda_7 = 0\ , \lambda_8 = 0.$

6.3.1 Hybrid (L_1, H_2, H_∞) Norm

In this section, the summary and results of AEO and MRFO experiments were presented, both algorithm were applied to solve the minimizing for hybrid (L_1, H_2, H_∞) error between original model Σ_N and order reduced model Σ_n (eq.6.2) by extraction the optimal reduced order representations $\sum_{AEO}$ and $\sum_{MRFO}$ for linear PEMFC system. The used parameters for AEO and MRFO Algorithms are given by:

Dimension of reduced order model: n=3
Population size: nPop= 100
The dimensionality of problem: Dim = 34
The low bound of search space: Low = -1
The up bound of search space: Up=1
The maximum number of iterations MaxIt = 2000

The 3^{rd} reduced models result of the hybrid (L_1, H_2, H_∞) norms model reduction approach on the 8^{th} linear PEMFC 500W model using the AEO and MRFO algorithms are given by following:

$$\sum_{AEO}: \begin{cases} x_n(k+1) = \begin{bmatrix} 0.364 & -0.129 & -0.341 \\ 0.443 & 0.111 & 0.493 \\ 0.368 & 0.561 & 0.207 \end{bmatrix} x(k) + \begin{bmatrix} 0.409 & 0.428 \\ 0.329 & 0.315 \\ 0.381 & 0.400 \end{bmatrix} u(k) + \begin{bmatrix} 0.666 & 0.649 \\ 0.164 & 0.300 \\ 0.625 & 0.751 \end{bmatrix} e(k) \\ y(k) = \begin{bmatrix} -0.310 & -0.032 & -0.461 \\ -0.479 & 0.315 & 0.223 \end{bmatrix} x(k) + \begin{bmatrix} -0.022 & 0.077 \\ 0.029 & 0.033 \end{bmatrix} u(k) + e(k) \\ x(o) = [-0.2395; 0.1262;\ 0.9285] \end{cases} \quad (6.9)$$

Eigenvalues: $\lambda_{1,2} = 0.5336 \pm 0.4132\, i, \lambda_3 = -0.3841 + 0.000i$

$$\sum_{\text{MRFO}}: \begin{cases} x_n(k+1) = \begin{bmatrix} 0.068 & -0.370 & -0.552 \\ 0.144 & 0.1327 & 0.566 \\ 0.543 & 0.017 & 0.984 \end{bmatrix} x(k) + \begin{bmatrix} -0.609 & -0.617 \\ 0.273 & 0.231 \\ -0.188 & -0.194 \end{bmatrix} u(k) + \begin{bmatrix} 0.492 & -0.470 \\ -0.050 & -0.248 \\ -0.225 & 0.181 \end{bmatrix} e(k) \\ y(k) = \begin{bmatrix} 0.259 & -0.263 & 0.497 \\ 0.016 & -0.194 & -0.338 \end{bmatrix} x(k) + \begin{bmatrix} 0.000 & -0.0031 \\ 0.0003 & -0.000 \end{bmatrix} u(k) + e(k) \\ x(o) = [-0.476; 0.298; -0.372] \end{cases} \quad (6.10)$$

Eigenvalues: $\lambda_{1,2} = 0.5683 \pm 0.4410\, i$, $\lambda_3 = -0.2166$

6.3.1.1 Comparative Study of the Meta-Heuristic Algorithms

The convergence process of both AEO and MRFO algorithms with 2000 iterations are shown in figure (6.1), note that, the MRFO approach has a faster convergence compared with AEO algorithm towards the best solution. Where, the MRFO approach reach to the best solution 0.272 at 1196 iteration. Whilemean, the AEO approach reach to the best fitness 0.429 at 1963 iteration.

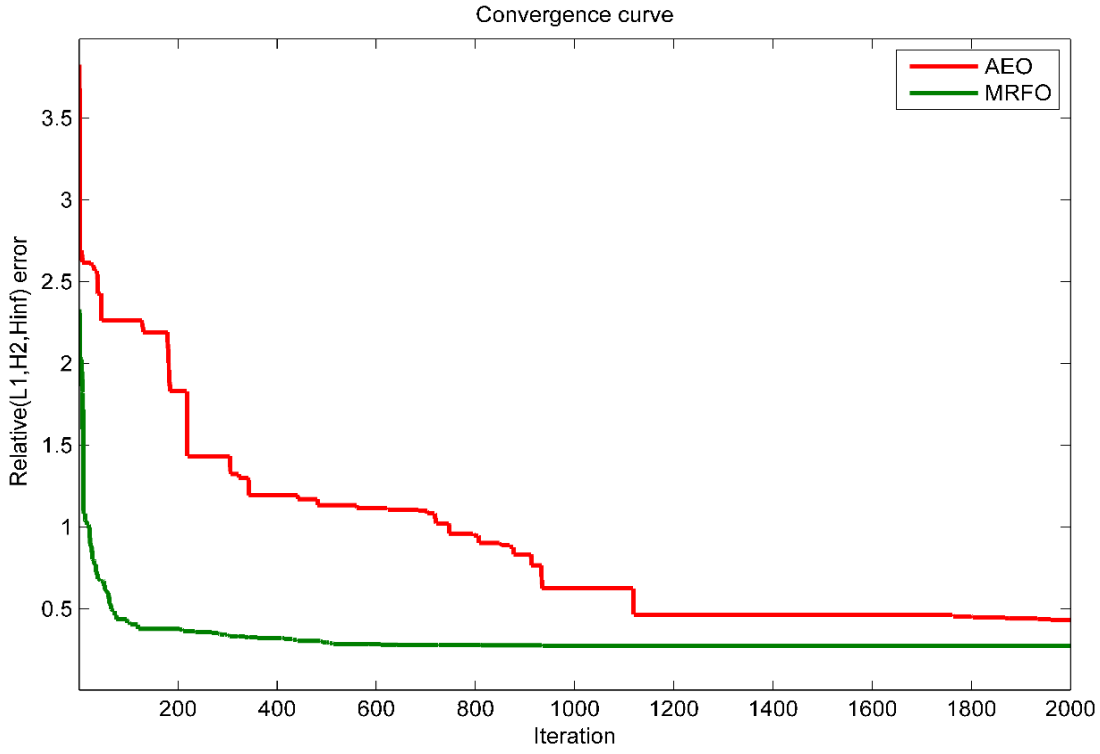

Figure 6.1 Convergence rate of AEO and MRFO for hybrid (L_1 , H_2, H_∞) norms

The following sections compare the results of the both AEO and MRFO algorithms with balanced truncation (BT) for reduction order of the linear 500 W SR-12 PEMFC model.

6.3.1.2 Norms and Steady State Errors

Table 6.1 presents the comparisons of the relative L_1, H_2, H_∞, hybrid (L_1 H_2, H_∞) norms of errors and steady state errors (SSE) of the reduced models obtained by AEO , MRFO , and BT with dimension n= 3.

Table 6. 1 Comparison between the relative L_1, H_2, H_∞, hybrid (L_1 H_2, H_∞) norms of errors and SSE

	L_1 norm		H_2 norm	H_∞ norm	hybrid (L_1, H_2, H_∞)		SSE
AEO	L1_AEO(:,:,1) =0.143	0.239	0.169	0.116	hybrid_AEO(:,:,1) = 0.429	0.526	0.0012
	L1_AEO(:,:,2) =0.168	0.258			hybrid _AEO(:,:,2) = 0.455	0.544	
MRFO	L1_MRFO(:,:,1)=0.103	0.175	0.104	0.066	hybrid _MRFO(:,:,1)=0.273	0.345	0.00007
	L1_MRFO(:,:,2)=0.115	0.184			hybrid _MRFO(:,:,2)=0.284	0.354	
BT	L1_BT(:,:,1) =0.022	0.133	0.103	0.092	hybrid _BT(:,:,1) = 0.218	0.328	0.002
	L1_BT(:,:,2) =0.022	0.133			hybrid _BT(:,:,2) = 0.218	0.328	

In the table 6.1, note that, the MRFO approach result is the lowest H_∞ norm and steady state error. While, the BT approach result is the lowest L_1 , H_2 and hybrid (L_1, H_2, H_∞) norms. However, the MRFO technique outperformed the AEO approach with the lowest in all of the norms.

To better evaluate the approximants quality, the temporal responses, the frequency responses and steady state errors for original PEMFC SR-12 500W model and the reduced order models of all AEO, MRFO and BT approaches were traced in next section.

6.3.1.3 Impulse Responses

Figure (6.2) presents the comparison of the impulse responses for the original PEMFC 500 W model to the result of the BT 3rd model order reduction approach and the results of the AEO and MRFO 3rd reduced order algorithms.

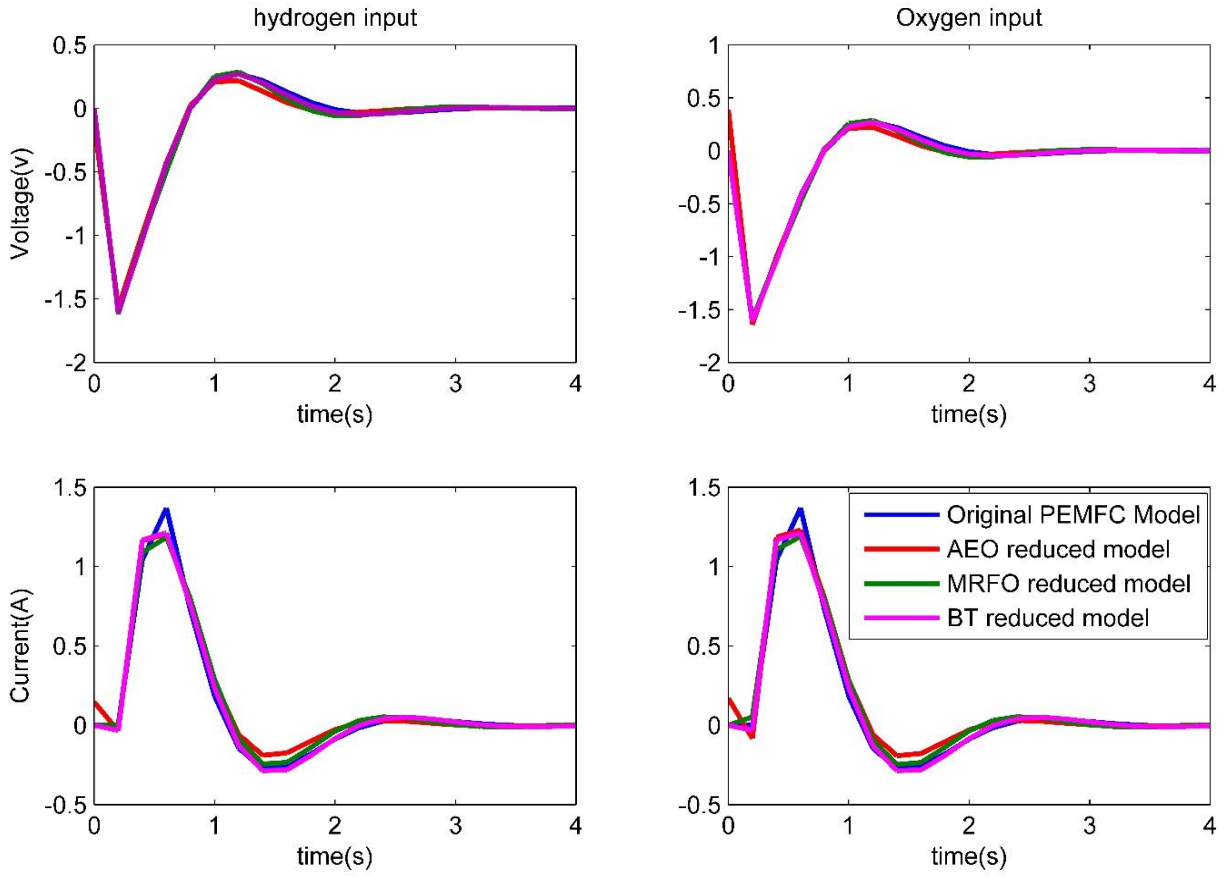

Figure 6.2 Impulse responses of original PEMFC model and hybrid (L_1, H_2, H_∞) reduced models via AEO, MRFO and BT

To know more precisely which algorithm is close to original PEMFC model , the impulse responses of the figure (6.2) is zoomed into figure (6.3) to compare the initial values of impulse responses for the original PEMFC model and AEO ,MRFO and BT reduced order models

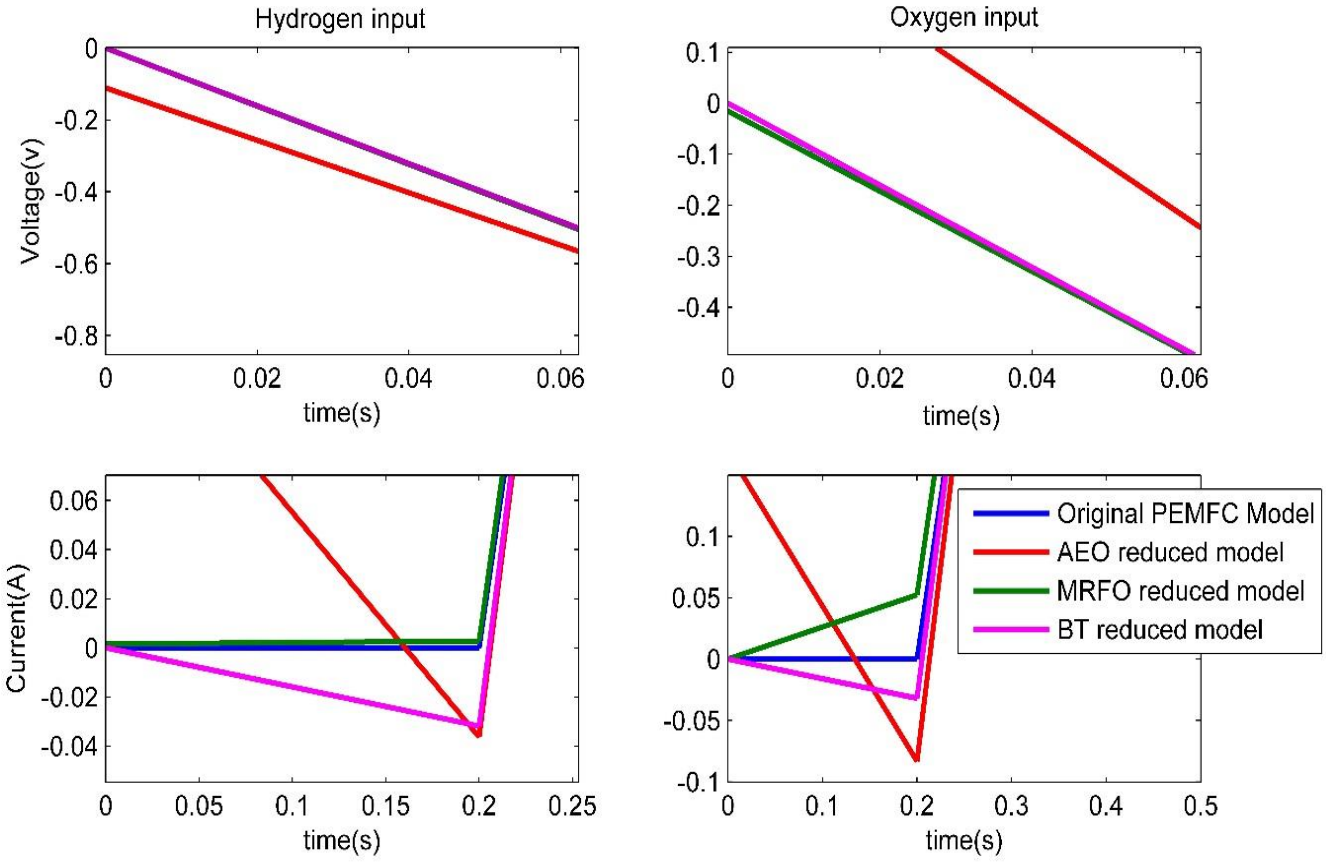

Figure 6.3 Initial values of the impulse responses of original PEMFC model and hybrid (L_1, H_2, H_∞) reduced models

6.3.1.4 Step Responses

Figure (6.4) represents the comparison of the step responses for the original PEMFC 500 W model to the result of the BT 3rd model order reduction approach and the results of the AEO and MRFO 3rd reduced order algorithms.

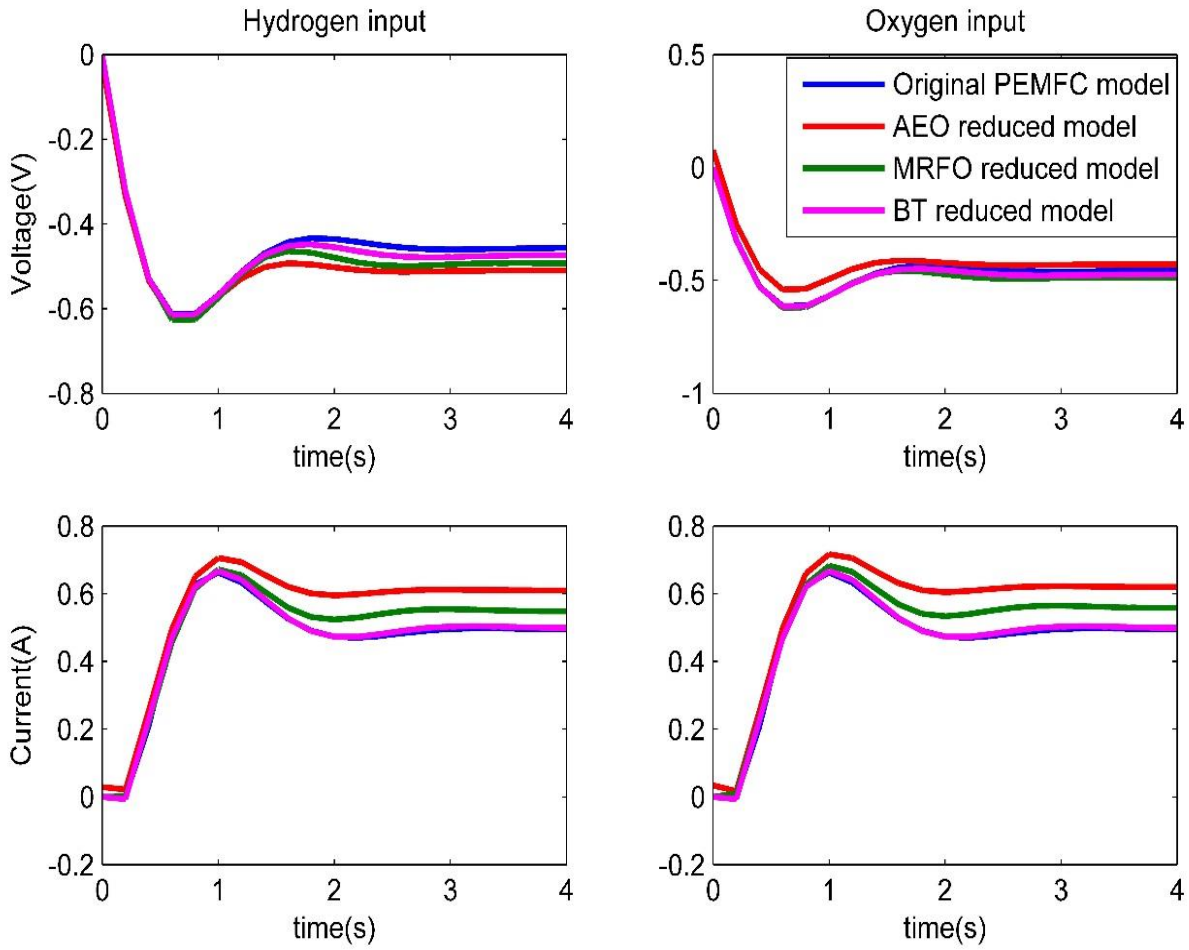

Figure 6. 4 Step responses of original PEMFC model and hybrid (L_1, H_2, H_∞) reduced models via AEO,MRFO and BT

Figure (6.5) zooms into the figure (6.4) to compare the initial values of step responses of the original PEMFC model and different reduced order models

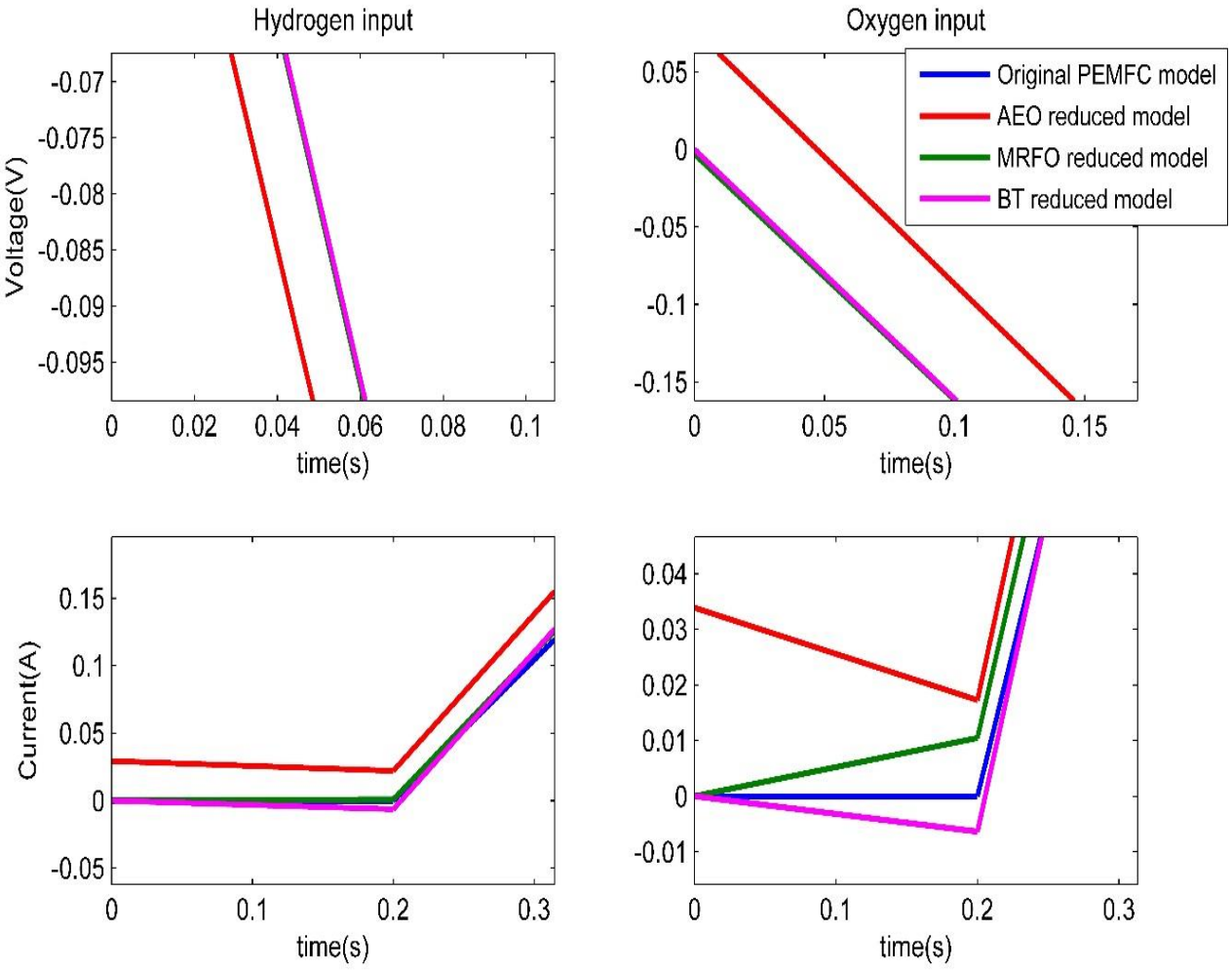

Figure 6.5 Initial values of the steps responses of original PEMFC model and hybrid (L_1, H_2, H_∞) reduced models

6.3.1.5 Frequency Responses and Steady State Error

Figure (6.6) represents the comparison of the frequency responses for the original PEMFC 500 W model to the result of the 3rd model order reduction by AEO , MRFO algorithms and the results of the 3rd reduced order model using BT approach.

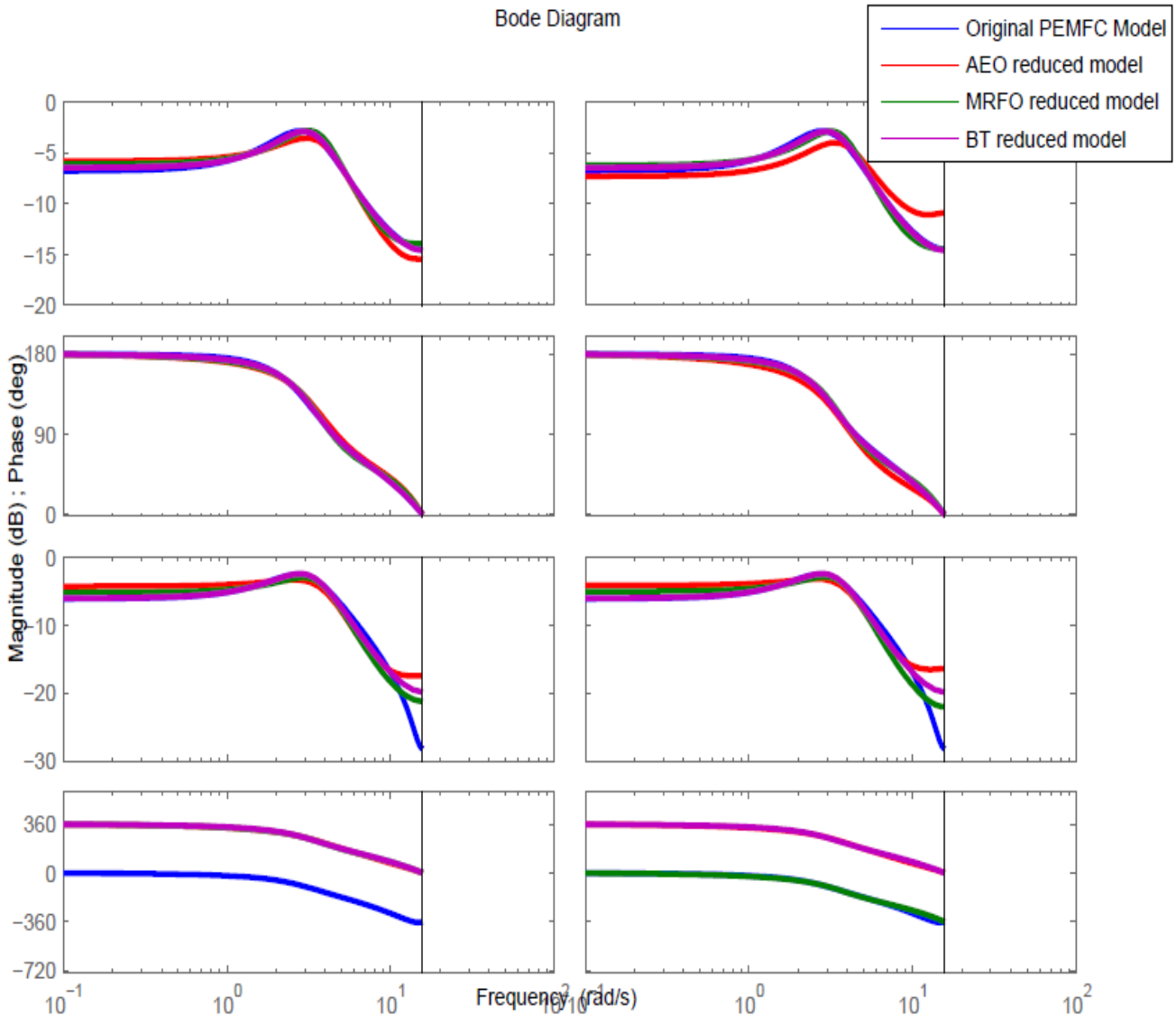

Figure 6.6 Frequency responses of original PEMFC model and hybrid (L_1, H_2, H_∞) reduced models via AEO,MRFO and BT

Figure (6.7) shows the comparison of step response error between original linear PEMFC model and AEO, MRFO, BT reduced order models

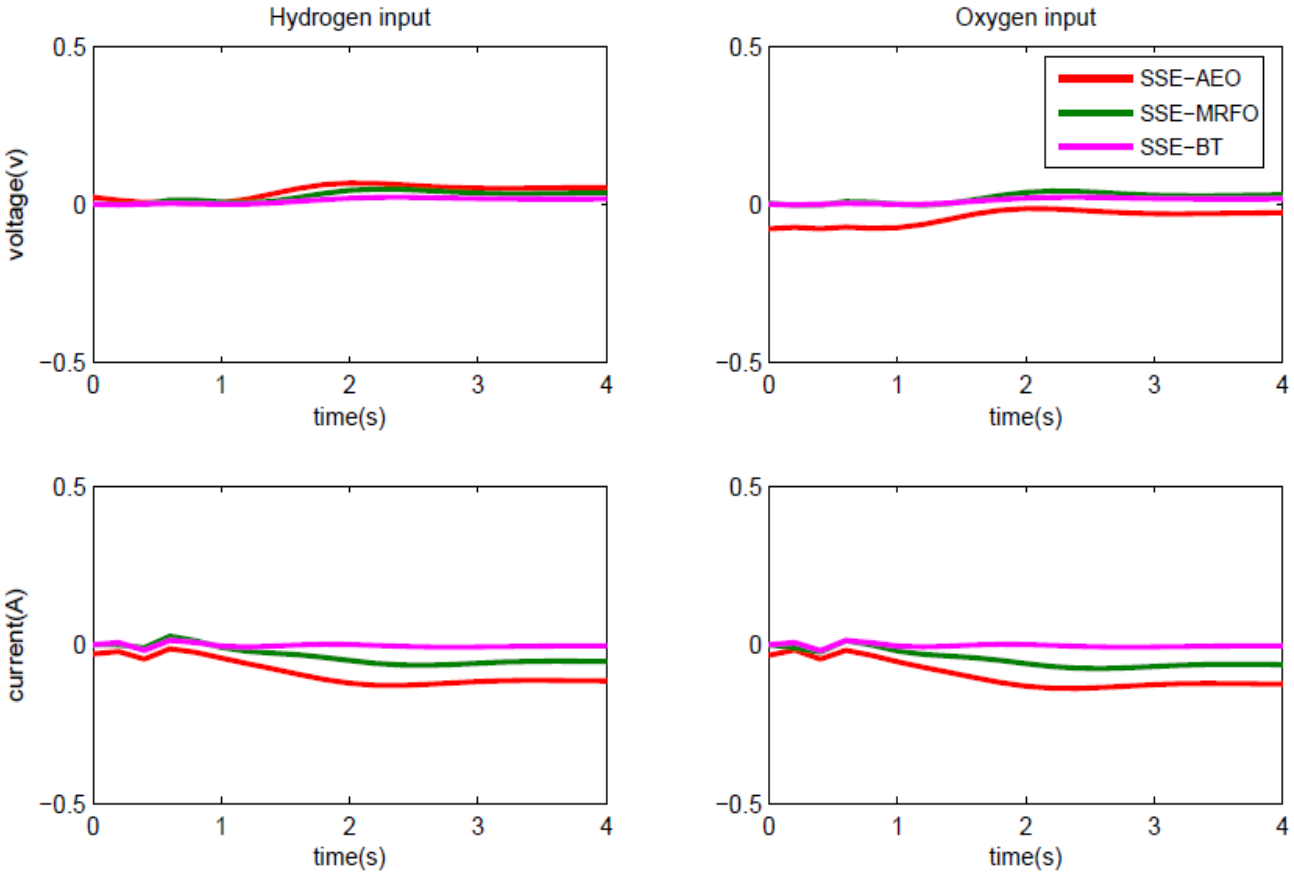

Figure 6.7 Step error comparison between the original PEMFC model and AEO, MRFO, BT reduced order models

Generally, it can observe that, the steady state of the impulse and step responses of hybrid (L_1, H_2, H_∞) reduced-order models by AEO, MRFO and BT techniques in figures (6.2) and (6.4) are close to those of the original PEMFC 500W model. More precisely, the initial values of transit state of both impulse and step responses of hybrid (L_1, H_2, H_∞) reduced-order models by MRFO and BT techniques in figures (6.3) and (6.5) are close match to those of the original PEMFC 500W model more than AEO approach. The same for the frequency responses, the results of the reduced-order models by MRFO and BT approaches are closely similar to an original model more than AEO technique. The figure (6.7) shows the comparison of steady state errors between hybrid (L_1, H_2, H_∞) reduced order models by AEO , MRFO and BT approaches

through drawing the step of error between original PEMFC model and reduced order models, the results are very close and satisfactory.

6.3.1.6 Comparative study of The Hybrid (L_1, H_2, H_∞) Reduced Models and Nonlinear PEMFC Model

To further validate the hybrid (L_1, H_2, H_∞) reduced order models, the outputs of AEO, MRFO and BT 3rd reduced models are compared with measured data, nonlinear and linear for PEMFC 500W models. Figure (6.8) shows these comparisons with exhibit the fit percentages between the outputs of AEO, MRFO and BT 3rd reduced models and their counterparts of the 8th order linear PEMFC model that was obtained via a local linearization technique, as well as the outputs of a nonlinear PEMFC model and measured data.

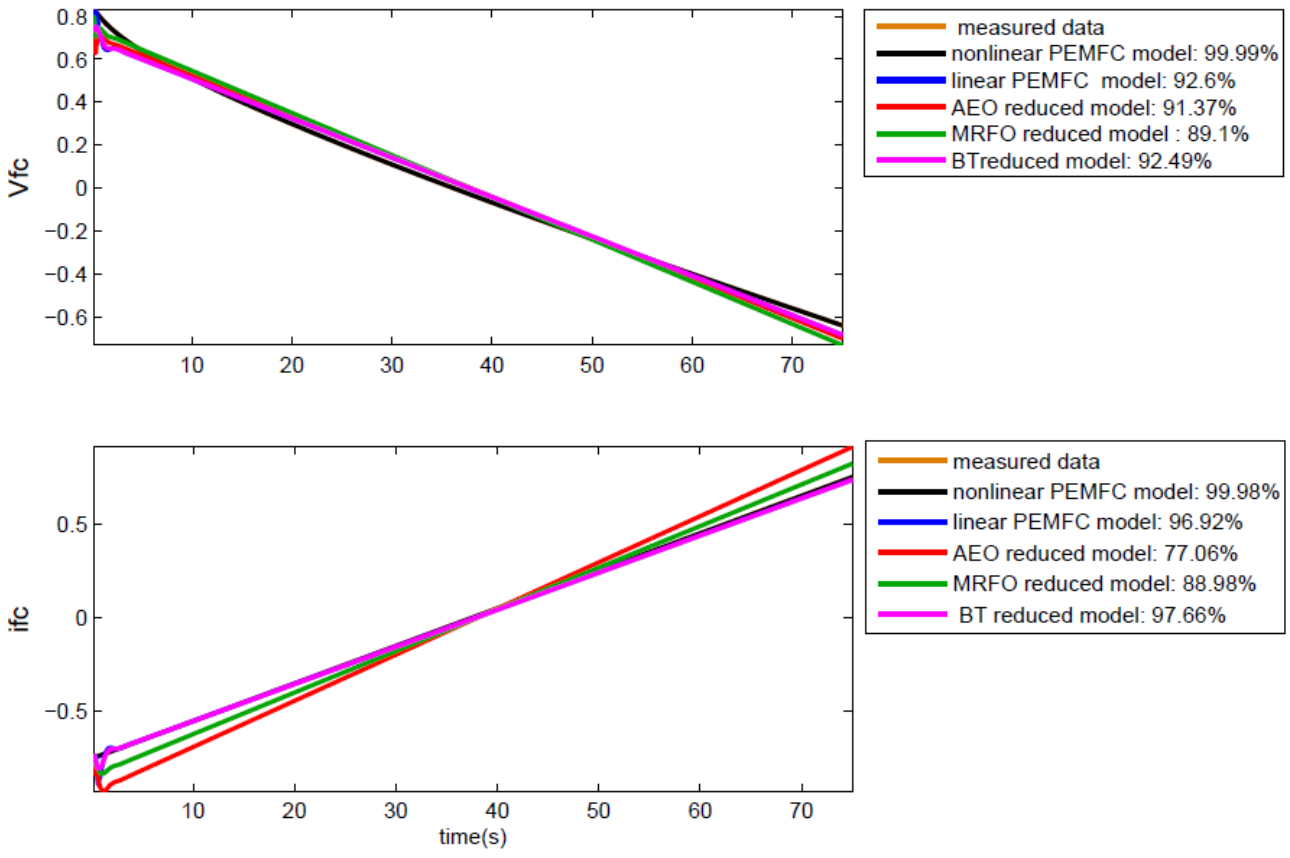

Figure 6.8 Comparison the outputs of hybrid (L_1, H_2, H_∞) reduced models, the linearized 8th order model, nonlinear model with PEMFC measured data

Note that, the fit percentage for BT 3^{rd} reduced model is highest percentage compared with AEO, MRFO 3^{rd} reduced models, it reaches to 92.49% for output voltage and 97.66% for output current. Generally, the fit percentage between the estimated outputs of the AEO, MRFO and BT 3rd reduced models, linear PEMFC model and nonlinear PEMFC model are close enough of the measured data for PEMFC system. Where, the fit percentage of output voltage (V_{fc}) varied between 89.1% and 99.99%, while the output current (i_{fc}) varied between 77.06% and 99.98%.

Figure (6.9) represents the comparison of the step responses for nonlinear PEMFC 500 W model to the result of 8th linear fuel cell model that was obtained by linearization technique and the AEO, MRFO and BT 3rd model order reduction approaches.

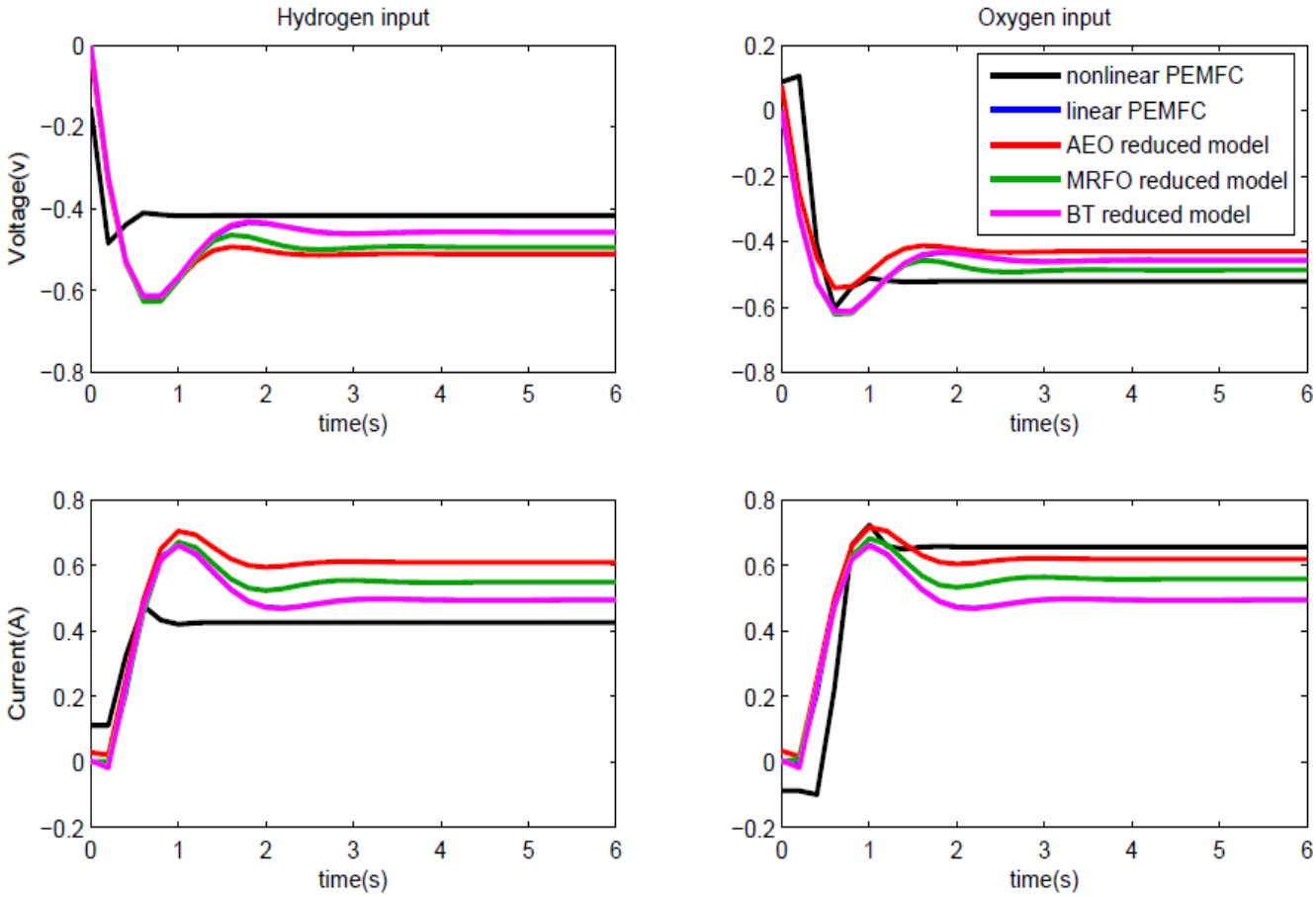

Figure 6.9 Step responses of nonlinear ,linear PEMFC models and hybrid (L_1, H_2, H_∞) reduced models via AEO, MRFO and BT

Observe that, the steady state of step responses of hybrid (L_1, H_2, H_∞) reduced-order models by AEO, MRFO and BT techniques in figure (6.9) are similar to those of linear and nonlinear PEMFC 500W model. While, the transit state of step responses for hybrid (L_1, H_2, H_∞) AEO, MRFO and BT reduced-order models are slightly different from the nonlinear PEMFC model. Furthermore, the step responses for BT approach and linear PEMFC model were identical.

6.3.2 Hybrid (H_2, H_∞) Norms

With application of AEO and MRFO algorithms, considering the same parameters which are presented in section (6.3.1) for minimizing optimal the hybrid (H_2, H_∞) norm for PEMFC 500W model. Hence, these parameters are summarize as follows:

Dimension of reduced order model: n=3

Population size: nPop= 100

The dimensionality of problem: Dim = 34

The low bound of search space: Low = -1

The up bound of search space: Up=1

The maximum number of iterations MaxIt = 2000

The systems represent the 3^{rd} order result of the hybrid (H_2, H_∞) norm Model reduction approach on the 8^{th} order PEMFC 500W model using the AEO and MRFO algorithms are given by following:

$$\sum_{\text{AEO}}: \begin{cases} x_n(k+1) = \begin{bmatrix} -0.117 & -0.249 & 0.210 \\ -0.205 & 0.637 & 0.590 \\ 0.751 & -0.347 & 0.130 \end{bmatrix} x(k) + \begin{bmatrix} 0.496 & -0.166 \\ 0.863 & 0.431 \\ 0.104 & 0.683 \end{bmatrix} u(k) + \begin{bmatrix} 0.401 & 0.071 \\ -0.425 & 0.348 \\ 0.106 & 0.377 \end{bmatrix} e(k) \\ y(k) = \begin{bmatrix} 0.063 & -0.371 & -0.197 \\ -0.408 & 0.274 & -0.263 \end{bmatrix} x(k) + \begin{bmatrix} -0.001 & -0.001 \\ -0.002 & 0.000 \end{bmatrix} u(k) + e(k) \\ x(o) = [-0.2876; \ -0.0781; \ -0.6706] \end{cases} \quad (6.11)$$

Eigenvalues: $\lambda_1 = -0.466, \ \ \lambda_{2,3} = 0.558 \pm 0.444\, i$

$$\sum_{\text{MRFO}}: \begin{cases} x_n(k+1) = \begin{bmatrix} 0.677 & 0.401 & 0.836 \\ 0.033 & 0.712 & 0.561 \\ -0.254 & -0.064 & 0.244 \end{bmatrix} x(k) + \begin{bmatrix} -0.346 & -0.337 \\ -0.140 & 0.136 \\ -0.389 & -0.398 \end{bmatrix} u(k) + \begin{bmatrix} 0.112 & 0.611 \\ 0.161 & -0.671 \\ -0.157 & 0.63 \end{bmatrix} e(k) \\ y(k) = \begin{bmatrix} 0.313 & 0.036 & 0.532 \\ -0.209 & -0.289 & 0.285 \end{bmatrix} x(k) + \begin{bmatrix} -0.000 & -0.0015 \\ 0.002 & -0.0041 \end{bmatrix} u(k) + e(k) \\ x(o) = [0.2436\,;\ -0.5999\,;\ -0.1391] \end{cases} \quad (6.12)$$

Eigenvalues: $\lambda_{1,2} = 0.6033 \pm 0.4221\,i, \lambda_3 = 0.4275$

6.3.2.1 Comparative Study of the Two Algorithms

The convergence process for hybrid (H_2, H_∞) norm of both AEO and MRFO reduced models with 2000 iterations are shown in figure (6.10) , note that, the MRFO approach has a best convergence compared with AEO algorithm towards the optimum solution. Where, the MRFO approach reaches to the best solution 0.1323 at 1996 iteration. While, the AEO approach reach to the best fitness 0.1797 at 1981 iteration.

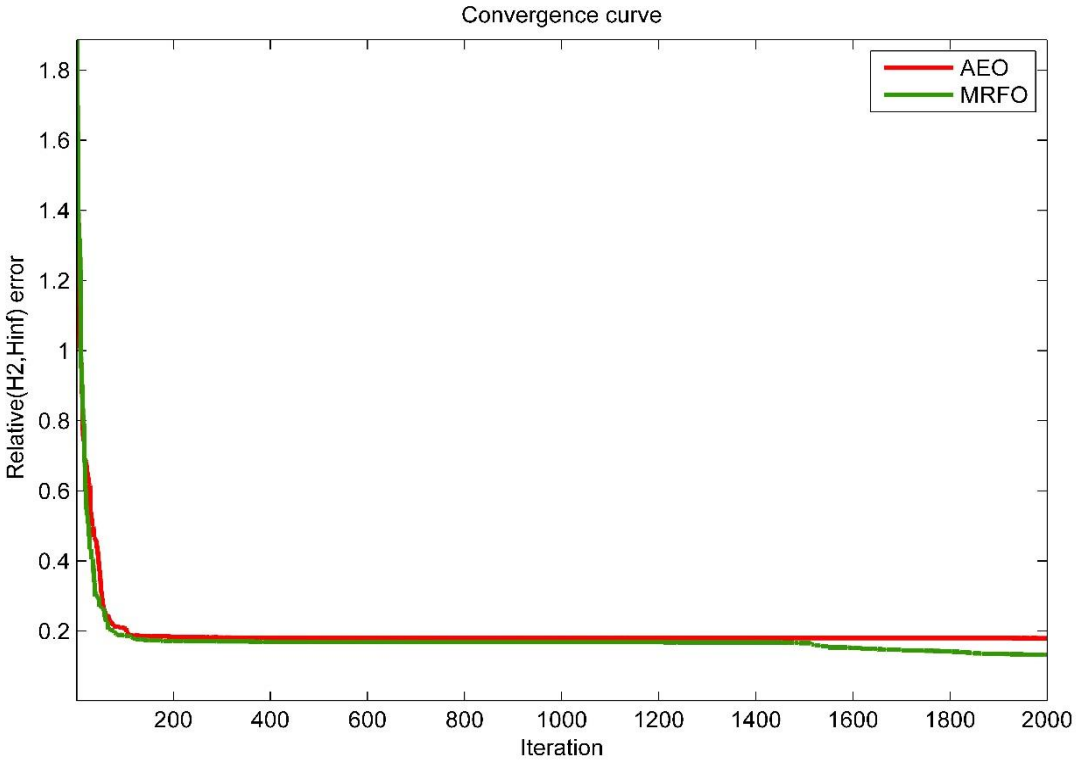

Figure 6. 10 Convergence rate of AEO and MRFO for hybrid (H_2 H_∞) norms

6.3.2.2 Norms and Steady State Errors

Table 6.2 presents the comparisons of the relative L_1 H_2, H_∞, hybrid (H_2, H_∞) of errors and steady state errors (SSE) of the reduced models obtained by AEO , MRFO , and BT with dimension n= 3.

Table 6. 2 Comparison between the relative L_1, H_2, H_∞, hybrid (H_2, H_∞) norms of error and SSE

	L_1 norm		H_2 norm	H_∞ norm	hybrid (H_2, H_∞)	SSE
AEO	L1_AEO(:,:,1) =0.174	0.177	0.112	0.067	0.179	0.0129
	L1_AEO(:,:,2) =0.180	0.178				
MRFO	L1_MRFO(:,:,1)=0.064	0.138	0.083	0.049	0.132	0.0019
	L1_MRFO(:,:,2)=0.066	0.144				
BT	L1_BT(:,:,1) =0.045	0.119	0.0799	0.0604	0.1403	0.002
	L1_BT(:,:,2) =0.045	0.119				

The MRFO approach has the lowest value of the hybrid (H_2, H_∞) , H_∞ and SSE compared to both AEO and BT techniques , the BT technique resulted in the lowest L_1 , H_2. However, the MRFO algorithm outperformed the AEO approach with the lowest all of the norms.

To better evaluate the approximants quality, the temporal responses, the frequency responses and errors steady state for PEMFC SR-12 500W original model and the reduced order models of all AEO , MRFO and BT approaches were traced in next sections.

6.3.2.3 Impulse Responses

Figure (6.11) represents the comparison of the impulse responses for the linear PEMFC 500 W model to the result of the hybrid (H_2, H_∞) norms of the 3^{rd} order reduction model approaches using AEO , MRFO and BT.

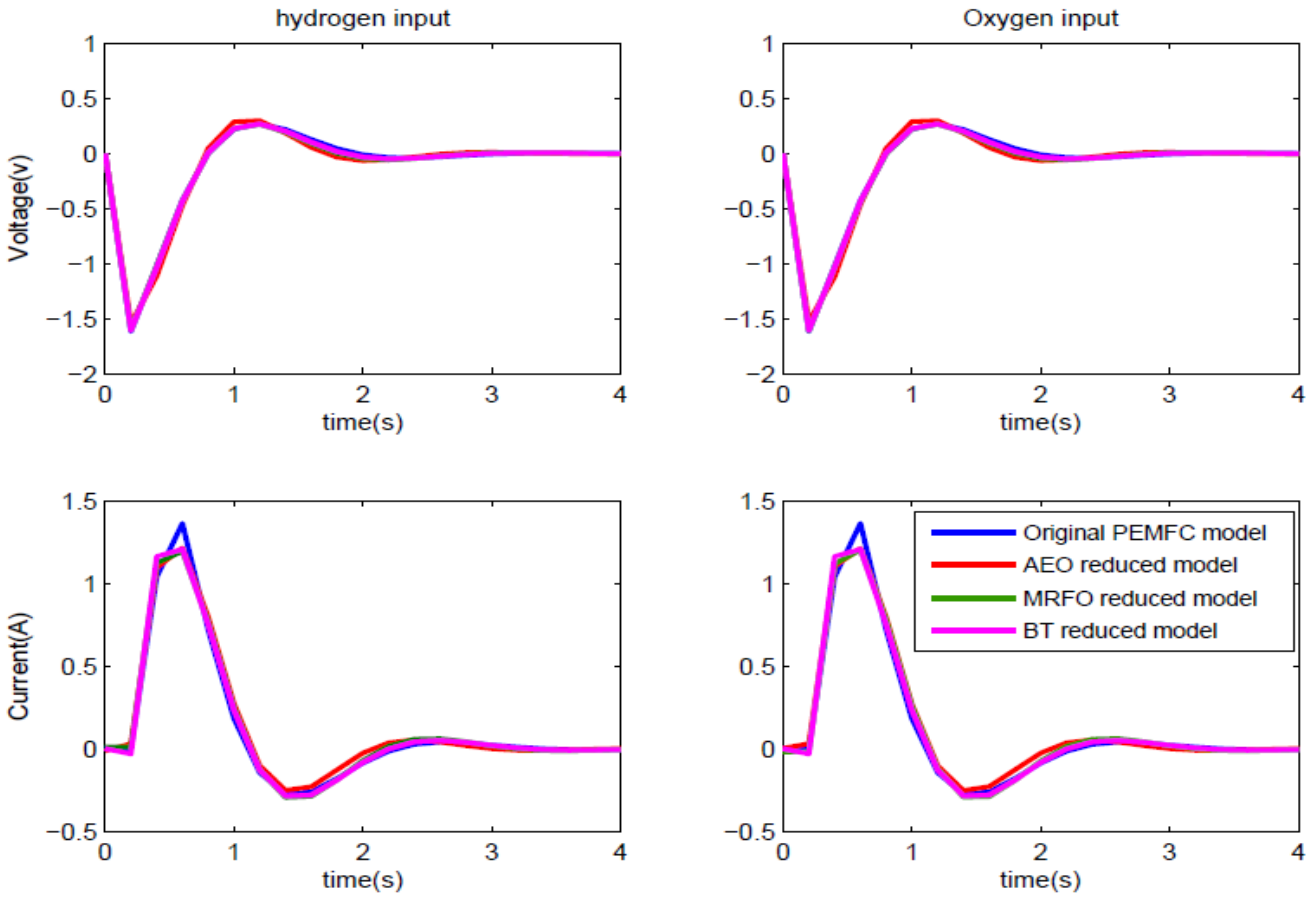

Figure 6. 11 Impulse responses of original PEMFC model and hybrid (H_2, H_∞) reduced models via AEO, MRFO and BT

To know more precisely which algorithm is close to original linear model , the impulse responses of the figure (6.11) is zoomed into figure (6.12) to compare the initial values of impulse responses for the original PEMFC model and AEO ,MRFO and BT reduced order models

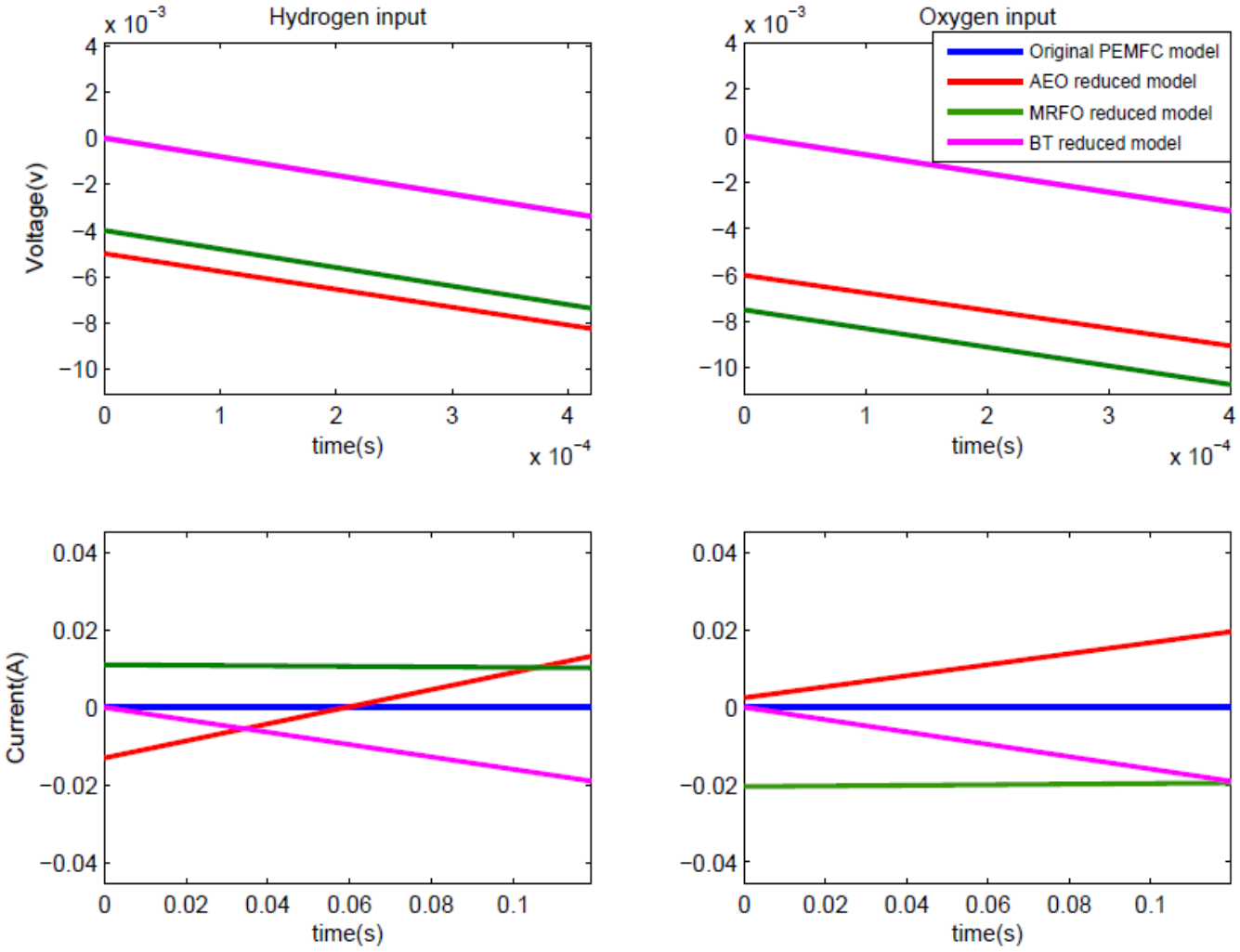

Figure 6.12 Initial values of the impulse responses of original PEMFC model and hybrid (H_2, H_∞) reduced models

6.3.2.4 Step Responses

Figure (6.13) represents the comparison of the step responses for the original PEMFC 500 W model to the result of the hybrid (H_2, H_∞) norms of the 3^{rd} order reduction model approaches using AEO , MRFO and BT.

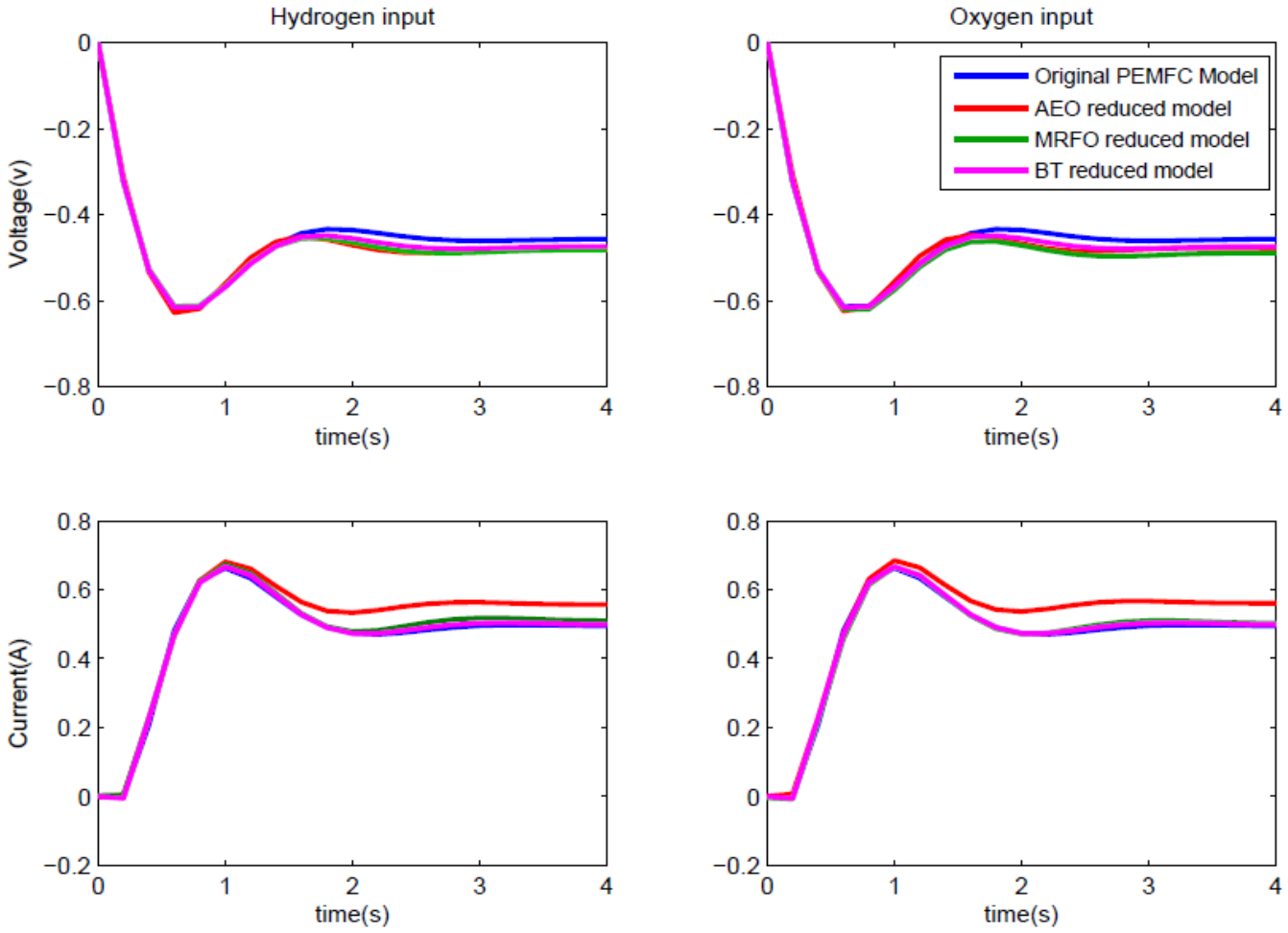

Figure 6.13 Step responses of original PEMFC model and hybrid (H_2, H_∞) reduced models via AEO, MRFO and BT

Figure (6.14) zooms into the figure (6.13) to compare the initial values of step responses of the original PEMFC model and all of AEO, MRFO and BT reduced order models

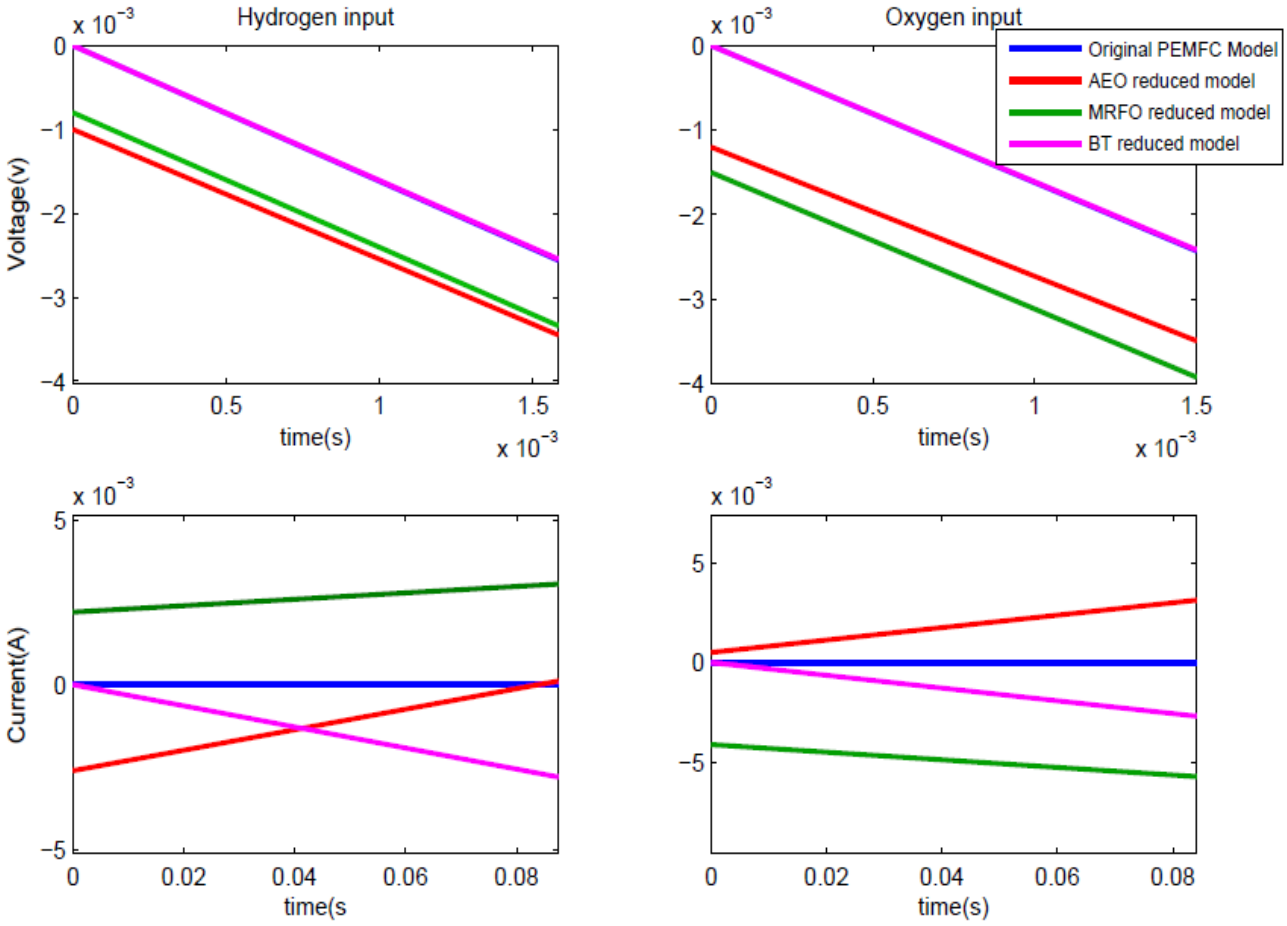

Figure 6.14 Initial values of the step responses of original PEMFC model and hybrid (H_2, H_∞) reduced models

6.3.2.6 Frequency Responses and Steady State Error

Figure (6.15) represents the comparison of the frequency responses for the original PEMFC 500 W model to the result of the hybrid (H_2, H_∞) norms of the 3^{rd} order reduction model approaches using AEO , MRFO and BT.

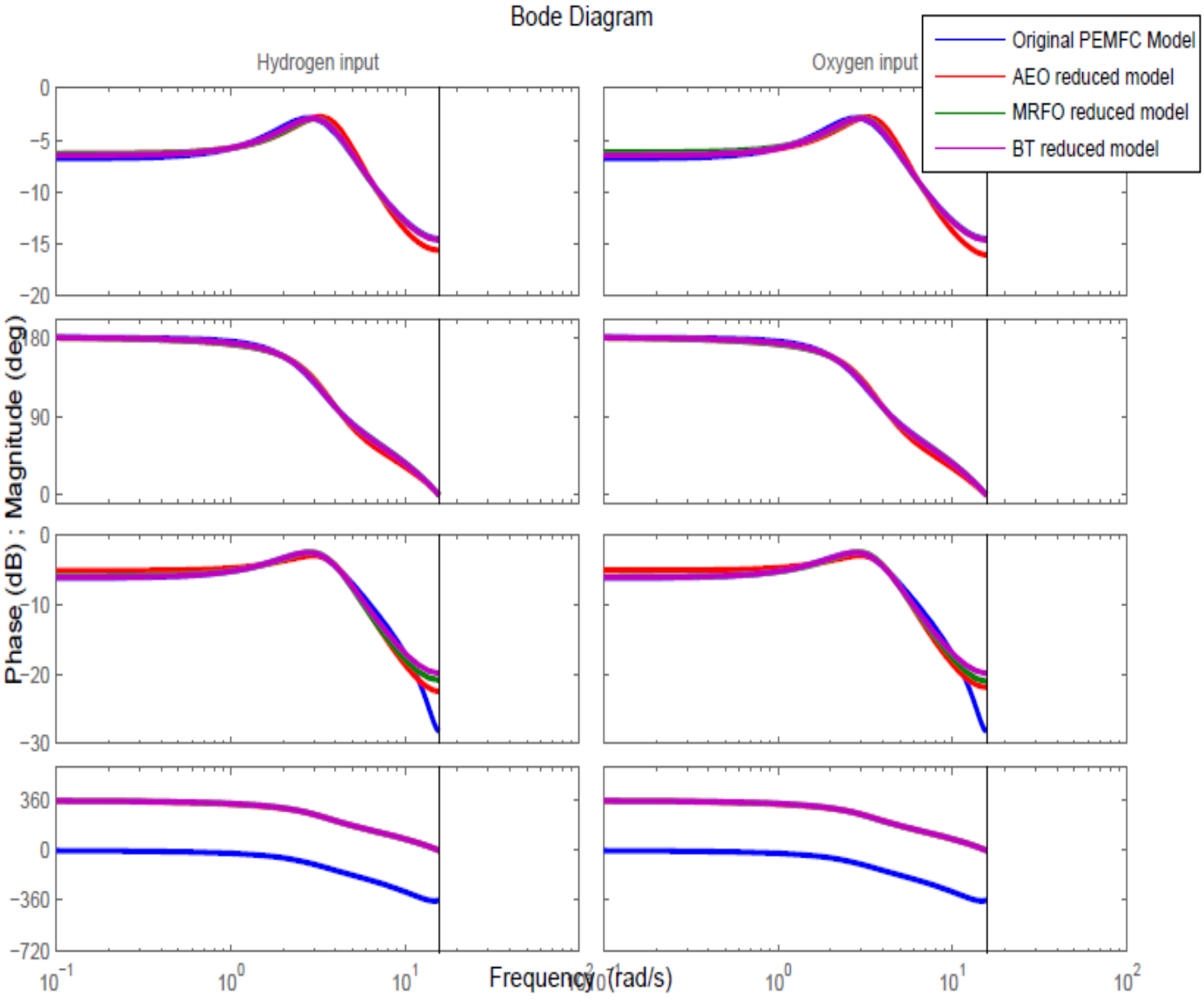

Figure 6.15 Frequency responses of original PEMFC model and hybrid (H_2, H_∞)

Reduced models via AEO, MRFO and BT

Figure (6.16) shows the comparison of step response error between original linear PEMFC model and AEO, MRFO, BT reduced order models

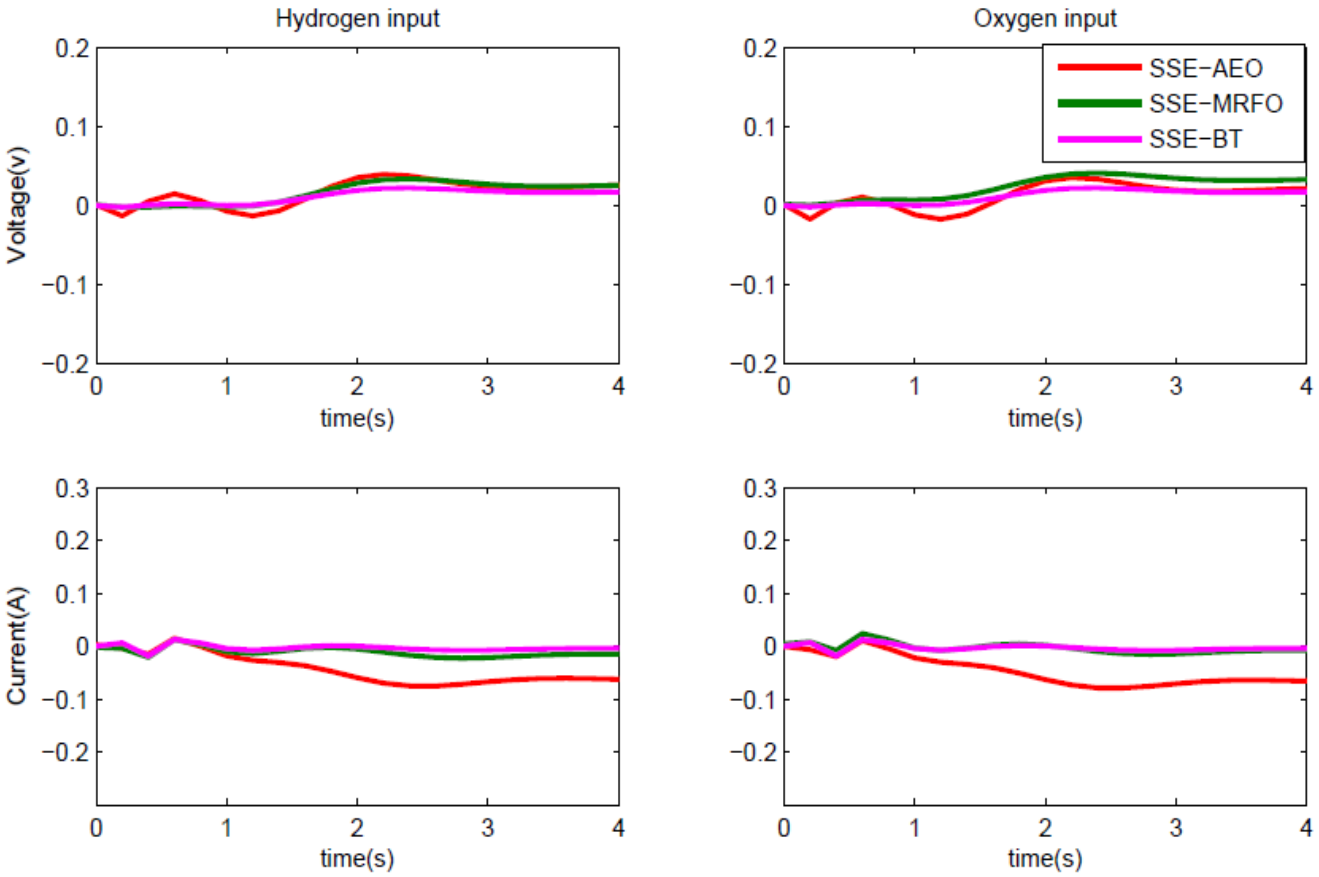

Figure 6.16 Step error comparison between original PEMFC model and hybrid (H_2, H_∞) reduced models

Note that, the steady state of the impulse and step responses of hybrid (H_2, H_∞) reduced-order models by AEO, MRFO and BT approaches in figures (6.11) and (6.13) are close match to those of the original PEMFC 500W model. More precisely, the initial values of transit state of both impulse and step responses of hybrid (H_2, H_∞) reduced-order models by MRFO and BT methods in figures (6.12) and (6.14) are close much to the original PEMFC 500W model more than AEO approach. For the frequency responses, the results of the reduced-order models by AEO, MRFO and BT approaches are closely similar to the original model.

The results of comparison of steady state errors between hybrid (H_2, H_∞) reduced order models by AEO , MRFO and BT approaches have been very close and satisfactory.

6.3.2.7 Comparative Study of The hybrid (H_2, H_∞) Reduced Models And Nonlinear PEMFC Model

To further validate the hybrid (H_2, H_∞) reduced order models, the outputs of AEO, MRFO and BT 3^{rd} reduced models are compared with nonlinear and linear for PEMFC 500W models further with measured data, . Figure (6.17) shows these comparisons with exhibit the fit percentages between the outputs of AEO, MRFO and BT 3rd reduced models and their counterparts of the 8^{th} order linear PEMFC model, outputs of the nonlinear PEMFC model and measured data.

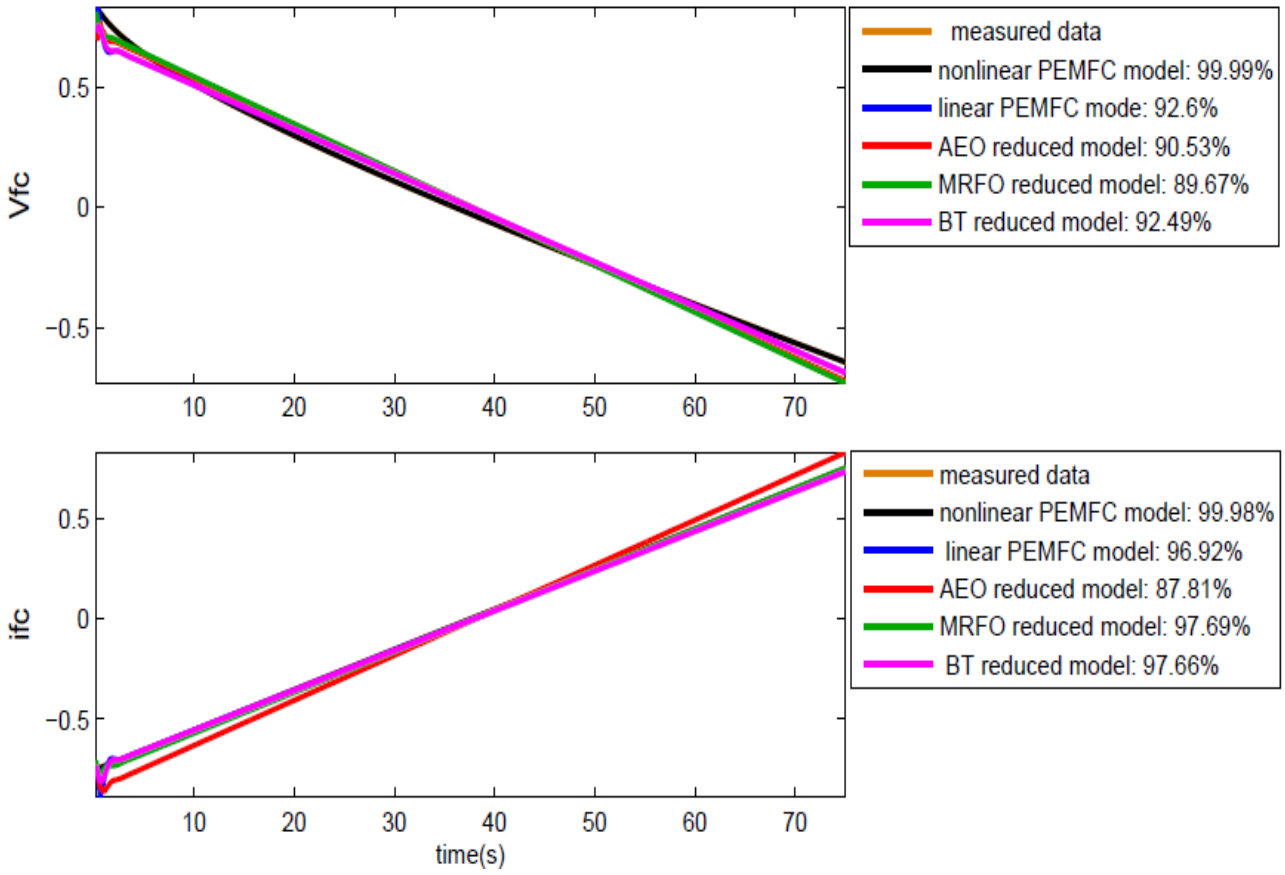

Figure 6.17 Comparison the outputs of hybrid (H_2, H_∞) reduced models, the linearized 8th order model, nonlinear model with PEMFC measured data

Note that, the fit percentage between the estimated outputs of the AEO, MRFO and BT 3rd reduced models, linear PEMFC model and nonlinear PEMFC model remained high. Where, the fit percentage of output voltage (V_{fc}) varied between 89.67% and 99.99%, while the output current (i_{fc}) varied between 87.81% and 99.98%. Therefore, all the outputs of reduced models, linear and nonlinear PEMFC models are close much to the measurement data for PEMFC system.

Figure 6.18 displays the comparison of the step responses for nonlinear PEMFC 500 W model to the result of 8th linear PEMFC model that was obtained by linearization technique section (3.7.3) and the AEO, MRFO and BT 3rd model order reduction approaches.

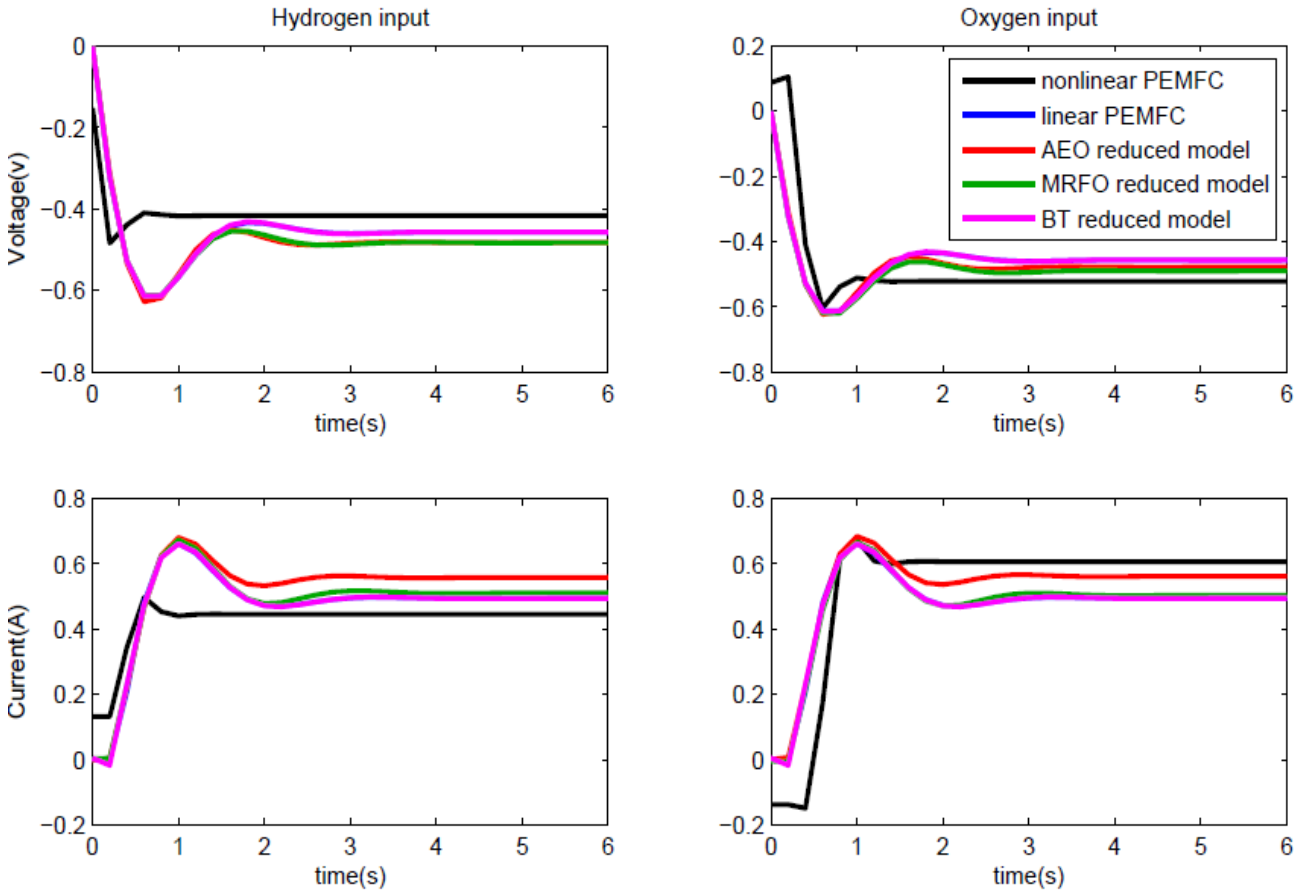

Figure 6. 18 Step responses of nonlinear ,linear PEMFC models and hybrid (H_2, H_∞) reduced models

In figure (6.18), the steady state of step responses of hybrid (H_2, H_∞) reduced-order models by AEO, MRFO and BT techniques are similar to those linear and nonlinear PEMFC 500W model. While, the transit state of step responses for hybrid (H_2, H_∞) AEO, MRFO and BT reduced-order models are slightly different from the nonlinear PEMFC model. Furthermore, the step responses for BT approach and linear PEMFC model are identical.

6.4 PEMFC Meta-Heuristic Model Reduction Approaches vs. Previous Studies

In this section, a comparison between the PEMFC model reduction approaches of research paper S.M. Elashhab et.al [1] with the AEO , MRFO and BT proposed techniques was presented . this paper used two approaches to generate a low order linear MIMO continuous time state space model equivalent to the nonlinear Proton Exchange Membrane Fuel Cell (PEMFC) power system developed . The input-output system identification (prediction-error minimization) and balanced model order reduction.

6.4.1 Model identification

S.M. Elashhab et.al [1] used the system identification technique for estimating a set of 8^{th}, 6^{th}, 4^{th} order MIMO continuous time state space models for the PEMFC system. They utilized the prediction-error minimization (pem) function to minimize the one step ahead prediction output error of the identified model using a maximum likelihood algorithm. The optimization technique employed with this function was Gauss-Newton line search for minimizing the cost function defined as follows:

$$V_N(B,C) = \sum_{t=1}^{N} e^2(t) \tag{6.13}$$

Where: N is samples number and e(t) is the error function defined as following:

$$e(t) = C^{-1}(q)[y(t) - B(q)u(t)] \tag{6.14}$$

To know how well a one step ahead prediction outputs of three estimated models close to the outputs of measured data. the percentage of fit given by equation (3.18) was used as criterion to select the best linear model to represent the PEMFC system.

The results of the three estimation linear models were validated via comparing their one step ahead prediction outputs and the outputs of the nonlinear model generated by identification data set. The comparison results displayed that, the PEMFC power system is best represented by 8^{th} order linear model which scored the highest fit percentage. while, the one step ahead prediction outputs of the 6^{th} and the 4^{th} order models were close much to the outputs of nonlinear model as well as the outputs of the 8^{th} order model .

6.4.2 Balanced Model Order Reduction

S.M. Elashhab et.al [1] applied the approximation concept for higher order state space PEMFC model with a lower order state space model while preserving the properties of the original system, they used balanced model order reduction method in order to achieve such task directly from the identified 8^{th} order PEMFC model. This technique computed a n^{th} order model given by:

$$G_n(s) = C_n(Is - A_n)^{-1}B_n + D \quad (6.15)$$

Of a possibly non-minimal and not necessarily stable N^{th} order system described by:

$$G_N(s) = C_N(Is - A_N)^{-1}B_N + D \quad (6.16)$$

$$\|G_N(s) - G_n(s)\|_\infty \leq total$$

Where $n < N$, $\|.\|_\infty$ denotes the infinity norm of the difference between the full order and the reduced models, *total* is the total error.

$$total = 2\sum_{i=n+1}^{N} svd(i) \quad (6.17)$$

$svd(i)$ denotes Hankel Singular Values of the full order model.

Hankel singular values of the system are determined as the square-roots of the eigenvalues of the reachability and observability grammians of the system .They are the energy measure of each state in the system and an indication of its contribution to properties of the system. Hence, preserving the high energy states that contribute the most to system dynamics and eliminating the low energy states will reduce the order of the model while keeping most of their characteristics in terms of stability, temporal and frequency responses.

The results of Hankel singular values for identified the 8^{th} order model showed that, it is reasonable to keep only four states in order to retain the characteristics of the initial order model. the comparison results of balanced model order reduction technique showed that, the simulated outputs of the truncated 4^{th} order linear model and its counterparts of the 8^{th} order linear model that was generated by a local linearization technique are close much to the outputs of the nonlinear PEMFC model, as well as ,the one step ahead prediction outputs of the truncated 4^{th} order model, and the identified 4^{th} order model are identical to the nonlinear model[1].Table 6.3 below compares the results of the hybrid (L_1, H_2, H_∞) norms model reduction for PEMFC system to the results of Shady M. Elashhab paper research:

Table 6. 3 Comparisons results of the hybrid (L_1, H_2, H_∞) norms and Shady's reduced models

PEMFC Model Reduction Approaches	Fit percentage $\binom{y_1\%}{y_2\%}$
Shady's identified 8th PEMFC model	98.3% 93.85%
Shady's identified 4th PEMFC model	98.32% 92.79%
Shady's truncated 4th PEMFC model	98.33% 91.27%
Proposed identified 8th PEMFC model	92.6% 96.92%
Proposed AEO 3rd PEMFC model	91.37% 77.06%
Proposed MRFO 3rd PEMFC model	89.1% 88.98%
Proposed truncated 3rd PEMFC model	92.49% 97.66%

Although the fit percentages of Shady's low order models are high compared with AEO and MRFO reduced models. However, the proposed approaches have proven better results , that

due to the 3rd AEO and MRFO reduced order models are simpler than 4th Shady's low order models with an appropriate fit percentage. In addition, the 3rd BT proposed method is better fit percentage compared with truncated 4th model.

6.5 Conclusion

In this chapter, AEO,MRFO and BT model order reduction approaches were presented in order to obtain low order linear MIMO models equivalent to the nonlinear model developed by Shahine [33].these techniques were used for minimizing both of hybrids (L_1 ,H_2, H_∞) and (H_2, H_∞) norms of errors between full PEMFC model and reduced order models. The convergence processes results of proposed meta-heuristic algorithms showed that , the MRFO approach has a faster convergence compared with AEO algorithm towards the best solution as displayed in figures (6.1) and (6.10). in addition, the simulation results of temporal and frequency responses for model reduction approaches have proven that, the AEO ,MRFO and BT 3rd reduced models were close much to the linear 8th PEMFC model as depicted in figures (6.2), (6.4), (6.6), (6.11), (6.13) and (6.15). finally, the simulated outputs of the AEO ,MRFO , BT 3rd reduced linear models and the outputs of the linearized 8th order PEMFC model were compared to the nonlinear PEMFC model as well as the measured data . According to this simulation, the outputs of AEO, MRFO and BT 3rd reduced models significantly similar to those of the nonlinear model and the measured data.

General Conclusion

General Conclusion

In this dissertation, an optimal model reduction for nonlinear complex proton exchange membrane (PEM) fuel cell 500W model was presented. Three steps were used to model the behavior of PEM fuel cell. The first step is preparing the measurement data (inputs-outputs) using the simulation of the nonlinear state space model of the PEM fuel cell 500W in Matlab environment programming.

The second step concerns system identification employing a nonlinear autoregressive exogenous (NLARX) structure for a PEMFC 500-W using a cascade-forward neural network. This model shows that, the nonlinear dynamics of the PEM fuel cell can be effectively modeled using three hidden layers neural network. The data set required to train the neural network was generated by implementing the nonlinear state space model of the PEM fuel cell 500W. Where the neural network is trained for voltage/current outputs values of the PEM fuel cell. Then, the obtained model was linearized to obtain the linear space state matrices of the PEM fuel cell. Based on the percentage of models fit, the results show that the linear and nonlinear models have a nearly similar trend of outputs data of the PEMFC stack. Overall, the NN-NLRAX and ARX structures with neural network estimator are capable of representing the PEMFC stack under tests. As a conclusion, the results of the best ARX and NNARX models are given by regressors n_a=[2 0,2 0] , n_b= [2 2,0 0] and n_k = [1 1,1 1], three hidden layers neurons [2 5 2]. Where, the best fit of the nonlinear model is given by: $y_{Vfc} = 99.99\%$, $y_{ifc} = 99.99\%$ for estimation data and $y_{Vfc} = 76.89\%$,$y_{ifc} = 98.88\%$ for validation data, the loss function is 5.5713e-019 and MSE performance for nonlinear model structures with neural network estimator is 6.7991e-009. For the linear model, the best fit is given by: $y_{Vfc} = 92.6\%$, $y_{ifc} = 96.92\%$ for estimation data and $y_{Vfc} = 88.4\%$, $y_{ifc} = 95.24\%$ for validation data, the loss function is 5.6797e-007 and the final prediction error FPE is 5.9220e-007.

The third step is an optimal reduction order model techniques for PEMFC model were performed using two new meta-heuristic techniques: nature-inspired Artificial Ecosystem Optimization (AEO) and bio-inspired optimization Manta Ray Foraging Optimization (MRFO) algorithms

.these algorithms were used to find the optimum reduced models for high order multiple input-output linearized PEM fuel cell 500w model, these approaches were applied to minimize the both of hybrids (L_1 ,H_2, H_∞) and (H_2, H_∞) norms of errors between full linearized PEMFC model and reduced order models, the process convergence results of AEO and MFRO approaches for hybrids (L_1 ,H_2, H_∞) and (H_2, H_∞) norms showed that the MRFO approach has a faster convergence compared with AEO algorithm towards the best solution. Both algorithms have been compared with standard balanced truncation (BT) technique, the obtained results have proved that, the performance of both MRFO and BT approaches are better than the obtained results by AEO algorithm in finding the lower order PEMFC model in terms of the minimum values of L_1 ,H_2, H_∞, hybrid (L_1 ,H_2, H_∞) and hybrid (H_2, H_∞) norms. The simulation results of temporal, frequency responses and steady state errors (SSE) showed that the AEO, MRFO and BT 3rd reduced models were much close to the linearized 8th PEMFC model. The simulated outputs of the AEO, MRFO, and BT 3rd reduced linear models and the outputs of the linearized 8th order PEMFC model were compared to the nonlinear PEMFC model as well as the measured data. According to the simulation, the outputs of AEO, MRFO and BT 3rd reduced models are significantly similar to those of the nonlinear model and the measured data.

In the future, both of state space model and NN-NLRAX model of the PEM fuel cell that were performed in this dissertation, can be used to develop the advanced control strategies to control the outputs of the PEM fuel cell. Also, other renewable energy technologies models, such as photovoltaic cells, wind turbines, and other fuel cells as, AFC,PAFC,SOFC, MCFC, MCFC, can be developed based on the proposed nonlinear space state PEM fuel cell modeling and neural network NLRAX approaches presented in this thesis.

This work uses meta-heuristic model order reduction methods for complex PEMFC 500W model. The obtained optimal reduced models can be used to develop a simple controller to control the voltage and current outputs of PEM fuel cell as well as these techniques can be used to other MIMO or SISO linear complex systems. .

Bibliography

Bibliography

[1] S. M. Elashhab and M. A. Zohdy, “PEM fuel cell system identification and model order reduction for H ∞ loop shaping controller design,” *2008 IEEE Int. Conf. Electro/Information Technol. IEEE EIT 2008 Conf.*, pp. 60–65, 2008, doi: 10.1109/EIT.2008.4554268.

[2] W. H. A. Schilders, H. A. van der Vorst, and J. Rommes, "Model Order Reduction: Theory, Research Aspects and Applications". 2008.

[3] J.Lachaize, “Etude des stratégies et des structures de commande pour le pilotage des systèmes énergétiques à Pile à Combustible (PAC) destinés à la traction. Soutenue,” Doctoteur de l’institut national polytechnique de Toulouse, 2004.

[4] C. Kunusch, P. Puleston, and M. Mayosky, "Sliding-Mode Control of PEM Fuel Cells". 2012.

[5] J. H. Scott, ‘The development of fuel cell technology for electric power generation: From NASA’s manned space program to the hydrogen economy,” *Proc. IEEE*, vol. 94, no. 10, pp. 1815–1825, 2006, doi: 10.1109/JPROC.2006.883702.

[6] M. W. Ellis, M. R. Von Spakovsky, and D. J. Nelson, “Fuel Cell Systems: Efficient, Flexible Energy Conversion for the 21st Century,” *Proc. IEEE*, vol. 89, no. 12, pp. 1808–1817, 2001, doi: 10.1109/5.975914.

[7] J. H. Hirschenhofer, “Fuel cell status: 1996,” *IEEE Aerosp. Electron. Syst. Mag.*, vol. 12, no. 3, pp. 23–28, 1997, doi: 10.1109/62.579205.

[8] K. Javed, R. Gouriveau, N. Zerhouni, and D. Hissel, “PEM fuel cell prognostics under variable load: A data-driven ensemble with new incremental learning,” *Int. Conf. Control. Decis. Inf. Technol. CoDIT 2016*, no. November 2017, pp. 252–257, 2016, doi: 10.1109/CoDIT.2016.7593569.

[9] A. R.Seyezhai and A. B.L.Mathur, “Mathematical Modeling of Proton Exchange Membrane Fuel Cell,” *Int. J. Comput. Appl.*, vol. 20, no. 5, pp. 1–6, 2011, doi: 10.5120/2433-3272.

[10] S. Jemei, “Modélisation d ’ une pile à combustible de type PEM par réseaux de neurones,” Energie électrique. Université de Franche-Comté; Universit_e de Technologie de Belfort-Montbeliard, 2013.

[11] P. Ovidiu, "The Study of the Efficiency of a Direct Methanol Fuel Cell," *J. Electr. Electron. Eng.*, vol. 7, no. 2, pp. 31–34, 2014. https://www.researchgate.net/publication/286098921.

[12] M. Khaled, "Modélisation et commande des systèmes energitiques à pile à combustible utilisation de la logique flou et des réseaux de neurones" ,Ecole Normal Supérieure de l'Enseignement Technologique d'Oran.

[13] F. C. Wang, L. H. Lin, and M. C. Chou, "Multivariable robust control for a 500W self-humidified PEMFC system," *Eur. J. Control*, vol. 17, no. 4, pp. 429–441, 2011, doi: 10.3166/ejc.17.429-441.

[14] C. Qin, J. Wang, D. Yang, B. Li, and C. Zhang, "Proton exchange membrane fuel cell reversal: A review," *Catalysts*, vol. 6, no. 12, pp. 1–21, 2016, doi: 10.3390/catal6120197.

[15] A. Albarbar and M. Alrweq, "Proton exchange membrane fuel cells: Design, modelling and performance assessment techniques". 2017.

[16] J. P. Kone, X. Zhang, Y. Yan, G. Hu, and G. Ahmadi, "Three-dimensional multiphase flow computational fluid dynamics models for proton exchange membrane fuel cell: A theoretical development," *J. Comput. Multiph. Flows*, vol. 9, no. 1, pp. 3–25, 2017, doi: 10.1177/1757482X17692341.

[17] A. Dudek and R. Wlodarczyk, "Corrosion resistance of composites based to graphite used as bipolar plates in fuel cells," *Corros. Resist.*, no. March, 2012, doi: 10.5772/31991.

[18] G. Fontès, "'Modélisation et caractérisation de la pile PEM pour l'étude des interactions avec les convertisseurs statiques,'" 2005.

[19] N. Margareth and C. Cuello, "Study of the Microstructure and Properties of a Pemfc Catalyst," University of Tennessee, Knoxville, 2018.

[20] K. A. Page and B. W. Rowe, "An overview of polymer electrolyte membranes for fuel cell applications," *ACS Symp. Ser.*, vol. 1096, pp. 147–164, 2012, doi: 10.1021/bk-2012-1096.ch009.

[21] J.W.Kulikowska, J.Wolska, and H.Koroniak, "Polymers application in proton exchange membranes for fuel cells (PEMFCs)," pp. 1–34, 2017, doi: 10.1515/psr-2017-0018.

[22] S. N. H. Jaafar, L. J. Minggu, K. Arifin, M. B. Kassim, and W. R. D. Wan, "Natural dyes as TIO2 sensitizers with membranes for photoelectrochemical water splitting: An

overview," *Renew. Sustain. Energy Rev.*, vol. 78, no. October, pp. 698–709, 2017, doi: 10.1016/j.rser.2017.04.118.

[23] F. Dubas, C. Espanet, and A. Miraoui, "Design of a high-speed permanent magnet motor for the drive of a fuel cell air-compressor," *2005 IEEE Veh. Power Propuls. Conf. VPPC*, vol. 2005, no. October, pp. 603–610, 2005, doi: 10.1109/VPPC.2005.1554621.

[24] I.Matraji, "Contribution à la commande non-linéaire robuste des systèmes d'alimentation en air des piles à combustible de type PEM," Universite de Technologie Belford - Montbéliard, 2006.

[25] V. Reguillet, "Caractérisation d ' un système pile à combustible en vue de garantir son démarrage et fonctionnement à température ambiante négative," Université de Franche-Comté, Doctoral thesis, 2013, 2015.

[26] A.Haddad, "Modèle dynamique non linéaire de la pile à combustible du PEM : Application à la régulation de l'humidité dans la menbrane électrolytique.," 2009.

[27] A. A. Alshorman, "Design and Investigation of Optimal Cooling System for Operative Performance of PEM Fuel Cell," *Int. J. Emerg. Trends Eng. Dev.*, vol. 1, no. 8, 2018, doi: 10.26808/rs.ed.i8v1.04.

[28] K. W. Harrison, R.Remick, G. D. Martin, and A. Hoskin, "Hydrogen Production: Fundamentals and Case Study Summaries," *Hydrog. fuel cells*, no. January, pp. 207–226, 2010.

[29] N. K. Tuan, K. E. Karpukhin, A. S. Terenchenko, and A. F. Kolbasov, "World trends in the development of vehicles with alternative energy sources," *ARPN J. Eng. Appl. Sci.*, vol. 13, no. 7, pp. 2535–2542, 2018.

[30] M. C. Williams, "Fuel Cell Handbook", Seven., no. 4. 2004.

[31] A. Haddad, R. Bouyekhf, A. El Moudni, and M. Wack, "Non-linear dynamic modeling of proton exchange membrane fuel cell," *J. Power Sources*, vol. 163, no. 1 SPEC. ISS., pp. 420–432, 2006, doi: 10.1016/j.jpowsour.2006.09.012.

[32] C. Wang, M. H. Nehrir, and S. R. Shaw, "Dynamic Models and Model Validation for PEM Fuel Cells Using Electrical Circuits," vol. 20, no. 2, pp. 442–451, 2005.

[33] S. Puranik, "Control of fuel cell based green energy systems for distributed generation applications," The Ohio State University, 2009.

[34] M. H. Nehrir and C. Wang, "Modeling and control of fuel cells :Distributed Generation Applications". 2009.

[35] R. I. Salim, “System for Domestic Use in the UAE Using Genetic Algorithms,” in *IEEE 2013 IV International Conference on Power Engineering, Energy and Electrical Drives& POWERENG ;May 13-17, 2013, Istanbul, Turkey*, 2013, pp. 2–7.

[36] Colleen Spiegel, “Mathematical Modeling of Polymer Exchange Membrane Fuel Cells,” University of South Florida, 2008.

[37] C. Wang and M. H. Nehrir, “A physically based dynamic model for solid oxide fuel cells,” *IEEE Trans. Energy Convers.*, vol. 22, no. 4, pp. 887–897, 2007, doi: 10.1109/TEC.2007.895468.

[38] J. Liang and Z. Wu, “Simulation and Optimization of Air-Cooled PEMFC Stack for Lightweight Hybrid Vehicle Application,” *Math. Probl. Eng.*, vol. 2015, pp. 1–12, 2015, doi: 10.1155/2015/738207.

[39] Colleen Spiegel, "PEM Fuel Cell Modeling and Simulation Using MATLAB". MATLAB® is a registered trademark of The MathWorks, Inc., 2008.

[40] J. Larminie and A. Dicks, "Fuel Cell Systems Explained", Second Edi., vol. 93, no. 1–2. 2003.

[41] N. H. Saad, A. A. El-Sattar, and A. E. A. M. Mansour, “Adaptive neural controller for maximum power point tracking of ten parameter fuel cell model,” *J. Electr. Eng.*, vol. 13, no. 3, pp. 233–239, 2013.

[42] G. Guni and A. Irawan, “Identification and Characteristics of Parallel Actuation Robot ’ s Leg Configuration Using Hammerstein - Wiener Approach,” vol. 1, no. 10, 2016, [Online]. Available: Guni and Irawan, JEECIE, Vol. 1, No. 10, Jan 2016.

[43] I. M. A. IBRAHEM, “A Nonlinear Neural Network-Based Model Predictive Control for Industrial Gas Turbine,” Superior Technology school university of Quebec, 2020.

[44] M. A. Ayob, W. N. W. Zakaria, J. Jalani, N. Mohamed Nasir, and M. R. M. Tomari, “Estimation of nonlinear ARX model for soft tissue by wavenet and sigmoid estimators,” *J. Telecommun. Electron. Comput. Eng.*, vol. 8, no. 7, pp. 123–128, 2016.

[45] S. A. H. Alrubaie, “Cascade-Forward Neural Network for Volterra Integral Equation Solution,” *Ibn AL- Haitham J. Pure Appl. Sci.*, vol. 34, no. 3, pp. 104–115, 2021, doi:

10.30526/34.3.2683.

[46] S. Rachad, B. Nsiri, and B. Bensassi, "System Identification of Inventory System Using ARX and ARMAX Models," *Int. J. Control Autom.*, vol. 8, no. 12, pp. 283–294, 2015, doi: 10.14257/ijca.2015.8.12.26.

[47] H. Fouraiji and B. Bensassi, "Identification of a production system using Hammerstein-Wiener and Narx Models," *J. Theor. Appl. Inf. Technol.*, no. 1, pp. 111–116, 2016, 10th February 2016. Vol.84. No.1.

[48] Tatang Mulyana, "Identification of Heat Exchanger by Neural Network Autoregressive with Exogenous Input Model," vol. i, no. tourism, p. 13, 2016, doi: DOI: http://dx.doi.org/10.5772/intechopen.83464.

[49] S. B. Salimbahrami, "Structure preserving order reduction of large scale second order systems," *IFAC Proc. Vol.*, p. 151, 2005, Doctoral thesis 2005.

[50] A. C.Antoulas and D.C.Sorensen, "Approximation of large scale dynamical systems: an overveiw," vol. 11, no. 5, pp. 1093–1121, 2001.

[51] V. D. Kubalinska, "Optimal interpolation-based model reduction," vol. 3, no. September, 2008, [Online]. Available: Doctoral thesis.

[52] B. C.Moore, "Principal Component Analysis in Linear Systems: Controllability, Observability, and Model Reduction," *IEEE Trans. Automat. Contr.*, vol. 26, no. 1, pp. 17–32, 1981, doi: 10.1109/TAC.1981.1102568.

[53] K. Glover, "Hankel-Norm Approximations," *Int. Inst. Appl. Syst. Anal.*, no. October, 1989, http://pure.iiasa.ac.at/3265/.

[54] Y. Liu and B. D.O. Anderson, "Singular Perturbation Approximation of Balanced Systems," in *Proceedings of the 28th Conference on Decision and Control Tampa, Florida December 1989*, 1989, vol. 2, no. December, doi: http://dx.doi.org/10.1080/00207178408933239.

[55] M. J. Rewienski, "A Trajectory Piecewise-Linear Approach to Model Order Reduction of Nonlinear Dynamical Systems," Massachusetts Institute of Technology, 2003.

[56] K. Gallivan, E. Grimme, and P. Van Dooren, "Asymptotic waveform evaluation via a Lanczos method," *Appl. Math. Lett.*, vol. 7, no. 5, pp. 75–80, 1994, doi: 10.1016/0893-9659(94)90077-9.

[57] K. Gallivan and P. Van Dooren, “Padé approximation of large-scale dynamic systems with Lanczos Methods,” *Proc. IEEE Conf. Decis. Control*, vol. 1, no. May 2014, pp. 443–448, 1995, doi: 10.1109/cdc.1994.410886.

[58] A. Odabasioglu, M. Celik, and L. T. Pileggi, “PRIMA: Passive reduced-order interconnect macromodeling algorithm,” vol. 17, no. 8, pp. 645–654, 1997.

[59] K. Gallivan, A. Vandendorpe, and P. Van Dooren, “Model reduction of mimo systems via tangential interpolation,” *SIAM J. Matrix Anal. Appl.*, vol. 26, no. 2, pp. 328–349, 2004, doi: 10.1137/S0895479803423925.

[60] J. M. A. Scherpen, “Balancing for nonlinear systems,” *Syst. Control Lett.*, vol. 21, no. 2, pp. 143–153, 1993.

[61] K. Fujimoto and J. M. A. Scherpen, "Nonlinear input-normal realizations based on the differential eigenstructure of hankel operators", vol. 50, no. 1. 2005.

[62] S. Lall, J. E. Marsden, and S. Glavaški, “A subspace approach to balanced truncation for model reduction of nonlinear control systems,” *Int. J. Robust Nonlinear Control*, vol. 12, no. 6, pp. 519–535, 2002, doi: 10.1002/rnc.657.

[63] Y. Chen and J. White, “A quadratic method for nonlinear model order reduction,” *2000 Int. Conf. Model. Simul. Microsystems - MSM 2000*, pp. 477–480, 2000.

[64] J. . Phillips, “Projection-based approaches for model reduction,” *Ieee Trans. Comput. Des. Integr. Circuits Syst.*, vol. 22, no. 2, pp. 171–187, 2003.

[65] L. Feng, X. Zeng, C. Chiang, D. Zhou, and Q. Fang, “Direct nonlinear order reduction with variational analysis,” *Proc. - Des. Autom. Test Eur. Conf. Exhib.*, vol. 2, no. March, pp. 1316–1321, 2004, doi: 10.1109/date.2004.1269077.

[66] D.A.Wilson, “Optimum Solution of Model-Reduction Problem,” vol. 117, no. 6, pp. 1161–1165, 1970, doi: 10.1049/piee.1970.0227.

[67] Z. Touati, “Réduction d’ordre optimale de systèmes complexes discrets MIMO par la norme H2,” Ziane Achour University, 2014.

[68] J. Doyle, B. Francis, and A. Tannenbaum, “Feedback Control Theory.” ,1990.

[69] D. C. Hyland and D. S. Bernstein, “The Optimal Projection Equations for Model Reduction and the Relationships Among the Methods of Wilson, Skelton, and Moore,” *IEEE Trans. Automat. Contr.*, vol. 30, no. 12, pp. 1201–1211, 1985, doi:

10.1109/TAC.1985.1103865.

[70] W. Yan and J. Lam, "An Approximate Approach to H2 Optimal Model Reduction," *IEEE Trans. Automat. Contr.*, vol. 44, no. 7, pp. 1341–1358, 1999.

[71] S. Gugercin, C. Beattie, and AC, "Rational Krylov methods for optimal H2 model reduction,",*Submitt.*,2006, . http://www.modelreduction.math.vt.edu/publications/gab_h2.pdf.

[72] C. Magruder, C. Beattie, and S. Gugercin, "Rational Krylov methods for optimal ℒ2 model reduction," *Proc. IEEE Conf. Decis. Control*, pp. 6797–6802, 2010, doi: 10.1109/CDC.2010.5717454.

[73] C. A. Beattie and S. Gugercin, "Krylov-based minimization for optimal H2 model reduction," *Proc. IEEE Conf. Decis. Control*, pp. 4385–4390, 2007, doi: 10.1109/CDC.2007.4434939.

[74] P. Van Dooren, K. A. Gallivan, and P. A. Absil, "H2-optimal model reduction of MIMO systems," *Appl. Math. Lett.*, vol. 21, no. 12, pp. 1267–1273, 2008, doi: 10.1016/j.aml.2007.09.015.

[75] A. Bunse-Gerstner, D. Kubalińska, G. Vossen, and D. Wilczek, "h2-norm optimal model reduction for large scale discrete dynamical MIMO systems," *J. Comput. Appl. Math.*, vol. 233, no. 5, pp. 1202–1216, 2010, doi: 10.1016/j.cam.2008.12.029.

[76] D. Kavranoğlu, M. Bettayeb, and M. F. Anjum, "L∞ norm simulataneous system approximation," *Novemb. 1996International J. Robust Nonlinear Control 6(910)999-1014*, vol. 6, pp. 999–1014, 1996, doi: 10.1002/(SIC1099-1239(199611)6:9/103.3.CO;2-F.

[77] D. Kavranoğlu and M. Bettayeb, "Characterization of the solution to the optimal H∞ model reduction problem," *Syst. Control Lett.*, vol. 20, no. 2, pp. 99–107, 1993, doi: 10.1016/0167-6911(93)90021-W.

[78] D. Kavranoglu and M. Bettayeb, "Constant L∞ norm Approximations of Complex Rational Functions," *Numer. Funct. Anal. Optim.*, vol. 16, no. 1–2, pp. 197–217, 1995, doi: 10.1080/01630569508816613.

[79] M. B. Bettayebt, Davut Kavranoglu and M. F. Anjum, "Rational L∞ norm approximation of multivariable systems," in *Proceedings of the 34th Conference on Decision & Control*,

1995, no. December, pp. 790–795.

[80] D. Kavranoğlu and M. Bettayeb, "LMI Based Computational Schemes for H ∞ Model Reduction," pp. 3585–3590, doi: :10.1016/S1474-6670(17)58234-8.

[81] Y. Ebihara and T. Hagiwara, "On H∞ model reduction using LMI's," *Proc. Am. Control Conf.*, vol. 1, no. 7, pp. 774–779, 2004, doi: 10.1109/TAC.2004.831116.

[82] L. Zhang, P. Shi, E. K. Boukas, and C. Wang, "H∞ model reduction for uncertain switched linear discrete-time systems," *Automatica*, vol. 44, no. 11, pp. 2944–2949, 2008, doi: 10.1016/j.automatica.2008.03.025.

[83] R. A. El-attar; and M. Vidyasagar, "Optimal order reduction using the induced operator norm," *1977 IEEE Conf. Decis. Control Incl. 16th Symp. Adapt. Process. A Spec. Symp. Fuzzy Set Theory Appl.*, doi: 10.1109/CDC.1977.271605.

[84] O. A. Sebakhy; and M. N. Aly, "Discrete-time model reduction with optimal zero locations by norm minimization," *Proc. 1998 IEEE Int. Conf. Control Appl. (Cat. No.98CH36104)*, no. September, pp. 812–816, 1998, doi: 10.1109/CCA.1998.721571.

[85] Y. Li, Y. Qu, H. Gao, and C. Wang, "Robust L1 model reduction for uncertain stochastic systems with state delay," *Proc. Am. Control Conf.*, vol. 4, pp. 2602–2607, 2005, doi: 10.1109/acc.2005.1470359.

[86] K. C. Tan and Y. Li, "L∞ identification and model reduction using a learning genetic algorithm," *IEE Conf. Publ.*, no. 427 /2, pp. 1125–1130, 1996.

[87] H. Du, J. Lam, and B. Huang, "Constrained H2 approximation of multiple input-output delay systems using genetic algorithm," *ISA Trans.*, vol. 46, no. 2, pp. 211–221, 2007, doi: 10.1016/j.isatra.2006.06.007.

[88] M. Juneja, S. K. Nagar, and S. R. Mohanty, "PSO Based reduced order modelling of autonomous AC microgrid considering state perturbation," *Automatika*, vol. 61, no. 1, pp. 66–78, 2020, doi: 10.1080/00051144.2019.1682867.

[89] R. Salim and M. Bettayeb, "Optimal Model Reduction Using Genetic Algorithms and Particle Swarm Optimization," 2009.

[90] M. Seyedali, M. Seyed Mohammad, and L. Andrew, "Author Grey Wolf Optimizer," *Adv. Eng. Softw.*, 2014.

[91] W. Zhao and L. Wang, "Artificial ecosystem-based optimization : a novel nature-inspired

meta-heuristic algorithm," *Neural Comput. Appl.*, vol. 0123456789, 2019, doi: doi.org/10.1007/s00521-019-04452-x.

[92] A. S. Menesy, H. M. Sultan, A. Korashy, F. A. Banakhr, M. G. Ashmawy, and S. Kamel, "Effective Parameter Extraction of Different Polymer Electrolyte Membrane Fuel Cell Stack Models Using a Modified Artificial Ecosystem Optimization Algorithm," *IEEE Access*, vol. 8, no. February, pp. 31892–31909, 2020, doi: 10.1109/ACCESS.2020.2973351.

[93] W. Zhao, Z. Zhang, and L. Wang, "Manta ray foraging optimization: An effective bio-inspired optimizer for engineering applications," *Eng. Appl. Artif. Intell.*, vol. 87, no. October 2019, p. 25, 2020, doi: 10.1016/j.engappai.2019.103300.

[94] M. G. Hemeida, S. Alkhalaf, A. A. Mohamed, A. A. Ibrahim, and T. Senjyu, "Distributed Generators Optimization Based on Foraging Optimization Algorithm (MRFO)," *Energies*, vol. 35, 2020, doi: 10.3390/en13153847.

Annex

Annex A

Balanced truncation procedure

The idea of model reduction by balanced truncation is to build a reduced order model by transforming the original model into a balanced realization and removing states that are both less reachable and less observable.

Definition 1. The state representation of a stable, completely reachability and observable system Σ is called balanced if the reachability grammian and the observability grammian, are equal and diagonal.

$$\mathcal{P} = Q = S = \begin{bmatrix} \sigma_1 & & \\ & \ddots & \\ & & \sigma_N \end{bmatrix} \qquad (A.1)$$

Where $\sigma_k = \sqrt{\lambda(\mathcal{P}Q)}$ are real and positive values so-called *Hankel singular values (HSV)* such that:

$$\sigma_1 \geq \sigma_2 \geq \sigma_3 \geq \cdots \geq \sigma_N > 0$$

$\mathcal{P}$ and Q are unique solutions symmetric positive definite of Stein equations:

$$\begin{cases} A\mathcal{P}A^* + BB^* = \mathcal{P} \\ A^*QA + C^*C = Q \end{cases} \qquad (A.2)$$

We need to build an invertible transformation matrix T which simultaneously diagonalizes the reachability $\mathcal{P}$ and observability grammians Q.

Consider the algebraic representation of the equivalent state space of the system Σ_N equation(4.5). The equilibrium transformation in the state space parameters leads to produce another algebraic representation $\widetilde{\Sigma_N}$.

$$\widetilde{\Sigma_N}: \begin{cases} \tilde{x}(k+1) = T^{-1}AT\tilde{x}(k) + T^{-1}Bu(k) \\ y(k) = CT\tilde{x}(k) + Du(k) \end{cases} \quad (A.3)$$

Then the transformed grammians: $\tilde{\mathcal{P}} = T\mathcal{P}T^*$ and $\tilde{Q} = T^{-*}QT^{-1}$ are unique solutions symmetric positive definite of following Stein equations:

$$\begin{cases} \tilde{A}\tilde{\mathcal{P}}\,\widetilde{A^*} + \tilde{B}\widetilde{B^*} = \tilde{\mathcal{P}} \\ \widetilde{A^*}\tilde{Q}\tilde{A} + \widetilde{C^*}\tilde{C} = \tilde{Q} \end{cases} \quad (A.4)$$

Equilibrium algorithm

The equilibrium algorithm consists of the determination of the non-singular equilibrium transformation T whose computation is essentially based on reachability grammian and the observability grammian of the system, this algorithm is given as follows:

Step 1: Having the state space representation of order N (A, B, C, D)

Step 2 : Calculating the reachability grammian $\mathcal{P}$ and the observability grammian Q as solutions of Stein's equations

Step 3: Cholesky factorization of the pair ($\mathcal{P}$, Q) such as:

$$\mathcal{P} = \mathrm{L_C L_C^T} \quad (A.5)$$

$$Q = \mathrm{L_O L_O^T} \quad (A.6)$$

With $\mathrm{L_C}$ and $\mathrm{L_O}$ are the lower triangular matrices

Step 4: Decomposing the singular value of the product of Cholesky factors

$$\mathrm{L_O^T\, L_C = US\, V^T} \quad (A.7)$$

Where $\mathrm{U} \in \mathbb{R}^{N\times N}$ and $\mathrm{V} \in \mathbb{R}^{N\times N}$ are orthogonal matrices, S = diag [σ_1 ... σ_N] is singular values matrix of the system.

Step 5: Obtaining the equilibrium transformation T

$$\mathrm{T = L_C V\, S^{1/2}} \quad (A.8)$$

$$\mathrm{T^{-1} = S^{-1/2}\, U^T L_O^T} \quad (A.9)$$

Step 6: Constructing the balanced state matrices:

$$\widetilde{\mathrm{A}} = \mathrm{T^{-1}\, AT = S^{-\frac{1}{2}} U^T L_O^T A L_C V S^{\frac{1}{2}}} = \begin{pmatrix} A_{11} & A_{12} \\ A_{21} & A_{22} \end{pmatrix} \quad (A.10)$$

$$\widetilde{\mathrm{B}} = \mathrm{T}^{-1}\mathrm{B} = \mathrm{S}^{-1/2}\,\mathrm{U}^{\mathrm{T}}\mathrm{L}_{\mathrm{O}}^{\mathrm{T}}\,\mathrm{B} = \begin{pmatrix} B_1 \\ B_2 \end{pmatrix} \qquad (A.11)$$

$$\tilde{\mathrm{C}} = \mathrm{CT} = \mathrm{C}\,\mathrm{L}_{\mathrm{C}}\mathrm{V}\mathrm{S}^{1/2} = (C_1 \quad C_2) \qquad (A.12)$$

There are states which are difficult to observe, in this sense the observation energy is low, which corresponds to a significant component of the observability grammian with small eigenvalues.
In addition, there are states, which are difficult to reach the minimum cost to command these states is high. The eigenvalues of the reachability grammian are small. Hence, the states that are less reachable and less observable are removing.
Suppose that S in (A.1) is partitioned into:

$$S = \begin{bmatrix} S_1 & \\ & S_2 \end{bmatrix} \qquad (A.13)$$

Where $S_1 \in \mathbb{R}^{\mathrm{n}\times\mathrm{n}}$ contains the largest Hankel singular values, i.e. the eigenvalues of the product $\mathcal{P}\mathcal{Q}$ that corresponding to a strong subsystem with easily controllable and easily observable states. The S_2 contains the smallest Hankel singular values which correspond to a weak subsystem with states which are difficult to reach and difficult to observe.

Step 7: the reduced order model for balanced state matrices (A.10), (A.11) and (A.12) is obtained by truncating the weak subsystem and maintaining those parts of matrices, which correspond to the strong subsystems:

$$\begin{aligned} A_n &= A_{11} \\ B_n &= B_1 \\ C_n &= C_1 \end{aligned} \qquad (A.14)$$

Then Σ_{n} reduced order system obtained by balanced truncation is given by following:

$$\Sigma_{\mathrm{n}}: \begin{cases} x_n(k+1) = A_n x_n(k) + B_n u(k) \\ y_n(k) = C_n x_n(k) + Du(k) \end{cases} \qquad (A.15)$$

The quality of this approximation could be measured as follows:

$$\| \Sigma_{\mathrm{N}} - \Sigma_{\mathrm{n}} \|_{H\infty} < 2(\sigma_{k+1} + \cdots + \sigma_N) \qquad (A.16)$$